REACTIONS BETWEEN THE LIQUID ALKALI-METALS AND LIQUID WATER

A THESIS SUBMITTED TO THE UNIVERSITY OF NOTTINGHAM

for

THE DEGREE OF DOCTOR OF PHILOSOPHY

by

ALLAN B. ASHWORTH BSc.

DEPARTMENT OF CHEMISTRY

THE UNIVERSITY, NOTTINGHAM.

December, 1979

REACTIONS BETWEEN THE LIQUID ALKALI METALS AND LIQUID WATER

by

A.B. ASHWORTH

ABSTRACT

The rates of reaction of the constituents of sodium-potassium alloy with water have been determined in the temperature range 20 - 60°C. They fall into two categories; the first is applicable to the instant the alloy meets the water, and the second applies to reaction of the metal through a bubble of hydrogen. The rates are widely different for these two stages, yet the activation energies are similar, being 38.3 and 33.0 KJ/mole respectively for sodium, and 24.9 and 27.3 KJ/mole respectively for potassium. The rate of reaction of sodium alone at 30°C. has also been determined.

The behaviour of liquid metals when injected into water has been studied by high speed photography. Such jets disintegrate, after a short distance of travel, into small globules, each contained within a hydrogen gas bubble. These globules then travel upwards through water, and consequently react much more slowly.

The reaction rate may be reduced by the addition of small concentrations of mineral acids to the water, due to the formation of salts at the metal-water interface which are less soluble than sodium hydroxide. Strong solutions of acid however, increase the rate of reaction. The

addition of hydroxide ions as NH_4OH has little effect on the rates.

The metals undergo secondary reaction in that the hydrogen which is initially formed subsequently reacts with the metal to produce hydrides. These are eventually hydrolysed.

The most probable reaction intermediate in the solution phase of the reaction is the solvated electron, $e^-_{(aq)}$, which has been detected photographically due to its absorption of light in the visible region of the spectrum.

Overall reaction mechanisms for both reaction in solution and reactions at the metal surface have been proposed.

ACKNOWLEDGEMENTS

The author would like to thank the following for their help. His supervisors, Dr. R.J. Pulham and Dr. W.D. Halstead for their guidance during the course of this project. His wife, for her patience during the preparation of this thesis. His parents, for their support during the years of his education. His colleagues in the liquid-metals laboratories, and the technical staff in the department of Chemistry at Nottingham. His father-in-law, Mr. Ray Williamson for the preparation of this typescript, and finally, the C.E.G.B. and S.R.C. who provided the money which funded this work.

CONTENTS

LIST OF DIAGRAMS

C H A P T E R I

INTRODUCTION

Interest in the chemistry of the alkali-metals, and more particularly, in the chemistry of sodium has developed in recent years as a consequence of the development of the Liquid Metal Cooled Fast Breeder Reactor (L.M.F.B.R.). This generation of reactors, the fourth in the United Kingdom is already at an advanced stage of development, since their commercial use may be necessary in order to fill the 'energy gap' expected to occur towards the end of this century.[1] The use of fast reactors rather than thermal (moderated) reactors will extend the lifetime of known deposits of the main nuclear fuel, uranium, due to the breeder properties of the reactor. If uranium fuel is used in the more conventional thermal reactors e.g. gas cooled (Magnox, A.G.R.) or water cooled (P.W.R., S.G.H.W.R.etc) reactors, known deposits of uranium will supply approximately 2 Q energy equivalent[2], where Q = the energy from 30,000 tonnes of good quality coal. The equivalent figure for exclusive fast reactor use of the fuel is 100 Q. Corresponding figures for estimated, as opposed to known, uranium deposits are 12 Q and 600 Q.

Conduction of heat energy from the core of such a reactor creates many problems. These problems have been partially solved by the use of a liquid alkali-metal coolant. The Dounreay Fast Reactor (D.F.R.) used 50,000 Kg of sodium-potassium alloy with composition 70 wt. % Na in a liquid metal coolant loop.[3] This reactor, recently shut down, was an experimental 60 M W. machine. The new Prototype Fast Reactor (P.F.R.), also at Dounreay in Scotland, uses approximately 1,000,000 Kg of liquid sodium as coolant, and is planned to generate 250 M W. of electricity. There are already designs for the construction of a 1300 M W. commercial prototype fast reactor in Britain.[4]

In fast reactors, the uranium or plutonium ceramic fuel (oxide or carbide) is clad in stainless steel pins, and these are surrounded by more pins containing natural uranium as its oxide (natural uranium contains 0·718% U^{235}, the fissile isotope, and 99·276% U^{238}, the fertile isotope as its major constituents). The whole assembly is then immersed in the liquid metal coolant. Heat is generated due to the nuclear reactions represented by Equations 1.1, 1.2.

$$_{94}Pu^{239} + {}_{0}n^{1} \longrightarrow {}_{94}Pu^{240} + \text{'fission fragments'} + 0{\cdot}84\text{MeV} \quad (1.1)$$

$$_{92}U^{235} + {}_{0}n^{1} \longrightarrow {}_{92}U^{236} + \text{'fission fragments'} + 0{\cdot}79\text{MeV} \quad (1.2)$$

The heat removed by circulating metal is transferred to an intermediate (sodium to sodium) exchanger, and from there to a secondary (sodium to water) exchanger, or steam generator. Figure 1.1. shows the main features of this system.

The physical properties of sodium make this metal an ideal choice as coolant in these reactors.[5] The important physical properties are listed in Table 1.1., in comparison with other possible reactor coolants. One drawback in this context is that the alkali-metal in the primary circuit acquires intense radioactivity from the core.[6]

The chemical properties of the alkali-metals, however, lead to difficulties and potential dangers in their use as L.M.F.B.R. coolants. The chemistry is dominated by the loss of a single electron from the outer shell, and the ease with which this occurs determines the relative reactivity of the Group I elements. The molar ionisation

KEY TO FIGURE 1.1.

A. Primary sodium pump.

B. Core instrumentation and control rods assembly.

C. Fuel handling machines.

D. Intermediate heat exchanger.

E. Sodium-hydrogen separator.

F. Contaminated sodium dump tank.

G. To vent stæck.

H. Secondary sodium pump.

I. Steam generator (Secondary heat exchanger).

J. Stainless steel primary vessel.

K. Water in.

L. Steam out.

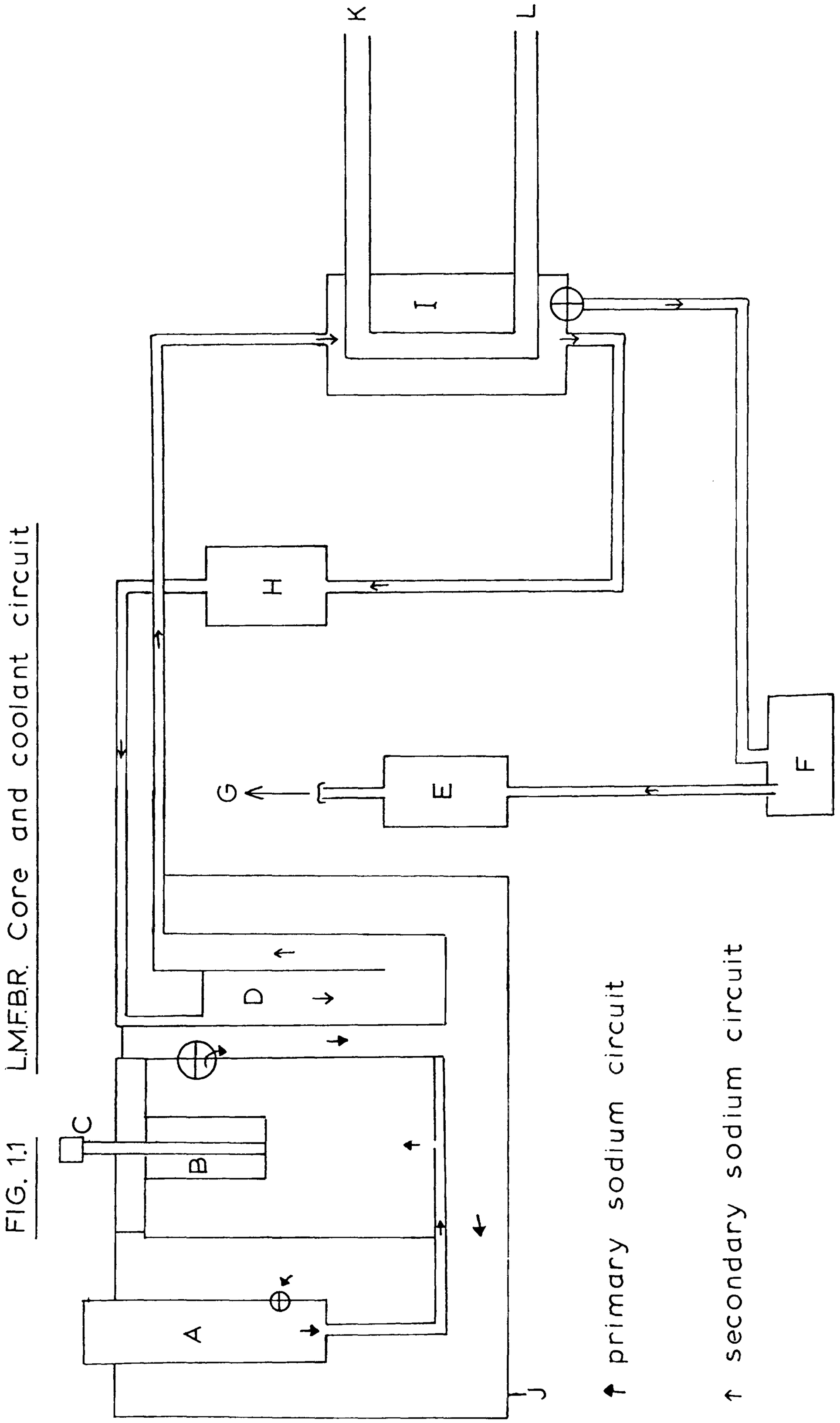
L.M.F.B.R. Core and coolant circuit
FIG. 1.1
A
B
C
D
E
F
G
H
I
J
primary sodium circuit
secondary sodium circuit

TABLE 1.1.

PHYSICAL PROPERTIES OF REACTOR COOLANTS

	Sodium	Water	Carbon Dioxide
Cross section for thermal neutron capture (millibarns)	400	0·33(H) 0·18(O)	3·4(C) 0·18(O)
Thermal conductivity at 100°C ($W.m^{-1}\ K^{-1}$)	88(l)	0·66(l) 0·0239(g)	0·0174(g)
Liquid range (°C)	97.8 -882.9	0.0 -100.0	[-78.5 (sub)]
Density (g/cm^3) at 298 K	0.97	1.00	-

energies for the reaction 1.3 are the lowest of all the

$$M \longrightarrow M^{+} + e \qquad (1.3)$$

elements and range from 520 KJ/mole (lithium) to 380 KJ/mole (caesium). The second ionisation energies i.e. for reaction 1.4 , are considerably higher, and range

$$M^{+} \longrightarrow M^{2+} + e \qquad (1.4)$$

from 7300 KJ/mole (lithium) to 2400 KJ/mole (caesium).[7] The metals, therefore, exhibit only the +1 oxidation state in their compounds. The most familiar reaction of the alkali-metals is, perhaps, the reaction with water (Equation 1.5), and this has a special relevance to the L.M.F.B.R.

$$M + H_2O \longrightarrow M\,O\,H + \tfrac{1}{2}H_2 \qquad (1.5)$$

coolant circuit.

There is a possibility of chemical reaction in the secondary heat exchanger due to a leak in the stainless steel dividing wall.[8] The partition is only 2.3mm thick, in order to give good heat conduction between the liquid sodium (350 - 520°C, 350 - 1000 KPa) and water (260 -480°C, up to 17,000 KPa).[9] It can be seen from the pressures of the two liquids that in the event of a leak, water will be forced into the liquid sodium side of the partition. Under these conditions, a non-explosive reaction results, since the reaction products dissolve smoothly in the liquid metal (Equations 1.6, 1.7 and 1.8). Also, there is no local heat build-up, the heat generated being conducted away in the liquid sodium. This is the expected reaction sequence

Primary reaction:

$$Na_{(excess,l)} + H_2O_{(l,g)} \longrightarrow Na_2O_{(s)} + H_{2(g)}\ ^{10} \qquad (1.6)$$

Secondary reactions:

$$Na_{(l)} + \tfrac{1}{2}H_{2(g)} \longrightarrow NaH_{(s)}\ ^{11} \qquad (1.7)$$

$$2Na_{(l)} + NaOH_{(s)} \longrightarrow Na_2O_{(s)} + NaH_{(s)}\ ^{12} \qquad (1.8)$$

when the sodium is in excess and when the temperature in the system is above the melting point of sodium hydroxide (318 C).

The main problem arising from such a leak is the enhanced corrosive nature of liquid sodium when it contains small quantities of the reaction products Na_2O [13], NaH [14], and NaOH [15]. Another problem is the temperature rise due to the reaction. Temperature rises of up to 1175 °C have been reported for sodium-water reactions, the theoretical temperature rises, for metal initially at 477 °C , being 1588 °C, (constant pressure) and 1682 °C (constant volume).[16]

This flow of high pressure fluid ($H_2O_{(l)}$ / $H_2O_{(g)}$) into relatively low pressure liquid ($Na_{(l)}$) is the major process occurring, but it is not the only one. Some metal, in fact, is found on the water side of the steam generator. One of the methods of detecting leaks depends upon this fact. It is possible then, that the minor process (Equation 1.9) occurs, the reaction shown being the same at all temperatures.

$$Na_{(l)} + H_2O_{(excess)} \longrightarrow NaOH + \tfrac{1}{2}H_2 \qquad (1.9)$$

All the products of this reaction do not dissolve smoothly in the medium, in this case, water. A large volume of hydrogen gas is produced. This may be dangerous for two reasons:-

(i) increased gas pressure in the exchanger, [17]

and (ii) the formation of an explosive (>4% O_2) H_2/O_2 mixture. [18]

It is important, then, to understand the chemistry of sodium/water reactions at a leak site in order to facilitate rapid leak detection. Current methods of detecting leaks are: [19]

(i)	detection of NaH in $Na_{(l)}$	"sodium side"
(ii)	detection of H_2 in gas space above Na	
(iii)	pressure rise in gas space a above Na	
(iv)	temperature rise in Na	
(v)	pH of boiler water	"water side"
(vi)	detection of Na^+ in boiler water by flame photometry	

A knowledge of the chemistry may enable improvement of these methods to be made, and indicate which method is best under certain circumstances.

From a fundamental chemical point of view, the reaction between the alkali-metals and water also commands considerable interest. The reaction has been examined under a wide variety of conditions. Generally, the reaction rates and reaction products depend primarily on the physical states of the reactants. Using solid metal, experiments have been carried out on the system $Na_{(s)} + H_2O_{(g)}$ using sodium 'mirrors' deposited from the vapour. With liquid metal, the reaction between $Na_{(l)}$ and $H_2O_{(g)}$ has been followed whilst the metal was agitated by electromagnetic pumps. The reaction $Na_{(s)} + H_2O_{(l)}$ has also been examined, with a view to determining the most likely intermediate species in the reaction. A range of values for the activation energy ($E^{\neq}$)

and rate of reaction at various temperatures have been reported, depending on the physical states of the reactants, whether or not the reaction products remain as a physical barrier between the reactants, and in the case of $H_2O_{(g)}$ experiments, whether static or flowing gas systems are used.

The reaction between $Na_{(l)}$ and $H_2O_{(l)}$ using a liquid alkali-metal jet beneath the surface of water promised to be useful for several reasons:-

(i) the physical processes occurring could be followed using optical methods (photography etc) if glass apparatus were used.

(ii) with a 'high speed' jet, the H_2O/Na contact time i.e. the time elapsing before separation of the reactants by product layers, would increase, thus facilitating more accurate timing of the reaction.

(iii) solid, water soluble products may be removed into excess water.

(iv) several products have been observed during sodium-water reactions (NaOH, H_2, NaH, Na_2O, Na_2O_2) depending upon reaction conditions. The correct observation and determination of these products in the reaction $Na_{(l)} + H_2O_{(l)}$ would add considerably to existing knowledge of alkali-metal chemistry.

SCOPE OF THE WORK

Simulation of a leak in the stainless steel partition dividing liquid sodium from water in the secondary heat exchanger is not a practical possibility on a laboratory scale. However, if the two processes occurring during such a leak (sodium + water $_{(excess)}$ - minor process and sodium $_{(excess)}$ + water - major process) can be separated, and studied independently, useful information may be forthcoming.

This work was an attempt to simulate the minor process and to provide information on the rates of reaction, reaction stoichiometry and reaction mechanism to help rationalisation of the minor process.

There are important differences, however, between such a laboratory simulation and a real leak. Firstly, water in the heat exchanger itself is either in the form of steam, or is highly pressurised at high temperatures. Secondly these simulations were carried out using glass apparatus. This ignores the problems of leak enlargement due to corrosion of the stainless steel by sodium hydroxide, which is a reaction product in both the major and minor processes.

By simplifying the processes occurring thus, a picture of the basic reactions could perhaps be built up.

C H A P T E R II

REVIEW OF PREVIOUS WORK

2.1 INTRODUCTION

This chapter reviews the two distinct systems:-

$$M + H_2O_{(vapour)} \longrightarrow \text{products}$$

$$M + H_2O_{(liquid)} \longrightarrow \text{products}$$

(M = Li, Na, K)

Rubidium and caesium will feature to a smaller extent since, firstly, only the first three Group I metals have been proposed for coolant materials in nuclear reactors. Lithium may have applications as a fuel and coolant in fusion reactors; [20] sodium, and to a lesser extent, potassium (as sodium-potassium alloy) have already been used as L.M.F.B.R. coolants. Secondly, it is well established that the reactivity of the alkali-metals increases down the group, and the number of papers published on the reactions of any given metal seems to have an inverse relationship with the reactivity of that metal.

Although this thesis deals primarily with experiments involving liquid water, it is not desirable to exclude the reactions of water vapour in the review. Thus in the familiar sodium/water experiment where sodium is cut into small pieces and placed on the surface of a pool of water, there is a rapid initial reaction (Equation 2.1)

$$Na_{(s)} + H_2O_{(l)} \longrightarrow NaOH_{(s)} + \tfrac{1}{2}H_{2(g)} \qquad (2.1)$$

but then sodium is seen to skid along the surface of the water, separated from it by a 'trapped bubble' of hydrogen gas. This gas space, however, also contains water vapour, from the vapourisation of the bulk water. At this stage, the much slower reaction (Equation 2.2) predominates.

$$Na_{(s,l)} + H_2O_{(g)} \longrightarrow NaOH_{(s)} + \tfrac{1}{2}H_{2(g)} \qquad (2.2)$$

The subscript (s,l) indicates that sodium fuses in contact with water. Reaction 2.1 may also continue during this stage, but the gaseous molecules much reduce the contact time between the two reactants.

2.2 $M + H_2O_{(g)}$

Due, perhaps, to the relatively low chemical reactivity of lithium as compared with the other alkali-metals, and hence the relative ease with which reaction rates can be measured, the system $Li_{(s)} + H_2O_{(g)}$ is the most researched, and hence the best understood of all the alkali-metal/water vapour reactions.

In air, the rate of oxidation of lithium is known to increase with increasing humidity.[21] At 50-70% humidity clean lithium darkens (LiOH can be black, due perhaps to excess metal, forming a non-stoichiometric compound) at 10-30 times the rate in a 1% humid atmosphere. This is attributed to the breakdown of the highly protective lithium oxide film by water vapour (Equation 2.3)

$$Li_2O_{(s)} + H_2O_{(g)} \longrightarrow 2LiOH_{(s)} \qquad (2.3)$$

Lithium nitride, Li_3N, may also be formed if there is moisture in the air,[22] and this may be correlated with the formation of LiOH, since this acts as a catalyst for nitride formation.[23] The rate of oxidation in these mixed (H_2O/O_2) atmospheres increases, as expected, with increasing temperature up to 35°C.

Several authors have investigated the system $Li_{(s)} + H_2O_{(g)}$ using water vapour or water vapour/inert gas mixtures, but excluding oxygen from the system. Deal and Svec[24] observed pressure changes in the system using rods of lithium. With pressures between 2.93 and 13.3 KPa they observed a logarithmic rate law, consistent with gas/solid reactions where protective film formation occurs. The rates measured at temperatures between 45 and 75°C gave an activation energy of between 23 and 26 KJ/mole. At pressures below 7.32KPa they found that the rate was independent of pressure. They also stated that the activation energy for the reaction decreased at these higher pressures.

Using partial pressures of water vapour of 1.68 KPa diluted in argon, at temperatures between 20 and 45°C, Irving and Lund [25] recognised three reaction stages:-

(i) linear rate, pressure dependent (pressure < 0.612KPa)

(ii) logarithmic rate law, pressure independent (0.612 - 1.68 KPa).

(iii) linear rate, pressure dependent (> 0.612KPa).

Besson and Pelloux [26] carried out the same reaction in the range of conditions 35 - 80°C, and 0.4KPa - 14.67KPa. They agreed with the above findings, but stated that stage (iii), reported above, only occurs when the pressure of water vapour is higher than the dissociation pressure of lithium hydroxide monohydrate, $LiOH.H_2O$. The process

when the pressure was higher than this value had an activation energy of 58.6 KJ/mole. Below this pressure, the activation energy was 41.2 KJ/mole.

The above findings can be explained in terms of three reaction stages:-

(i) uniform coverage of the lithium surface by hydroxide giving a linear, pressure dependent rate law (Equation 2.4)

$$Li_{(s)} + H_2O_{(g)} \longrightarrow LiOH_{(s)} + \tfrac{1}{2}H_{2(g)} \qquad (2.4)$$

(ii) growth of a protective hydroxide film, accompanied by nucleation and growth of lithium hydroxide monohydrate at the outer surfaces of the film, leading to a pressure independent logarithmic rate law (Equation 2.5)

$$LiOH_{(s)} + H_2O_{(g)} \longrightarrow LiOH.H_2O_{(s)} \qquad (2.5)$$

(iii) diffusion of water to the metal surface through the porous hydrate, giving a pressure dependent linear rate law.

These stages are shown in Figures 2.1 and 2.2.

The system $Na_{(s,l)} + H_2O_{(g)}$ is not so well understood. Again, water is known to catalyse the oxidation of sodium in the mixed oxidising atmosphere $H_2O_{(g)}/O_2$, the rate increasing with increasing humidity [7] due to the preliminary step shown by Equation 2.6.

FIG. 2.1 Stages in the reaction $Li + H_2O_{(g)}$ –

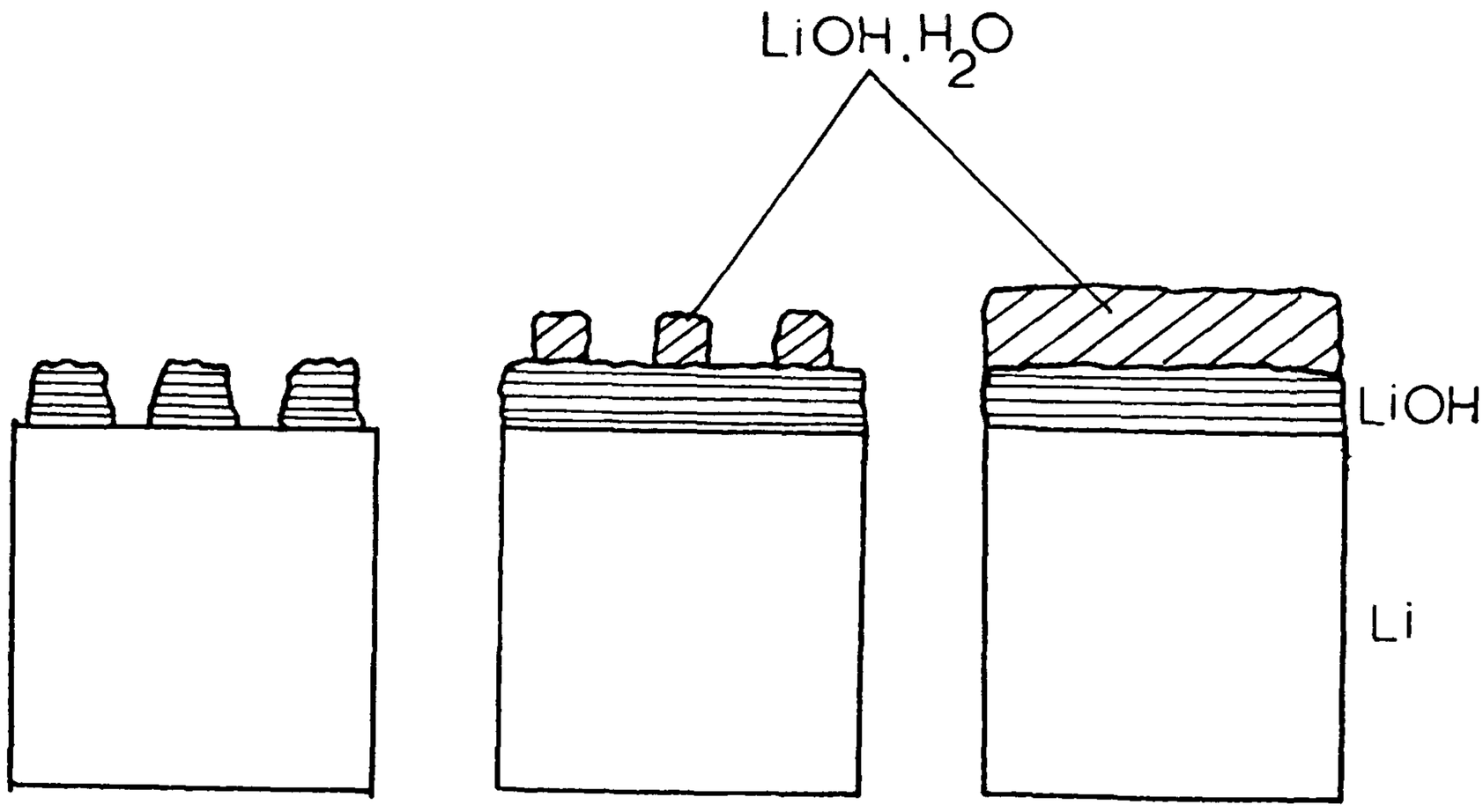

FIG. 2.2 Rate curves for $Li + H_2O_{(g)}$ –

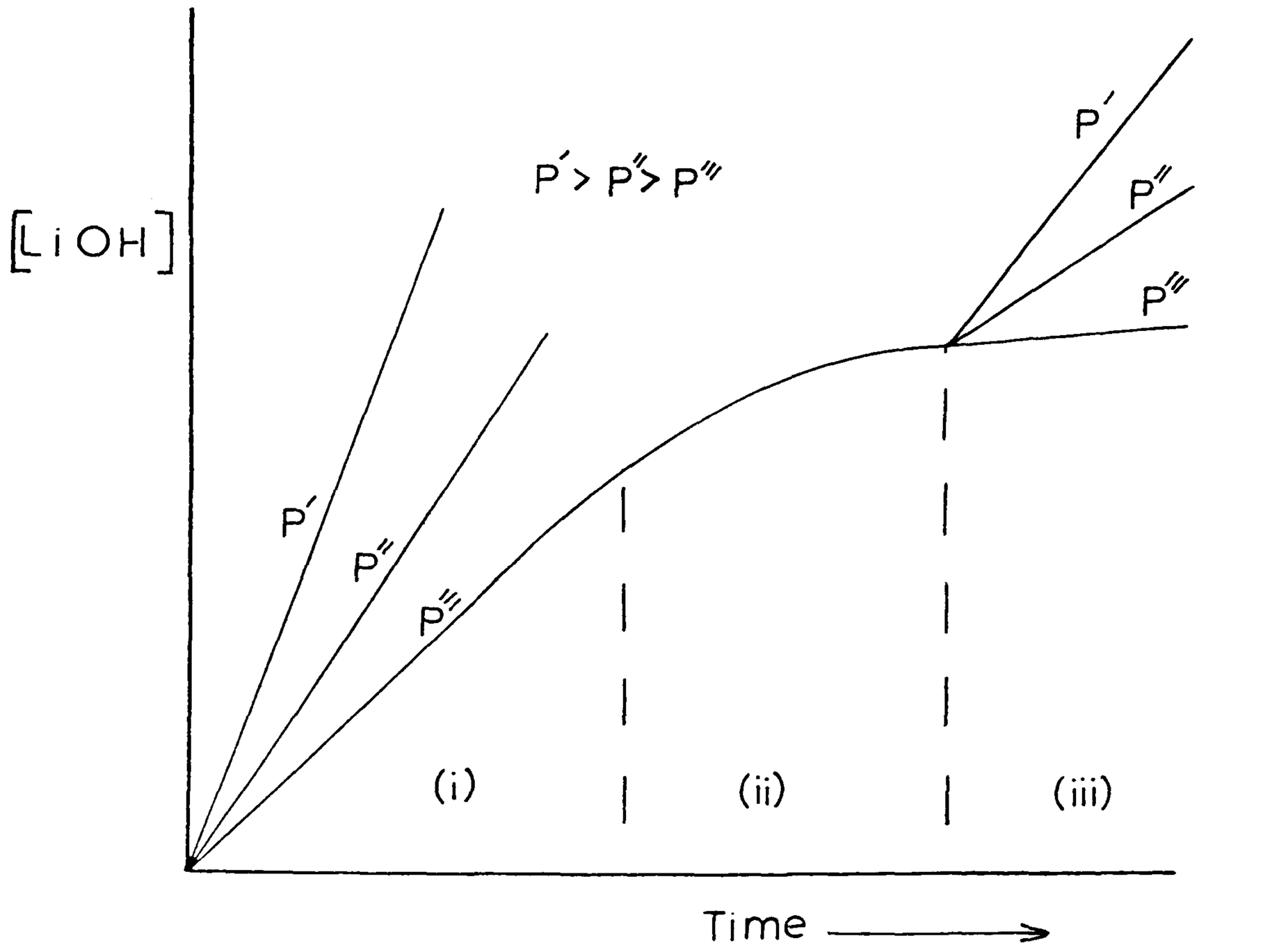

$$M + H_2O \longrightarrow M^+ + OH^- + \tfrac{1}{2}H_2 \qquad (2.6)$$

In water vapour/inert gas mixtures at least two reaction stages have been reported. Cornec and Sannier[28] observed a parabolic, leading to a linear rate law using vapour pressures of 2.67 KPa. The slope of the graph log.K against 1/T was linear up to the melting point of sodium, giving an activation energy of 20.9 KJ/mole. The conclusion from this work was that the rate of reaction was controlled by the migration of Na^+ ions through the hydroxide, since hydrated sodium hydroxide, $NaOH.H_2O$ was considered too porous to provide an effective barrier to further reaction. Besson and Pellaux[29], using pressures in the range 0.33 - 4.0 KPa and temperatures of 40 - 240°C, also claimed an initial parabolic rate law at temperatures below 179°C during the formation of NaOH, with a linear second stage observed for both $Na_{(s)} \geqslant 94°C$ and $Na_{(l)} \geqslant 130°C$. A third stage, intermediate between linear and parabolic complicated the system even further during the formation of hydrated sodium hydroxide.

The reaction may also be complicated by the formation, under certain conditions, of reaction products other than sodium hydroxide, its monohydrate, and hydrogen. Pulham and Simm [30] used water vapour in the pressure range 7.32 - 8.65 KPa in the reaction with liquid sodium at 300 - 450°C. Two reactions (Equations 2.7 and 2.8)occurred,

$$2Na + H_2O \longrightarrow NaOH + NaH \qquad (2.7)$$

$$2Na + NaOH \longrightarrow Na_2O + NaH \qquad (2.8)$$

2.8 tending to dominate at low water vapour pressures i.e.

when the sodium could be considered to be in excess.

McKnight and Brockway [31] provided confirmation of the above results by analysing the products using reflected X-ray diffraction techniques. The products were identified as sodium oxide and sodium hydroxide. The unfamiliar oxide product appears when the temperature of the reaction is at or above the melting point of sodium hydroxide (318.4°C) Above this temperature, reaction 2.8 occurs if the sodium is in excess. At higher temperatures, trace amounts of sodium peroxide have been detected by Wollen et al [32] according to reaction 2.9. Again, the sodium is in excess.

$$2Na + 2H_2O \xrightarrow{450^\circ C} Na_2O_2 + 2H_2 \qquad (2.9)$$

Addison and Manning[33], in addition to observing the previously described rate laws i.e. rapid initial coverage followed by a parabolic rate law followed by a linear rate law, also detected sodium hydride in the reaction between $H_2O_{(g)}$ and both $Na_{(s)}$ and $Na_{(l)}$. The hydride was formed under conditions of:

(i) high pressure (> dissociation pressure of NaH)

and (ii) low temperature (NaH is unstable above 250°C with low hydrogen pressures.

The overall process is described by Equation 2.10, where

$$Na + NaOH \xrightarrow{300^\circ C} \begin{cases} P > P_d \rightarrow Na_2O + NaH & (2.10a) \\ P < P_d \rightarrow Na_2O + H_2 & (2.10b) \end{cases}$$

P_d is the dissociation pressure of sodium hydride.

Very little data is available on the reaction $K + H_2O_{(g)}$ Experiments have been carried out by Saltsburg [34,35] using flow methods in the reaction between water vapour and sodium-potassium alloy. Due to complications in the measuring techniques no rate data were forthcoming from this work.

2.3. $M + H_2O_{(l)}$

The previous section has shown that the most important factor dominating the chemistry of the alkali-metals in their reaction with water vapour is the nature of the solid product protective film. In the case of lithium, this may extend to the reaction with liquid water, and the relative insolubility of lithium hydroxide may be the reason in part for the slower rate of reaction of this metal with water, when compared to the rest of the Group I elements.

The products NaOH, NaH, and Na_2O are all very soluble in liquid water, however, so that other factors become more important for the reaction $Na_{(s\ or\ l)} + H_2O_{(l)}$.

When a small piece of sodium is placed on the surface of a pool of water, the reaction can be explained in terms of Equations 2.11, 2.12, and 2.13 [36], 2.13 being an explosive

$$Na_{(s,l)} + H_2O_{(l,g)} \longrightarrow Na^+_{(aq)} + OH^-_{(aq)} + \tfrac{1}{2}H_{2(g)} \qquad (2.11)$$

$$2Na_{(s,l)} + \tfrac{1}{2}O_{2(g)} \longrightarrow Na_2O_{(s)} \qquad (2.12)$$

$$H_{2(g)} + \tfrac{1}{2}O_{2(g)} \longrightarrow H_2O_{(g)} \qquad (2.13)$$

chain reaction.[37] Results are different when oxygen is

excluded. Dumm and co-workers[38] broke sodium-filled tubes beneath the surface of liquid water. They concluded that hydrogen was produced between regions of sodium and water after the very rapid initial reaction (Equation 2.1.) This was followed by reaction 2.2 since the sodium fused in contact with water.

I. Iitaka [39] carried out the reaction between solid cubes of lithium, sodium and potassium, and water/acid solutions. He concluded that the metals reacted not only with the water molecules, but also with hydrogen ions (Equations 2.14, 2.15 and 2.16) even at very low hydrogen ion concentrations.

$$2H^+ + 2M \longrightarrow H_2 + 2M^+ \qquad (2.14)$$

$$2H_2O + 2M \longrightarrow H_2 + 2M^+ + 2OH^- \qquad (2.15)$$

$$H_2O \rightleftharpoons H^+ + OH^- \qquad (2.16)$$

M.M. Markowitz [36] decided that certain physical effects determined the rate of reaction, and could be used to explain the relative reaction rates of the alkali-metals. These effects are:-

(i) The number of metal atams exposed to the water. Table 2.1 shows that this number does in fact rise from lithium to sodium. The variation down the rest of the group, however, does not tally with the observed reaction rates, which are known to increase down the group.

(ii) The melting points of the metals. With all the metals except lithium, the maximum water

TABLE 2.1

PROPERTIES OF THE ALKALI-METALS HAVING AN EFFECT ON THEIR RATE OF REACTION WITH WATER

(a) $-\Delta H$ (KJ/mole) for $M_{(s)} + H_2O_{(l)} \longrightarrow MOH_{(aq)} + \frac{1}{2}H_{2(g)}$ [36]

Li	Na	K	Rb	Cs
508	469	481	475	478

(b) No. of atoms($\times 10^{14}$) exposed on immersion of a 1mm cube.[26]

Li	Na	K	Rb	Cs
26.1	36.1	18.2	18.5	15.7

(c) Solubility of metal hydroxides in water (mole%)[7]

Li	Na	K	Rb	Cs
$53.6^{(20)}$	$105.0^{(0)}$	$190.7^{(15)}$	$175.6^{(15)}$	$263.8^{(15)}$

(d) Melting points of the metals (°C).[7]

Li	Na	K	Rb	Cs
180.5	97.8	63.7	38.9	28.6

temperature (100°C) is sufficient for fusion. The molten metals fragment after a short time in contact with water, substantially increasing the number of metal atoms in contact. With lithium, the water behaves as a heat sink, and the temperature never rises high enough (180.5°C) to fuse the metal.

(iii) The solubility of the solid product. Note (Table 2.1.) that LiOH is relatively insoluble compared with the other alkali-metal hydroxides.

Energetic factors seem to be not so important in determining reaction rates. Although lithium reacts slowest, Table 2.1. shows that it has the highest heat of hydrolysis. However, it is the rate of energy evolution, and not the total, which indicates the relative reaction rate.

Reaction products can have a marked effect on the rate of reaction. Halstead[40] has carried out an experiment which illustrated clearly the influence of the gaseous product, hydrogen. After a rapid initial reaction on dropping liquid water into liquid sodium, the rate slowed due to the intervention of gaseous hydrogen. This is shown in Figure 2.3. The hydrogen separated the reactants. A secondary barrier of condensed phase reaction products separated the hydrogen/water vapour mixture in the gas space from sodium. A mathematical model has been set up to describe the above system.[41]

A drop of liquid sodium in water can be assumed to produce an equivalent system, but in reverse. This is shown in Figure 2.4. Again, the sequence is water - hydrogen - metal, but with the metal at the centre. The essential difference between the two systems, however, is that with excess water, the hydroxide can dissolve away in the water when the metal contacts the gas bubble walls. This is not possible in the first system, the

FIG. 2.3 A drop of liquid water in hot sodium

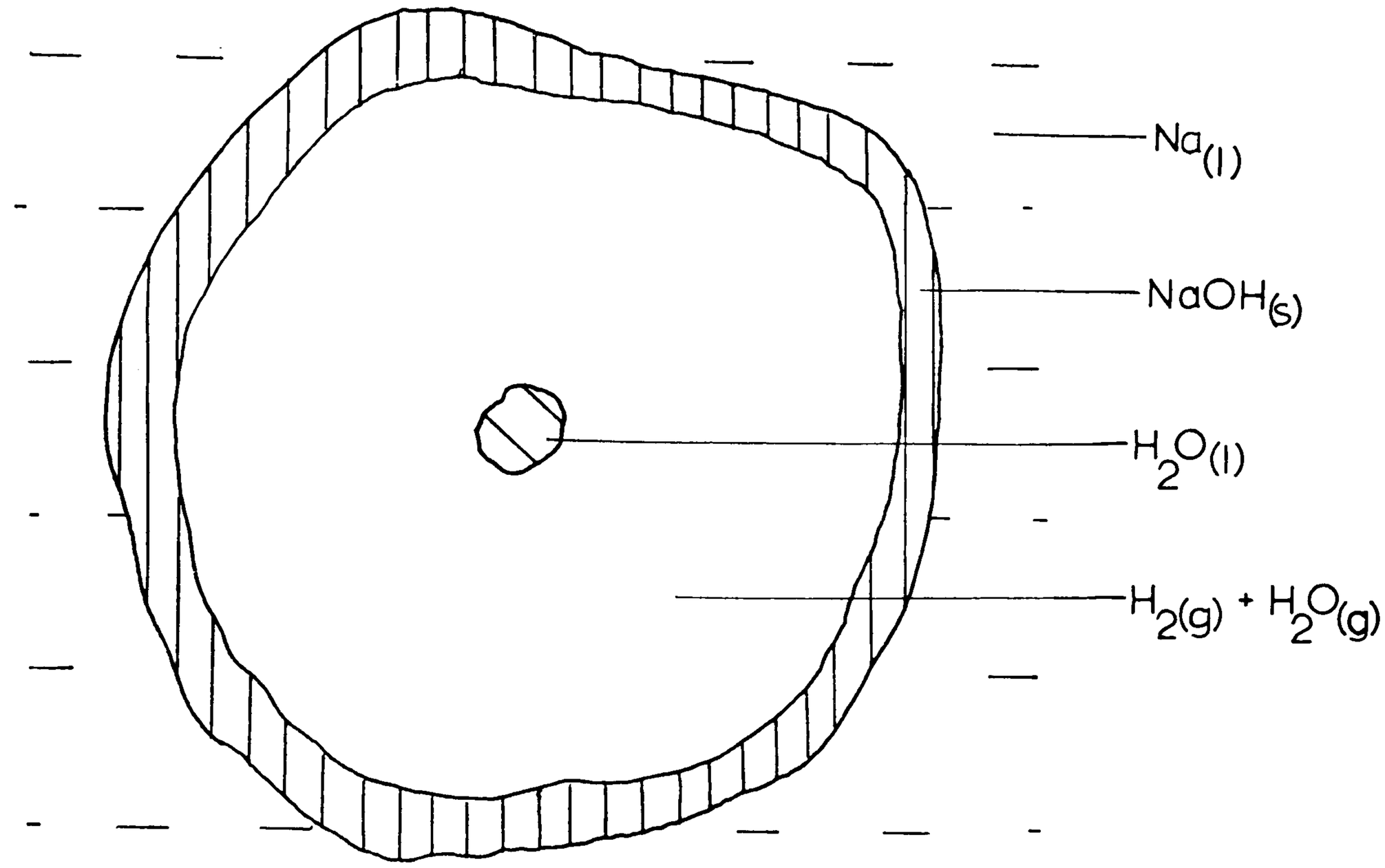

FIG. 2.4 A drop of liquid sodium in water

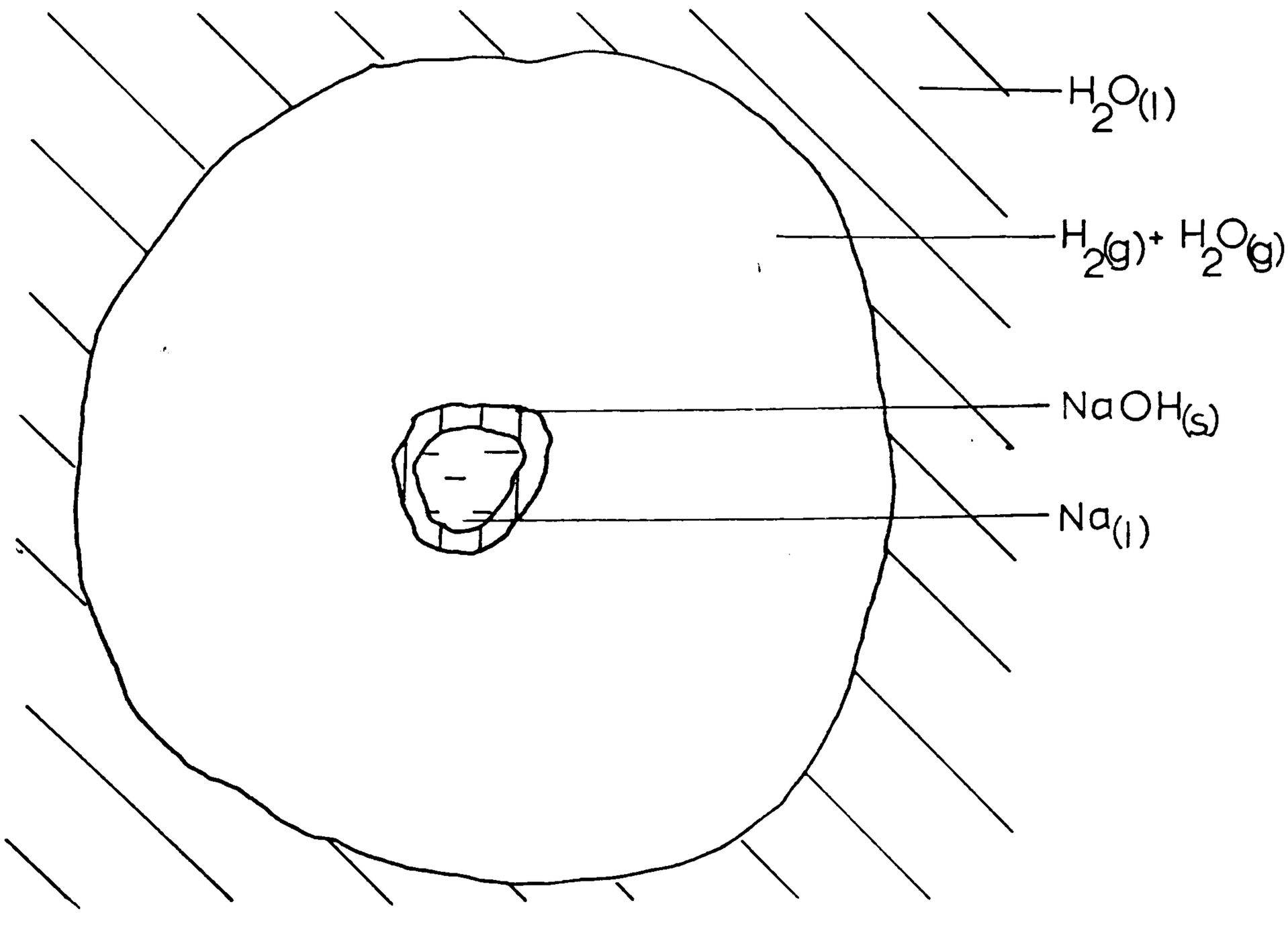

solubility of sodium hydroxide in liquid sodium being as low as 0.0038% at 100°C.[42]

2.4. M + H_2O IN F.B.R. DEVELOPMENT

In two reviews, by J.L. Henry [9] and J.A. Ford [19], the sodium/water reaction is considered with particular reference to the sodium-water steam generator. The temperatures and pressures used in such a generator, and therefore in experiments carried out to test the effects of a leak, set this work apart from the smaller scale laboratory experiments. Because of the wide range of conditions, all the reactions listed in Table 2.2. may occur.

Ford states that below 318.4°C (the melting point of NaOH) the ratio of reactants is not important, and reactions (1) and (2) are likely to dominate. Above this temperature, with excess sodium, (6) is the most likely reaction, followed by the secondary reactions (4) and (7). Na_2O_2 has been found in small quantities (< 0.1% of the total products) after sodium steam reactions, indicating the small extent of reaction 2.9 in these systems.[32]

The measured rate of each of the reactions listed depends primarily upon the surface areas of the reactants in contact.[43] For thin films of metal, the reaction is believed to be complete in less than one millisecond, so the measured rates for metal in bulk seem to be a function of the mixing of the reactants.[44]

TABLE 2.2

POSSIBLE REACTIONS DURING A STEAM-GENERATOR LEAK

(1) $Na_{(l)} + H_2O_{(l)} \longrightarrow NaOH_{(s)} + \frac{1}{2}H_{2(g)}$

(2) $Na_{(l)} + H_2O_{(g)} \longrightarrow NaOH_{(s)} + \frac{1}{2}H_{2(g)}$

(3) $2Na_{(l)} + H_2O_{(g)} \longrightarrow NaOH_{(s)} + NaH_{(s)}$

(4) $Na_{(l)} + \frac{1}{2}H_{2(g)} \longrightarrow NaH_{(s)}$

(5) $Na_{(l)} + NaOH_{(l)} \longrightarrow Na_2O_{(s)} + \frac{1}{2}H_{2(g)}$

(6) $2Na_{(l)} + H_2O_{(l)} \longrightarrow Na_2O_{(s)} + \frac{1}{2}H_{2(g)}$

(7) $2Na_{(l)} + NaOH_{(l)} \longrightarrow Na_2O_{(s)} + NaH_{(s)}$

A decrease in mixing can occur from:-

(i) vapourisation of water

(ii) the formation of a product film (gaseous or solid)

(iii) restriction of surface areas in contact

Increases occur due to:-

(i) the melting of NaO_H at 318.4°C.

(ii) dissolution or reaction of the products.

The reaction between sodium and water is highly exothermic,[45,46] and local temperature rises of up to 1093°C have been noted in leak simulations. Subsequent reactions, however, are by no means so violent e.g reaction (4). This reaction is of particular interest to workers in this field, since leak detection methods depend upon detection of hydrogen either as gas above the circulating metal or as H in NaH. In both cases, hydrogen is drawn through a hot nickel thimble and thence to a detector. Due presumably to reaction (4) the hydrogen pressure surges resulting from reactions (1) and (2) are less than 30% of those expected. The metal absorbs the hydrogen giving stable solutions.[14] Moreover, the gas pressure in the space above the metal appears to suppress the dissociation of sodium hydride.[11, 47] As the temperature rises, however, both solid NaH and its solutions in sodium progressively evolve hydrogen. Thus Wollen[32] has detected NaH in the products of the sodium/water reaction between 280–450°C, but not at 500°C.

All these observations are the result of the pressure–composition relationship which exists between hydrogen, hydride, and its solution in liquid sodium.[48] This relationship is depicted in Figure 2.5.

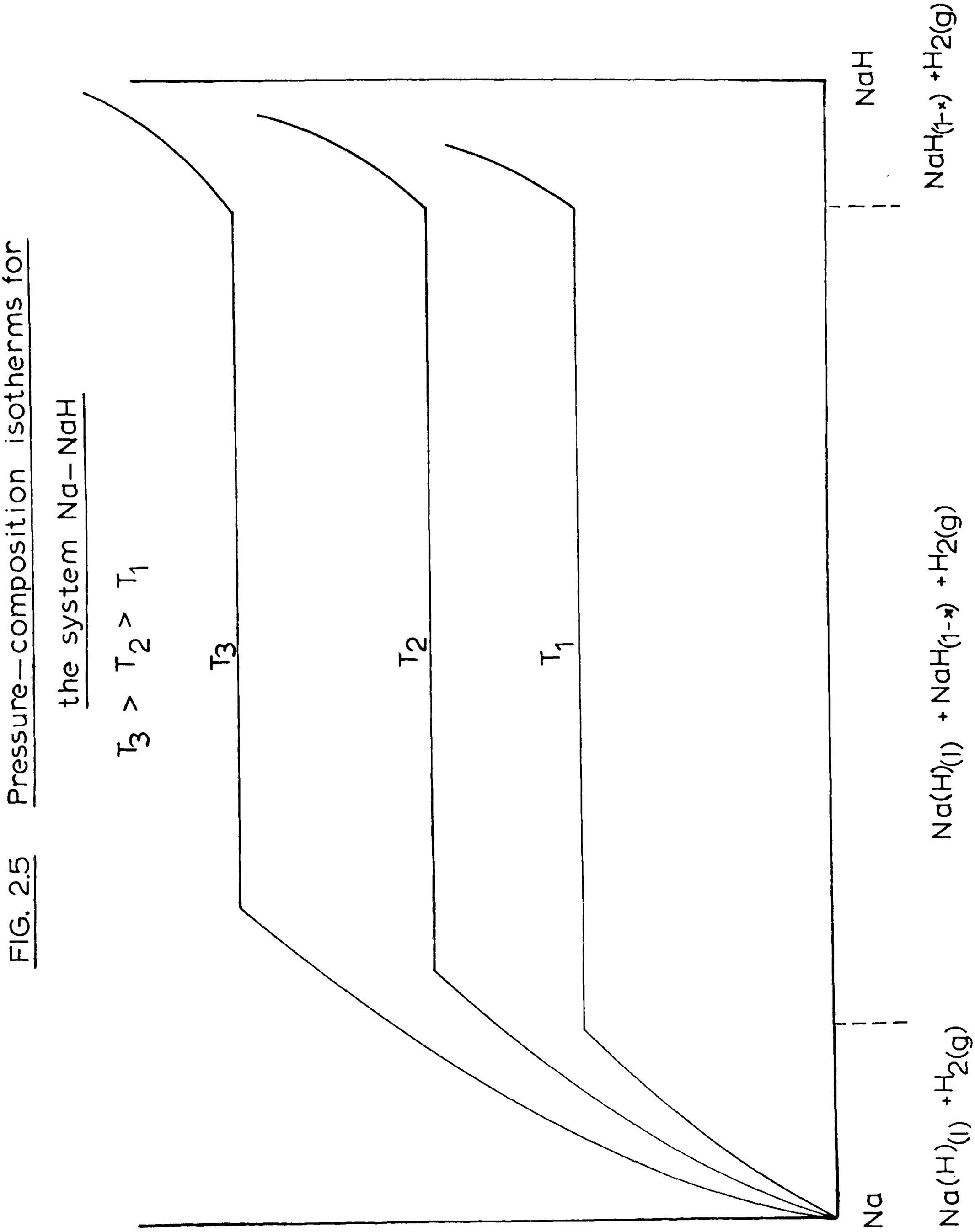

FIG. 2.5 Pressure—composition isotherms for the system Na—NaH

$T_3 > T_2 > T_1$

2.5. BACKGROUND TO PRESENT WORK

The scene was set for the present work by Dowling.[49] Initially, he established a dynamic system for investigating the reaction of water vapour as it was drawn past a moving column of liquid alkali-metal. Using water vapour pressures of ca. 10KPa at room temperature he attributed an activation energy of 38.8 KJ/mole to the reaction $NaK_{(l)} + H_2O_{(g)}$. The system was modified in that the column of metal was now run into liquid water, and this necessitated a completely re-designed apparatus. Sodium-potassium alloy of eutectic composition was injected into a reservoir of water through a narrow (0.1 - 0.4 mm diameter) capillary under pressure. In a series of experiments in which unreacted metal was 'trapped out' after certain distances of travel, he determined that the reaction was controllable and that less than 15% of the metal injected reacted instantly at 25°C. The rest of the metal broke up from the thread into individual globules which moved vertically through the water, each of them encapsulated in a protective bubble of hydrogen gas. He determined a reaction rate, in terms of water consumption, of 0.028 moles/s/cm^2 at 25°C, and an activation energy of 36.6 KJ/mole. Comparing the activation energies for $NaK_{(l)} + H_2O_{(g)}$ (38.8 KJ/mole) and $NaK_{(l)} + H_2O_{(l)}$ (36.6 KJ/mole) he concluded that the rate determining step was common to both systems.

The present work incorporates many of the essential features of the apparatus and methods employed by Dowling, and, in some respects, his work provided a platform on which to build up a picture of more precise rates, of the effect of alloy composition and temperature, and also of additives to the water. Some concepts of the reaction have been modified and considerably extended by the use of continuous and more sophisticated high speed photography.

CHAPTER III

EXPERIMENTAL ASPECTS

3.1. INTRODUCTION

Dowling [49] demonstrated that it was possible to produce a jet of liquid metal in water, by forcing liquid sodium-potassium alloy at high pressures through a narrow orifice beneath the surface of a vessel of water, and observe the reaction taking place. The apparatus described in this chapter was designed for the purpose of carrying out experiments which would give more detailed information about the reaction, in particular, the rates of reaction.

The original reason for producing threads of NaK under water was to determine reaction rates by direct measurement of the length of the jet. Knowing the flow rate of the metal (moles/second), measurement of the length would lead to values for the rate of reaction (moles/second/unit area of metal surface). However, since the preliminary experiments of Dowling showed that not all of the metal reacted on contact with water, but that metal could be transferred away from the site of injection, it was necessary to design a type of flow reactor vessel.

In this design, unreacted metal is 'trapped out' of the system after various times. Then, knowing the extent of reaction at various times, the rate of reaction can be calculated. In practice, it is not possible to vary the time of reaction directly, but by variation of the distance through which the metal has to travel, it is possible to vary the time factor indirectly.

3.2 THE SODIUM-POTASSIUM ALLOY

Most of the investigations described in this thesis employed an alloy of sodium and potassium, liquid at room temperature. Although dilution of sodium by potassium creates a more chemically reactive alloy, which is therefore potentially more hazardous and difficult to handle than sodium, the alloy had the advantage that neither it, nor the injection apparatus, had to be heated during an experiment. Some experiments (Chapter 6) did in fact use pure, un-alloyed sodium metal at higher temperatures, but the apparatus described in this chapter was designed primarily for the reactions of the alloy.

Sodium-potassium alloy has a large liquid range at room temperature. The phase diagram is shown in Figure 3.1. At 20°C, the alloy is liquid from 35-83 mole % K. The eutectic composition contains 77.8 wt. % K, and has a density of 0.867 g/cm^3 at 20°C, and a melting point of -12.6°C[50].

NaK alloy was manufactured from weighed quantities of clean sodium (BDH, > 99.8%) and potassium (Koch-Light, 99%) placed in a 500 cm^3 round bottom flask, and shaken till completely liquid under an argon atomosphere. Impurities (oxide and hydroxide) and undissolved metal were removed by filtration of the liquid under pressure through a glass wool plug into an argon filled flask. The filtration apparatus is shown in Figure 3.2.

The precise alloy composition was determined by removing a sample from the stock flask with a hyperdermic syringe and needle, and leaving this to hydrolyse on a clock glass. After a period of one week, the metal had reacted completely, and could be washed off the glass into a standard flask, and analysed for sodium and potassium content using atomic emission techniques.

The composition of the alloy when prepared in this way was not precisely constant. Similar compositions were chosen for each of the experiments described in Chapter 5 (Rates of

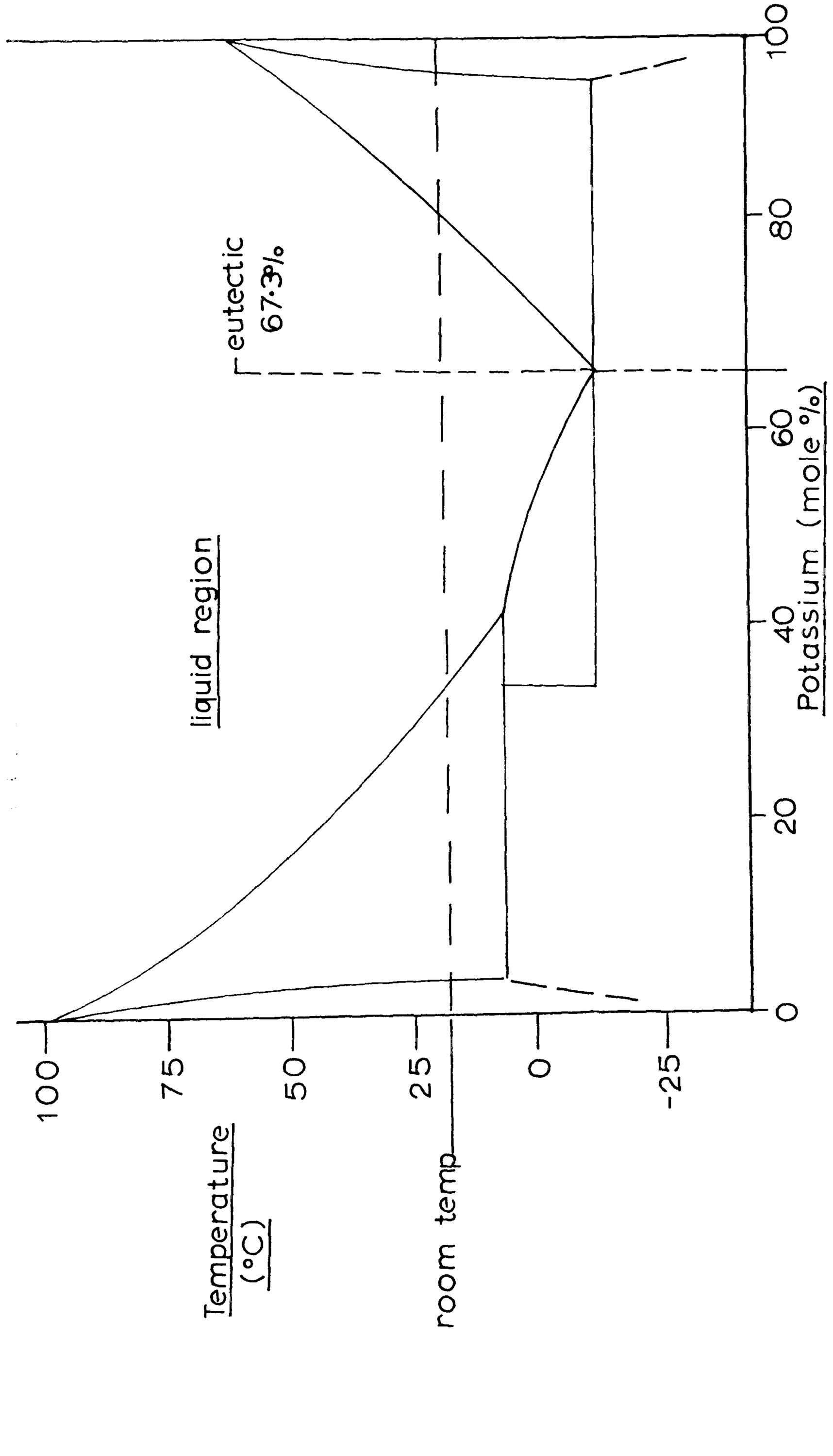

FIG. 3.1 The Na—K phase diagram

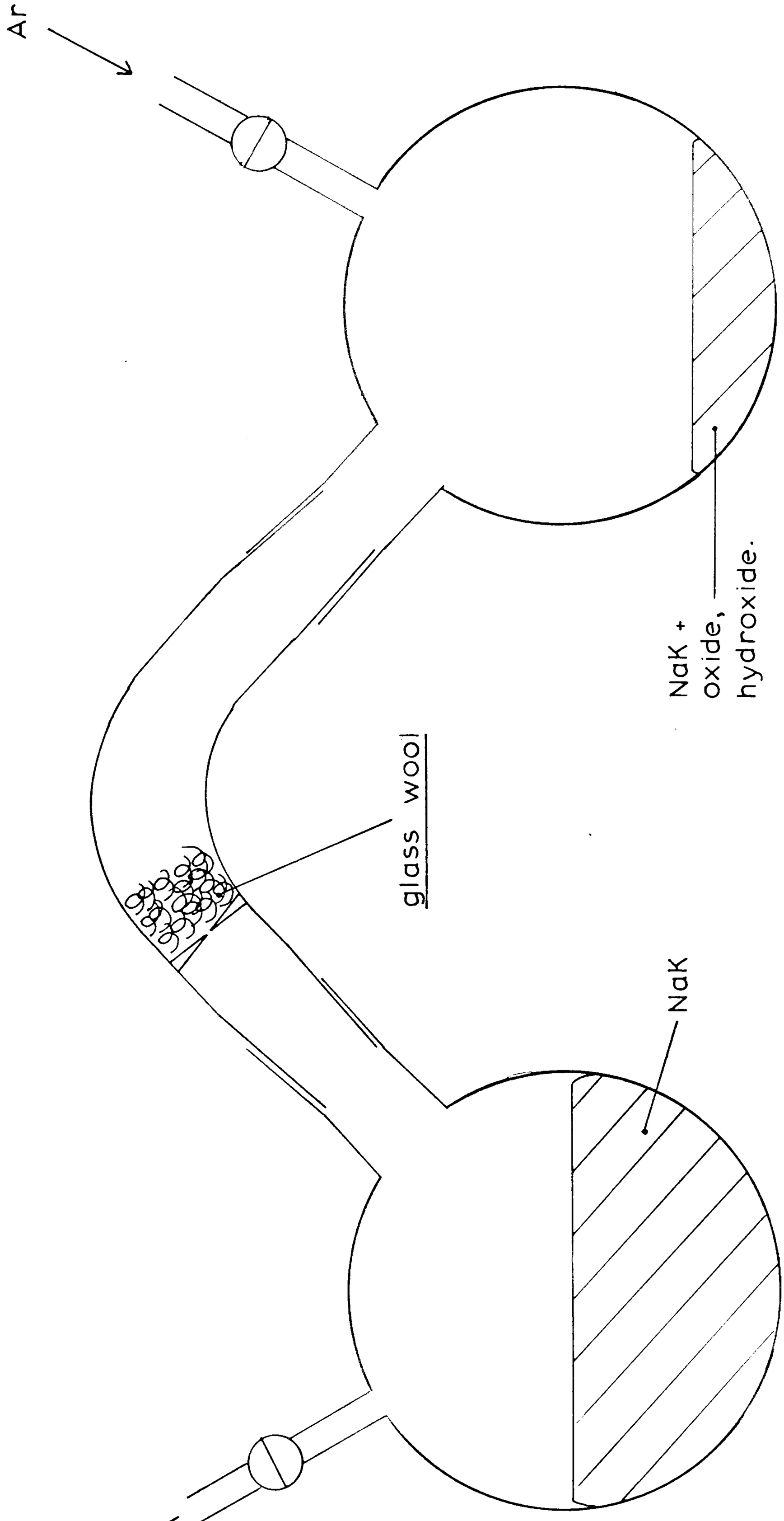

FIG. 3.2 The sodium potassium alloy filtration apparatus

Reaction). These were in the range 40-45 mole% potassium, and melted near 6°C.

3.3, THE REACTION VESSEL

The vessel is shown in Figure 3.3. A property of the metal is that, on leaving the site of injection, it always travelled vertically upwards. The reaction vessel, therefore, consisted of a vertically mounted pyrex glass column, 30 cm high, with a diameter of 6 cm, through which the metal could rise. The distance from the sidearm (A), through which the injection apparatus entered the vessel, to the stoppered top of the column, was 25 cm. The gas inlet (B) and outlet(C) were set as close to the open end of the column as possible, and the outlet was connceted by means of rubber tubing to a water-filled dreschell bottle. The lower tap(D) was used to run off the various layers for analysis.

3.4, THE METAL INJECTION APPARATUS

The metal injection apparatus is shown in Figure 3.4. It was designed to deliver clean sodium-potassium alloy to the water at constant pressure, and therefore, at constant flow rate, through a narrow orifice.

It consisted of a pyrex glass barrel (A) with a diameter of 2 cm, the open end topped by a tightly fitting septum cap (B). The gas inlet (C) was sited near the top of the barrel. The barrel was divided into two sections by a grade-0 sintered glass filter pad (E), the lower section bending a right angles, and narrowing to fit into the reaction vessel side arm. The seal between the injector and the reaction vessel was effected by means of a BIO ground glass watertight joint (F). The capillary was connected to the end of the narrow

FIG. 3.3 Apparatus for separation experiments

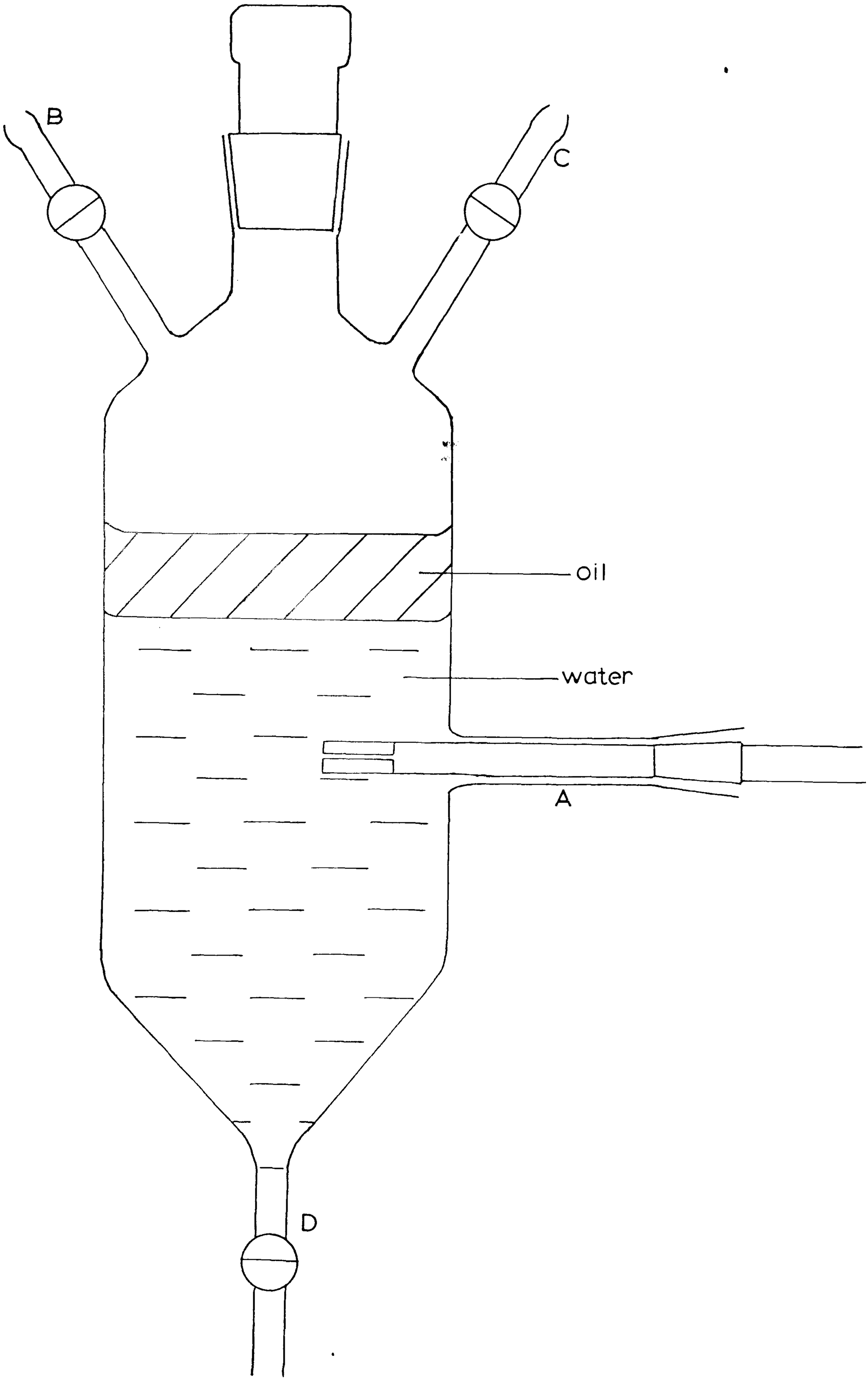

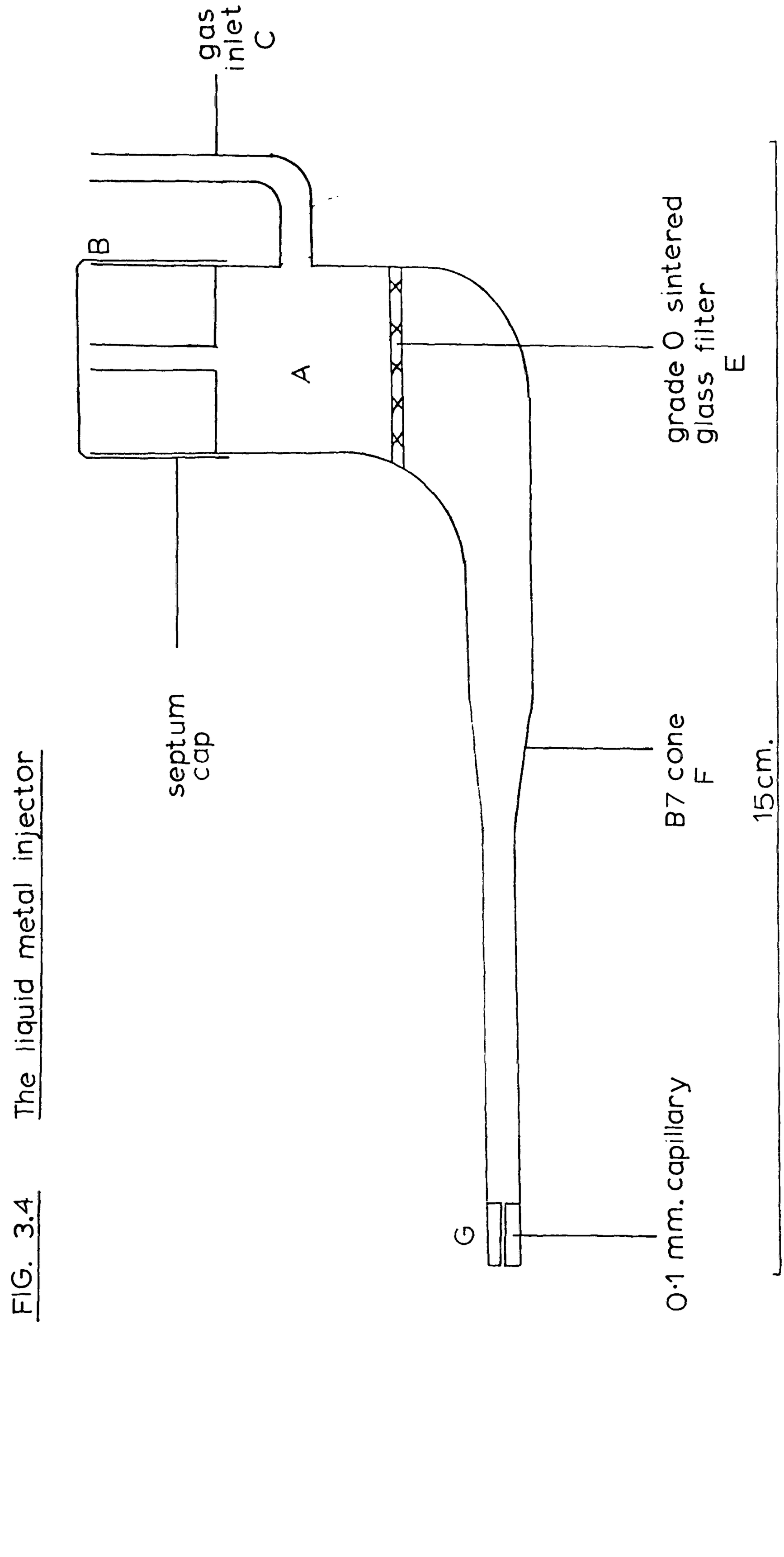

FIG. 3.4 The liquid metal injector

section, so that the opening (G) protuded approximately 2-3 cm inside the column of the reaction vessel.

The capillary glass used for most of the experiments described was standard, manufactured 0.1 mm internal diameter with an external diameter of 4 mm. Some of the orifices were produced by drawing down 2 mm capillary to diameters which varied between 0.1 and 0.3 mm, since exact reproducibility was not possible using this process. Capillary orifices produced in this way were measured using a travelling microscope with a vernier scale.

The capillary was replaced for each experiment, during which some metal adhered to its inside surfaces, burning to oxide when the injectorwas exposed to air prior to cleaning.

3.5, PROCEDURE

An argon cylinder was connected to the gas inlet port of the injector apparatus, and set to supply a pressure of 69 KPa. This was left to sweep out air from the injector for a period of one hour, before being connected, as described, to the reaction vessel.

The vessel was then filled to the required height with triply distilled de-ionised water. Argon bubbles were forced through the orifice, and streamed vertically upwards after some short horizontal movement. A layer of oil was poured carefully onto the surface of the water to a depth of 3 cm. At this stage the water height i.e. the distance from the capillary to the water/oil interface, was measured using a cathetometer. This distance could be adjusted slightly by either adding a few drops of water through the top of the vessel, or running water off through the lower tap of the vessel. The vessel was then securely stoppered.

A second source of argon was connected to the gas inlet tap of the vessel, and set to give a slow, but continuous

flow of argon through the space above the oil layer. This flow was monitored by the water filled dreschel bottle connected to the outlet port. The vessel was then flushed with argon for approximately one hour.

Liquid NaK was introduced to the injector. It was transferred in quantities of 1-2 g from the stock bottle using a hyperdermic needle and 2 cm plastic syringe, and injected through the septum cap and into the injector barrel. The metal rested on the filter until it was completely covered. Then, the pressure of argon gas forced the metal through the filter, leaving solid salt impurities behind. The metal then travelled along the length of capillary and out of the orifice to form a jet of alloy which reacted with the water.

Some metal, having left the site of injection, and travelled vertically through the water, appeared as pin-head sized globules in the oil layer above the water. Most of the metal reaching the oil rested on the surface, occasionally releasing some hydroxide smoke into the argon atmosphere above the oil. This smoke was swept out of the reaction vessel by the flow of argon, and it dissolved in the water in the dreschel bottle connected to the outlet port.

The time of injection i.e. the total time during which metal entered the water, was recorded. At the end of this period, the water in the vessel was immediately run off through the lower tap. This left the layer of oil, containing unreacted metal globules, in the vessel. This metal was hydrolysed carefully by pouring water onto the oil, while the flow of argon through the vessel was maintained. The resulting solution in water was run off as before, and the process repeated until no metal could be seen in the oil. Then, a final 100 cm of water was added, and shaken vigorously with the oil, after stoppering the vessel. The layers were allowed to separate, and the water run off as before. The contents of the dreschel bottle were added to the solution from the oil layer.

The solutions produced, from the water layer, and from hydrolysis of the oil layer were made up to 5000 cm^3 and analysed quantitatively for sodium and potassium content.

3.6 CALIBRATION OF THE JET

The metal flow rate for various capillary diameters was calculated using a pre-weighed oil filled vessel with a sidearm adapted to fit the metal injection apparatus. This is shown in Figure 3.5. Using conditions of a standard pressure of 69KPa and an alloy composition in the range 40 - 42 mole % K, the weight of metal injected during measured times was calculated from weight difference measurements. The results are shown in Table 3.1 and in graphical form in Figure 3.6.

TABLE 3.1.

FLOW RATE OF NaK THROUGH CAPILLARIES OF VARIOUS SIZE

Capillary diameter (mm)	Flow rate (mg/s)	Mole%K in alloy
0.080	2.0	41.6
0.090	9.0	41.8
0.100	20.0	40.3
0.110	25.0	41.4
0.119	30.0	40.0
0.125	41.5	41.0
0.135	60.0	41.9

A diameter of 0.1mm (the standard size of capillary used in the experiments described in Chapters 5 and 6) with a driving pressure of 69KPa therefore gives a flow rate of 20 mg/s.

FIG. 35 Apparatus for the determination of metal flow rates

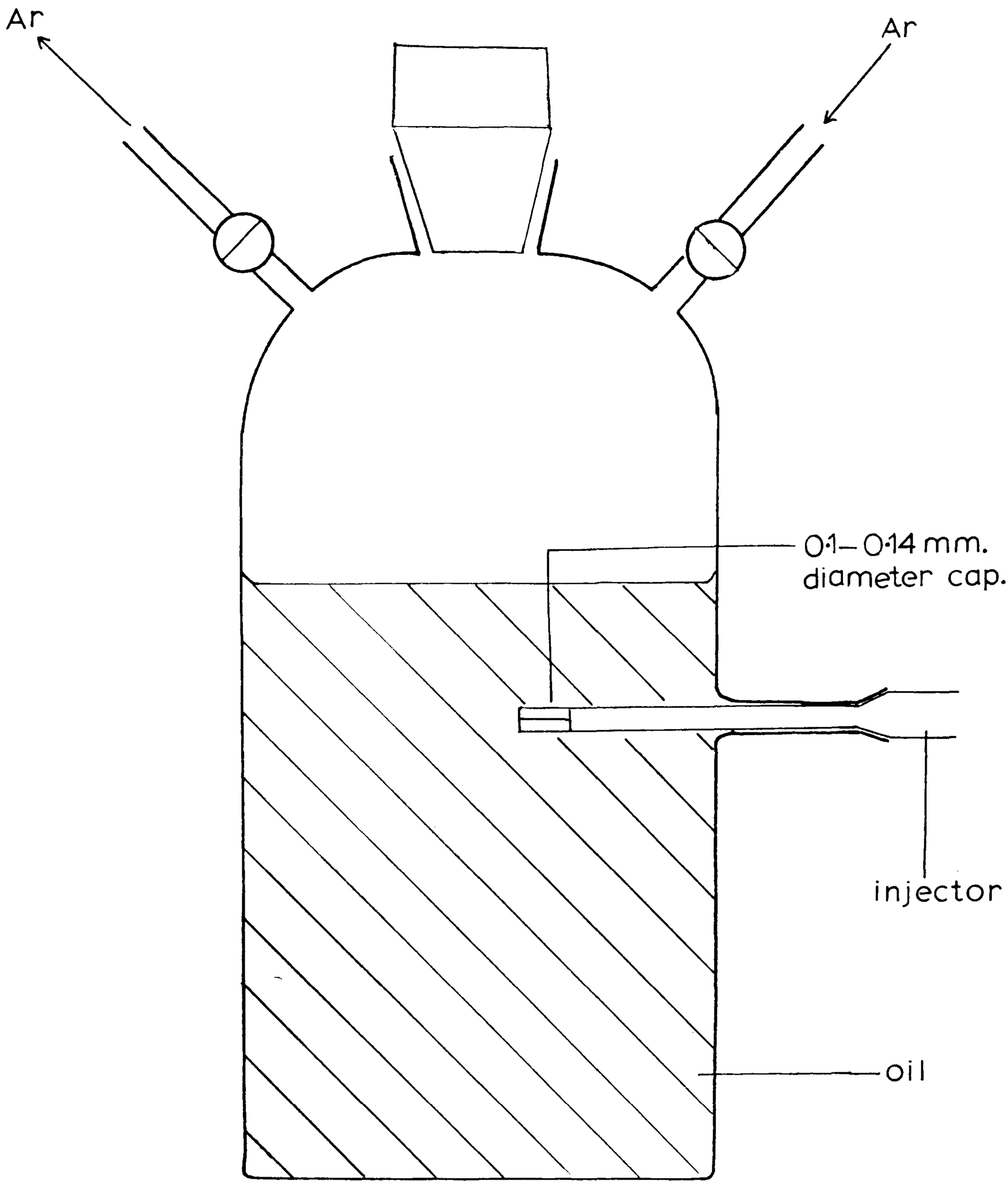

FIG. 3.6 Flow rate vs. capillary diameter

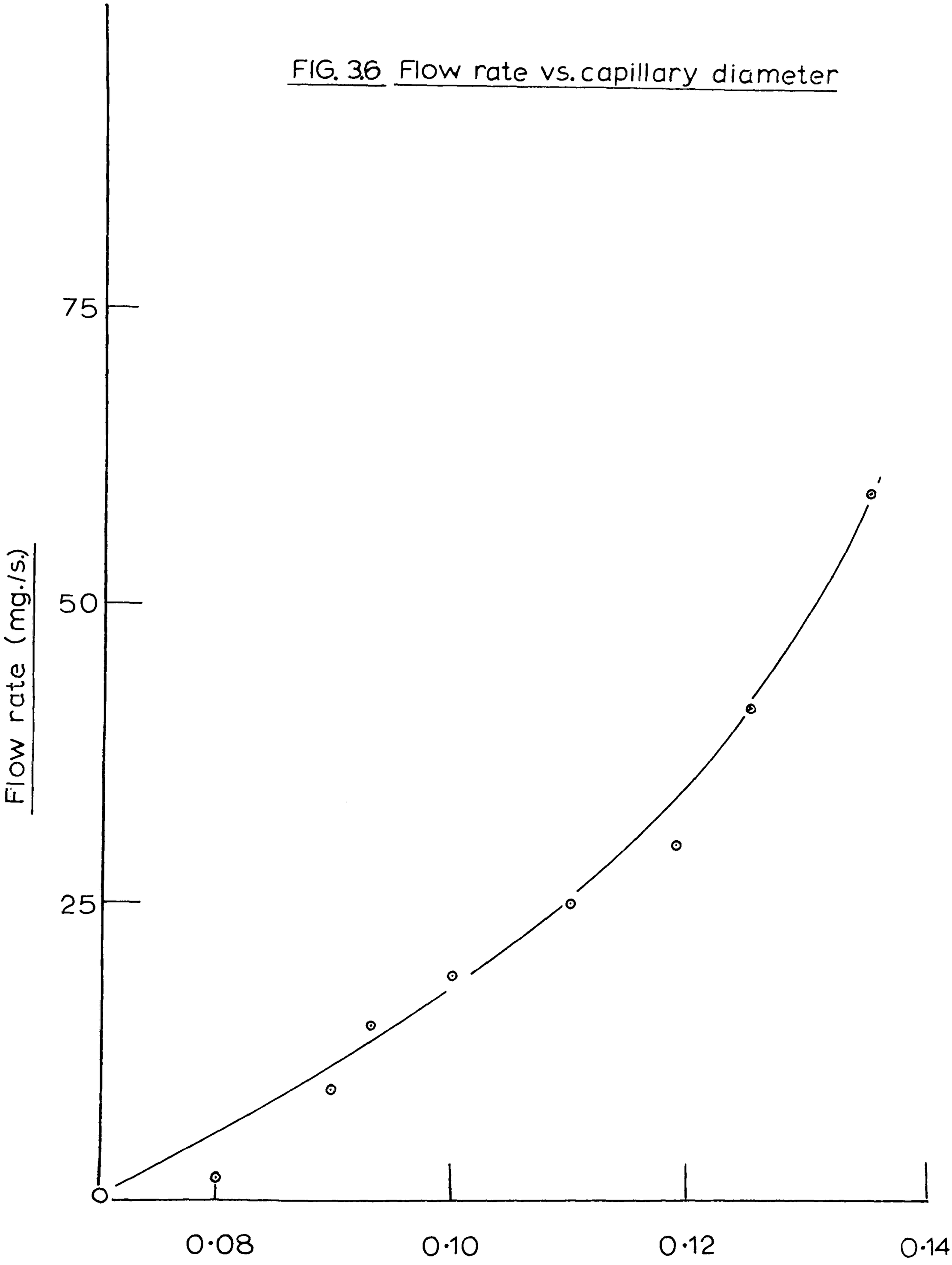

3.7 TEMPERATURE CONTROL AND MEASUREMENT

For variable temperature experiments, the apparatus was heated internally by immersion of a glass-clad heating coil (500w) through the B 24 neck of the vessel. Temperature gradients were minimised by external stirring, using a magnetic 'flea' and rotating magnet. The temperature was measured using a chart recorder (Bryans), so that temperature changes in the water bulk could be measured during the course of a reaction.

A test injection, at 30°C of approximately 2g of metal into water, gave an overall temperature rise of less than 0.5°C i.e. the bulk water temperature was found to be approximately constant over the course of an experiment, so that temperature rises due to NaK/water interactions in variable temperature experiments (Chapters 5 and 6) could generally be disregarded.

3.8. ANALYSIS

Dilution of the solutions to 5000cm^3 led to concentrations of each of the two metal ions in the range 20 - 100 p.p.m. The technique of atomic emission spectroscopy was used for the analysis. The instrument employed was a Perkin-Elmer 603 Atomic Absorption Spectrometer, using an air-acetylene flame. Measurement of the alkali-metal ion concentration relied upon the very strong emission lines at 589.0, 589.6 nm. for sodium, and 766.5 nm. for potassium. Full details of the conditions and procedure are contained in "Analytical Absorption Spectroscopy". [51]

CHAPTER IV

PHOTOGRAPHIC EXPERIMENTS

4.1 INTRODUCTION

Several photographs were obtained by Dowling[49] of the area around the end of a 0.106 mm diameter capillary through which liquid NaK was injected into water. An open shutter technique and electronic flash of duration one microsecond were used. Photographs obtained in this way led him to believe that a 'steady state' situation existed at the liquid metal jet. This is depicted in Figure 4.1. From the glass capillary (A) a jet of liquid metal (B) issues. This metal reacts in part with the water (Dowling's separation experiments indicated that 13.5% of metal injected reacted in the region between (B) and (D)) to produce an envelope of hydrogen gas (C).

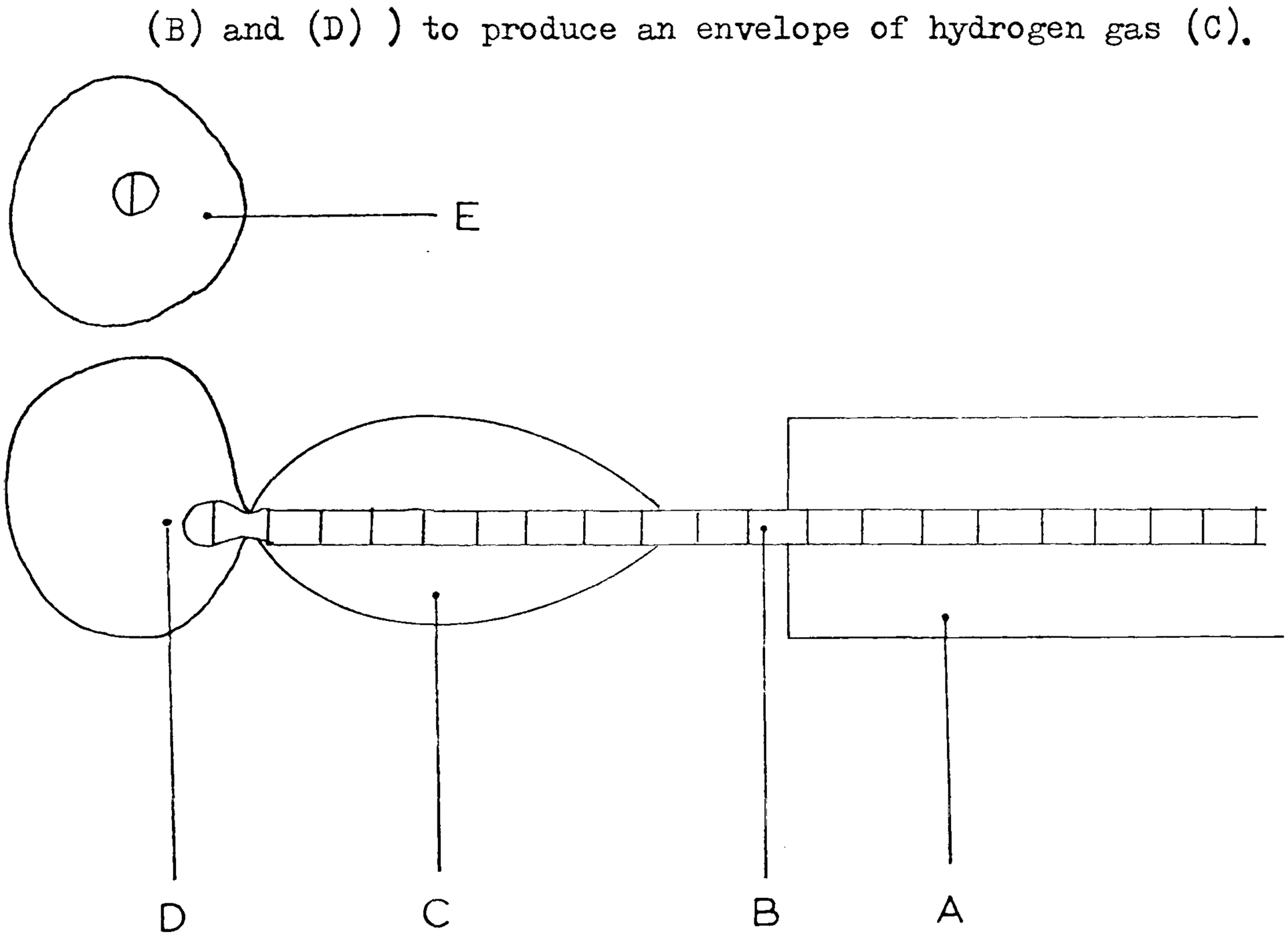

Fig. 4.1. THE SITUATION AT THE JET

This envelope collapses back onto the thread of metal, and direct (i.e. $M_{(l)} + H_2O_{(l)}$) reaction again occurs, producing more hydrogen (D). The jet then breaks into globules, each globule moving vertically away from the jet encased in a hydrogen bubble (E).

Double-exposure photographs enabled measurement of the rate of bubble rise, and the rate of bubble growth to be measured. The latter is significant in the determination of the reaction stoichiometry (Chapter 8).

In the present work, high speed photography was employed. This method was expected to fulfil two functions:-

(i) Provide information on the physical processes occurring i.e. the nature of bubble production and release, the transition from coherent metal thread to individual globules. Confirmation or not of the steady state situation shown in Figure 4.1. could only be provided by a series of continuous high speed exposures.

(ii) Enable certain physical measurements, in particular, the length of exposed metal thread, to be made. These measurements would then be used in the calculation of the rate of reaction.

4.2. EXPERIMENTAL

The standard reaction vessel (Figure 3.3) was modified to expose the area around the end of the capillary to the camera. The modified vessel is shown in Figure 4.2. One section of the glass column was replaced with flattened glass walls to produce a photographic 'cell' around the region of injection. The dimensions of the cell were 80 mm x 60 mm (in the plane of the liquid metal jet direction) x 15 mm

FIG. 4.2 Reaction vessel for photographic experiments

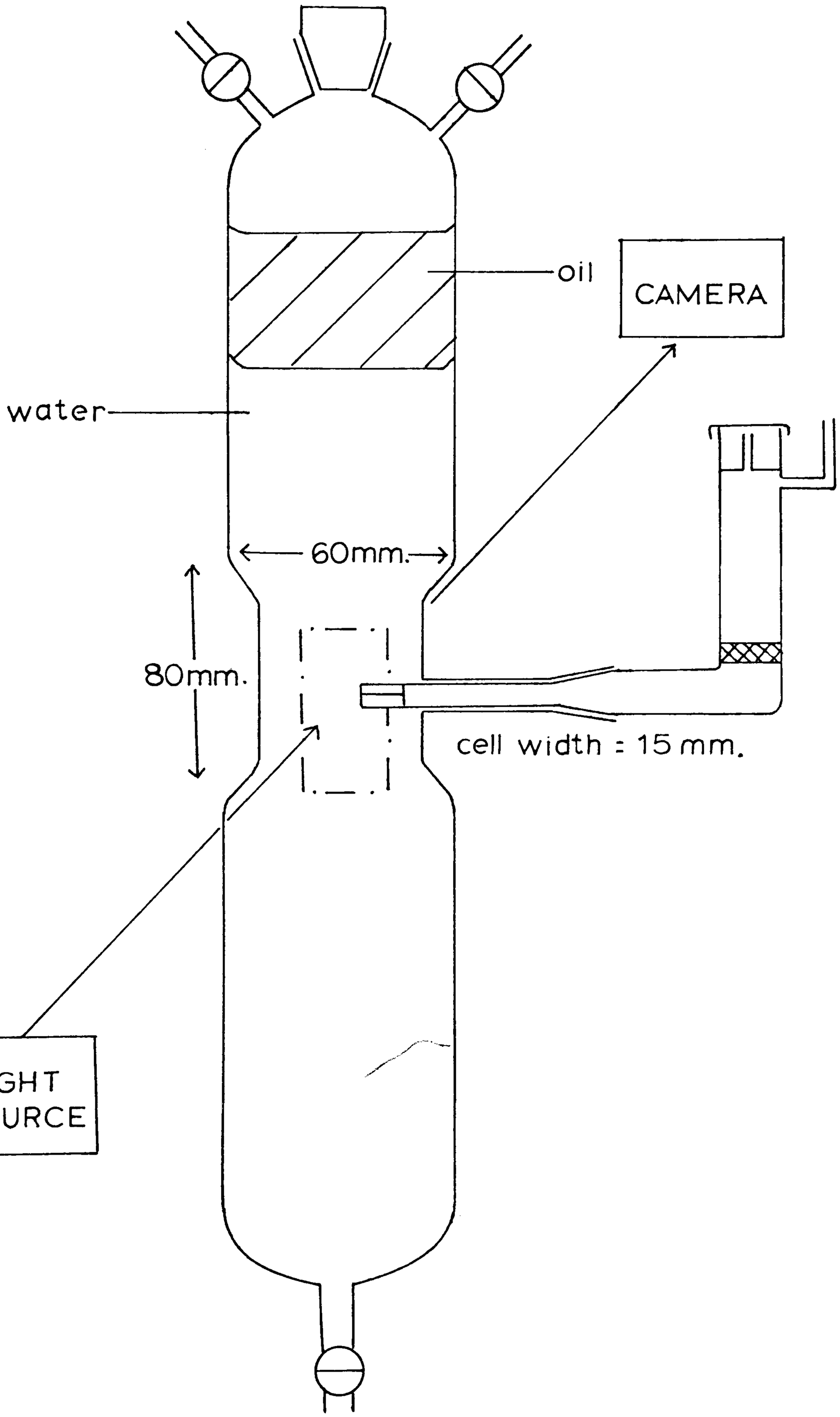

(perpendicular to the plane of jet direction). The photographs taken with a high speed camera (1000 frames/second) were therefore perpendicular to the jet direction (Fig 4.2).

Eleven experiments were filmed using this apparatus, each film of approximately 1000 frames (one second of action). The details are contained in Table 4.1. The alloy used in these experiments was in the composition range 40-50 mole % K, 50-60 mole % Na. Experiments 1-9 were filmed in black and white, 10 and 11 in colour.

A 1,000 cycle/second marker produced spots on the film at intervals of one millisecond. Preliminary examination of the films revealed that the frames 300-700 in each sequence were the closest to one millisecond apart, the frames 0-300 and 700-1000 being fractionally slower, corresponding respectively to periods of the film speeding up and slowing down. Analysis was therefore restricted to frames in the middle sequence.

4.3 RESULTS

The results are presented in two sections, the physical processes occurring, and the photographic measurements.

4.3.1 The physical processes

Experiments 1 and 2. The frames shown between pages 46 and 47 are from experiment 2, and correspond to the frames numbered 492-531 in the 100 frame film. With a driving (argon) pressure of 69 KPa and 0.1 mm diameter capillary, this experiment gave the clearest picture of jet breakdown and hydrogen bubble formation. Experiments 1 and 2 provide a comparison between gas bubble formation at the end of a capillary and product gas formation due to a reacting metal jet with the same size capillary. Whearas experiment 1 showed erratic bubble formation in 3 dimensions, with irregular bubble sizes

TABLE 4.1 FILMED EXPERIMENTS

Experiment no.	Injeted fluid	Vessel fluid	Cap. diameter (mm)
1	Argon	Water	0.100
2	NaK	Water	0.100
3	NaK	Water	0.132
4	Argon	Water	0.120
5	NaK	Water	0.120
6	Argon	Water	0.130
7	NaK	Water	0.130
8	NaK	0.67M.NaOH	0.100
9	NaK	0.398M.H_2SO_4	0.100
10	NaK	Water	0.100
11	NaK	5.50M.H_2SO_4	0.120

and release times, injection of NaK into water produced a regular, repeating pattern of bubble formation in 2 dimensions only ie. from a view perpendicular to the direction of the metal flow, the bubbles did not overlap.

The frames 1-39 reproduced in this chapter show a sequence of bubble formation over a time period of 39 milli seconds. The capillary appears at the bottom left hand corner of each frame. The dark area in the centre of the capillary is the liquid metal, and the flow is from left to right. The cycle of events begins at frame 2, as bubble detachment is about to occur. Two regions of bubble expansion can now be seen (frames 3-6), one around the body of the thread, and one at the right hand extremity. These regions continue to expand to become one elongated bubble, or envelope, enclosing the thread (frame 8). Yet another region of bubble growth appears adjecent to the capillary opening (frame 9) as more metal is pushed from the capillary. This new envelope then feeds gas forwards into the primary bubble (frame 11). Detachment of The main bubble occurs momentarily (frame 12). Meanwhile, another region of hydrogen production is evident, around the metal jet.

Frames 13-25 show this continuous process of gas envelope formation around the reacting metal jet, followed by gas flowing into the main bubble from these individual envelopes. A second temporary detachment occurs at frame 17.

The main bubble eventually reaches a stable size, and detaches to move vertically through the water (frame 26). This process has lasted 25 milliseconds. In most cases, this cycle then repeats itself with a remarkably consistent frequency.

In some cases, however, the process is not complete. Two bubbles, formed in the way described, may join together to form one bubble, of approximately twice the normal size. Frames 31-35 show such a bubble in formation. This bubble detaches

PHOTOGRAPHS 1 - 12

1

2a

3

4

5

6

7

8

9

10

11

12

PHOTOGRAPHS 13 - 24

13

14

15

16

17

18

19

20

21

22

23

24

PHOTOGRAPHS 25 - 36

25

26

27

28

29

30

31

32

33

34

35

36

PHOTOGRAPHS 37 - 39

37

38

39

(frame 36) to move, as before, vertically through the water. Frames 35 and 36 may be compared with frames 2 and 3, as the cycle begins to repeat. Frames 37-39 show the beginning of the formation of a new bubble.

Experiments 3-7. Using larger diameter capillary, the situation described for experiment 2 was repeated. Due to larger surface areas of reactants in contact, the reaction was more vigorous, the water more turbulent, and the sequence of events not so uniform. Bubble sizes were generally larger, but there was some variation in bubble size. For instance, with the largest capillary (0.132 mm diameter, experiment 3) very small bubbles were occasionally released, each travelling for considerable distances horizontally before moving vertically upwards through the water column.

Experiments 8 and 9. No difference in size or frequency of bubble formation could be observed. Films of these experiments were identical with those in experiment 2.

Experiment 10. Colour photography provided little extra information in terms of a description of the physical processes. However, in these films, individual metal globules could be seen very clearly. In experiment 2, the metal in bubbles appears as black dots (see frames 4, 24 and 37 in particular) but these are not very well defined. The film from this experiment shows that between one and four metal globules are present in each ascending hydrogen bubble, where previously, it was believed that there was only one per bubble.

Experiment 11. With strong acid, the reaction is more vigorous, and the water considerably turbulent. The basic system for NaK $\longrightarrow$ water and NaK $\longrightarrow$ dilute acids/alkalis still applies, but the metal globules could be seen burning within their protective hydrogen bubbles. Bubble production occurred at approximately twice the rate of that for experiment 2.

The salient features of the system described above are illustrated on a larger scale in photofraphs A, B and C.

Photograph A. This shows the injection of argon into water, at a pressure of 69 KPa. Over a large number of frames, no repeatable regular pattern occurred. The average bubble size was approximately of that for hydrogen bubbles in NaK + water reactions. The bubbles issued from the capillary and moved in three dimensions, although the general direction was, of course, vertically upwards.

Photograph B. This, by contrast, illustrates the regular bubble formation during an injection of NaK at the same pressure through the same capillary. Regions of gas expansion can be seen around the jet as the bubble begins to form. These regions flow, one by one, into the main bubble to the right of the jet. This will detach when a stable bubble size is reached. A globule of NaK can clearly be seen in the fully formed bubble closest to the jet, and appears as a black sphere. The bubble at the top of the picture is beginning to 'flatten out' from a sphere into an elipse.

Photograph C. Two important features descussed in connection with photographs 1-39, experiment 2, are illustrated in more detail here. Two regions of expansion can clearly be seen in the area of the metal jet, as the new bubble begins to form. The region closest to the capillary is about to flow through to the end. Comparing the sizes of the two detached bubbles, the lower one is approximately twice the size of the upper. It has been formed by a combination of two bubbles in the manner described from photographs 31-35. This bubble contains two globules of metal, as may be expected. These, again, appear as two black spheres in the lower centre of the bubble.

PHOTOGRAPH A

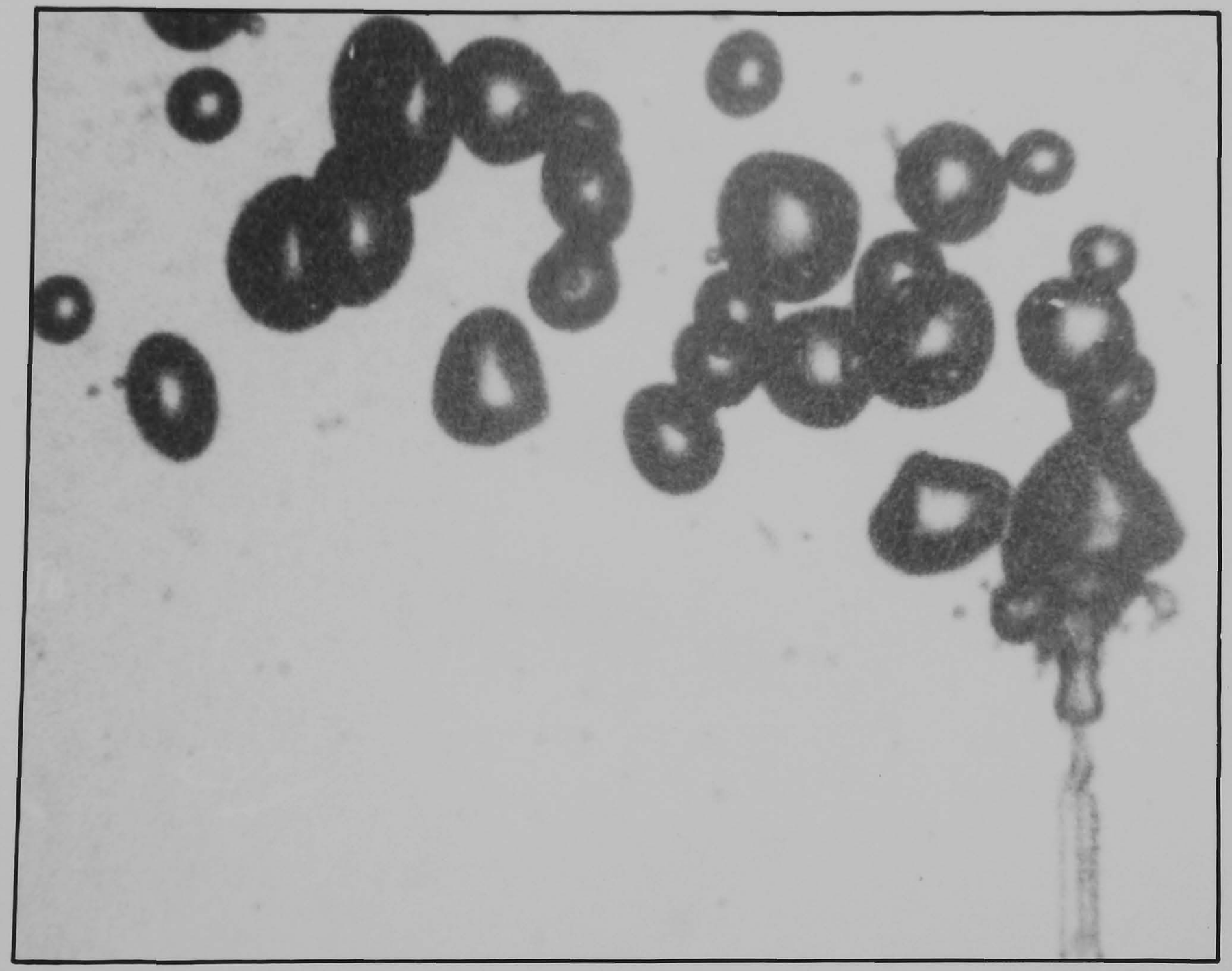

PHOTOGRAPH B

A9

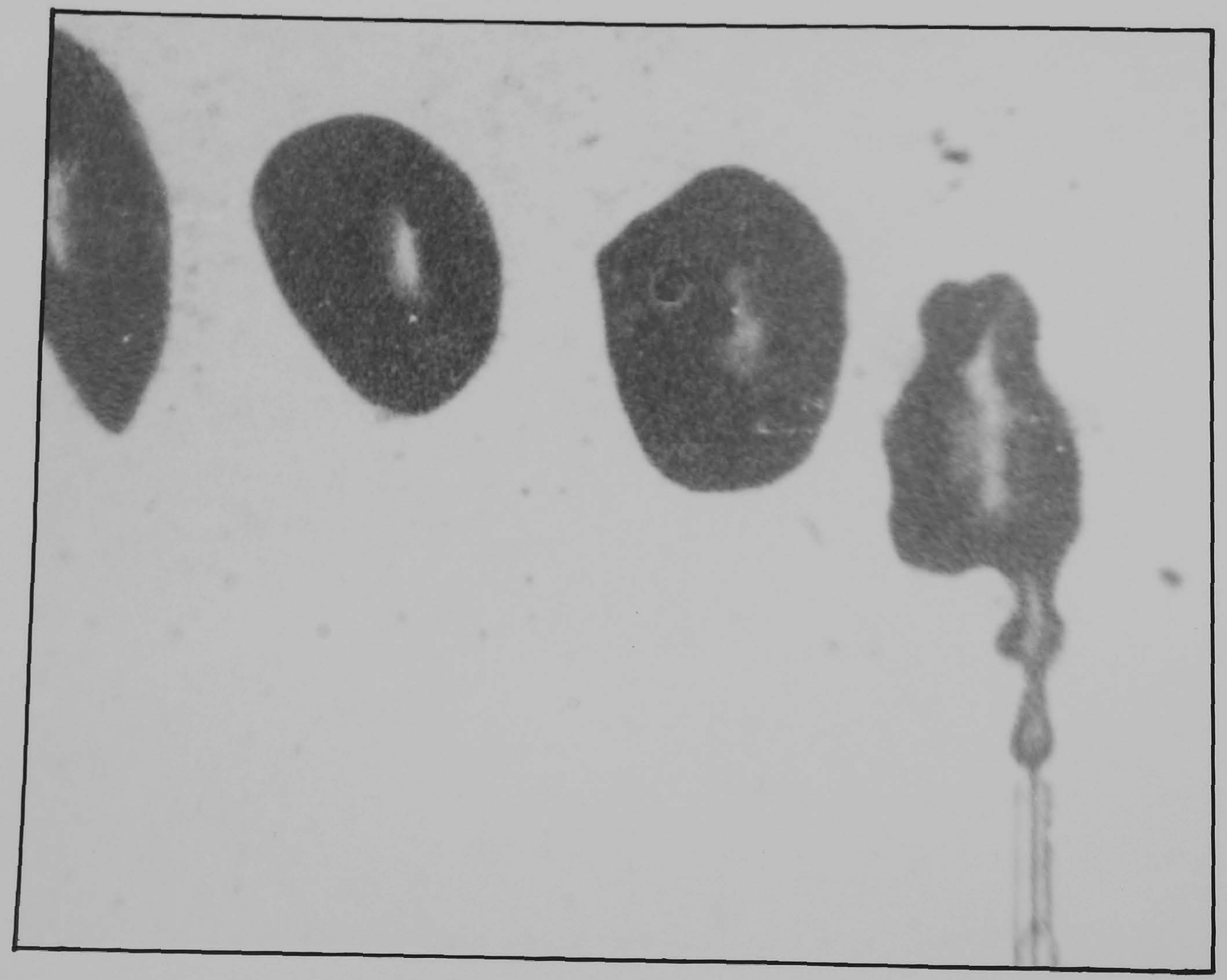

PHOTOGRAPH C

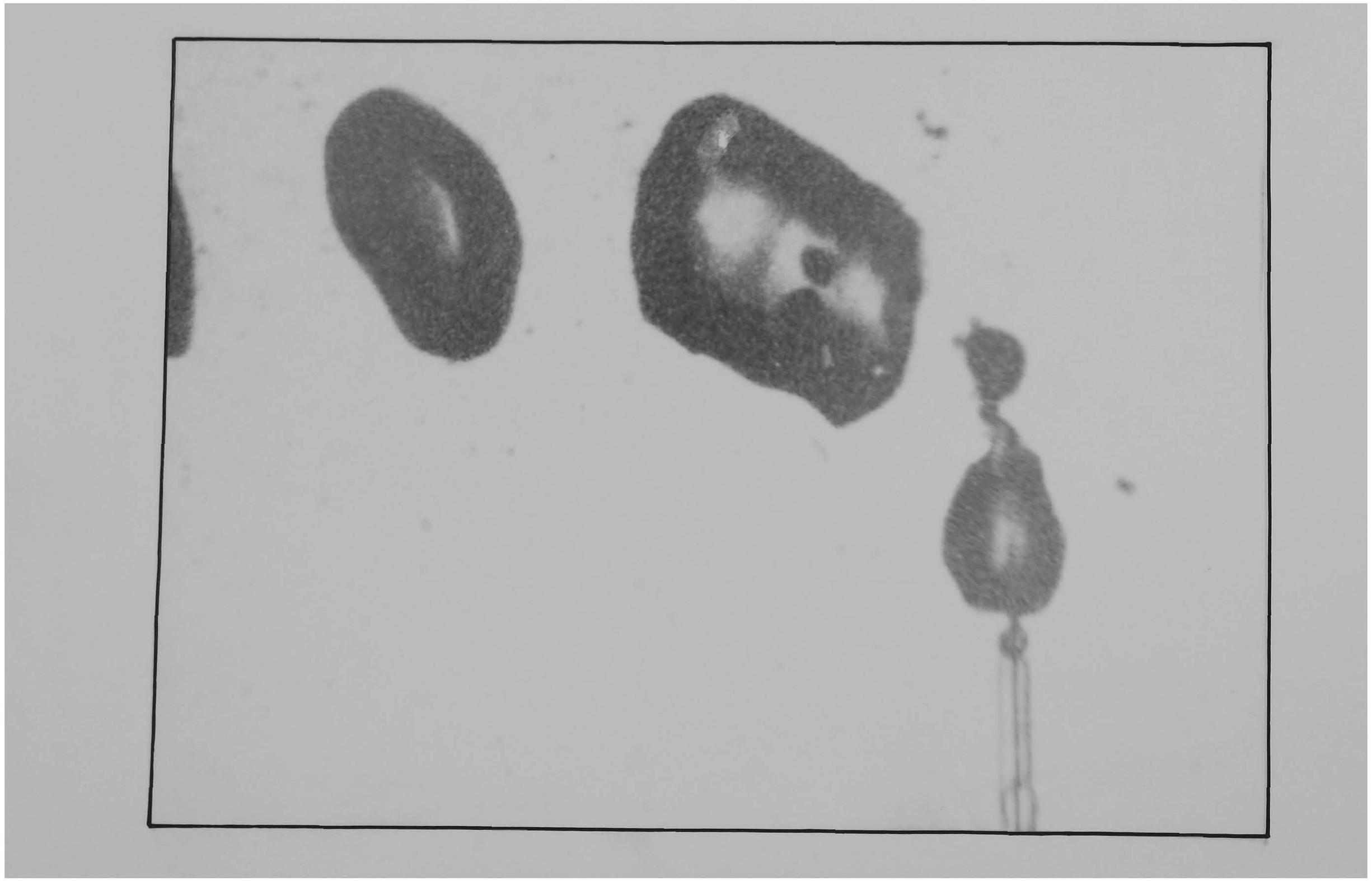

4.3.2 Photographic measurements

Measurements were taken from the films of experiments 2 and 10, which employed capillary diameters of 0.1 mm. The measurements were to be used in the calculation of the rates of reaction (Chapter 5), the experiments for which used this size of capillary exclusively.

(a) The length of metal thread. This was the distance from the open end of the capillary to the point on the metal jet where hydrogen gas protection could clearly be seen. Difficulties in measurement were encountered due both to fluctuation in the length and to poor definition of the position of the gas envelope. Measurements were taken directly from film scanner - editor by comparing the external diameter of the standard 0.1 mm capillary as it appeared on the screen with its actual diameter (4mm) to calculate the scale. The number of sample frames used was 300. Table 4.2 gives a sample of 48 measurements of the thread length compared with their frame number. The average length of exposed metal thread was 0.42 mm.

(b) The number of bubbles released per second. The time for 30 bubbles, a convienant number, to be released from the area of the jet was measured (15 bubbles from the centre regions of film 2, and 15 from film 10). These release times are collected in Table 4.3. One bubble was released, on average, every 26.5 milliseconds, which geves a bubble evolution rate of 37.7 per second.

(c) Rate of bubble ascent at 20°C. Ten bubbles were timed over a distance of 2 cm (experiment 2). The average bubble velocity was 0.28 metres/second.

(d) Number of metal globules per bubble. Of 32 bubbles examined on the film of experiment 10, two contained two globules of metal ie. approximately two bubbles of every 32 released were formed from a combination of two smaller

TABLE 4.2 SAMPLE OF 48 MEASUREMENTS OF THE LENGTH OF EXPOSED METAL THREAD

Frame No	Length (mm)	Frame No	Length (mm)	Frame No	Length (mm)
301	0.0	406	0.1	553	0.7
311	0.6	420	0.4	560	0.6
320	0.3	431	0.1	569	0.5
322	0.3	434	0.0	570	0.5
326	0.6	436	0.4	571	0.4
348	0.0	512	0.7	573	0.4
351	0.2	513	0.8	589	0.4
372	0.4	514	0.7	590	0.1
373	0.0	516	0.0	600	0.0
379	0.6	525	0.5	611	0.4
380	0.6	531	0.5	613	0.4
390	0.3	540	0.6	614	0.5
395	0.5	542	0.8	651	0.6
402	0.5	544	0.1	653	0.4
403	0.6	545	0.3	660	0.6
404	0.0	551	0.8	661	0.6

TABLE 4.3 TIMES OF BUBBLE RELEASE (milliseconds)

	FILM 2		FILM 10	
1	25	15 bubbles released in 394 milliseconds	29	15 bubbles released in 401 milliseconds
2	51		54	
3	81		87	
4	105		110	
5	133		131	
6	159		160	
7	180		185	
8	208		210	
9	235		238	
10	265		270	
11	290		295	
12	318		319	
13	345		348	
14	376		381	
15	394		401	

bubbles as in frames 31 - 36 of experiment 2. Then, if an average of 37.7 bubbles are released every second, and $\frac{1}{16}$ of all bubbles released contain two globules of metal, the metal thread appears to break down into 37.7 + 2.35 ± 40 globules every second.

(e) Rate of bubble rise. A number of bubbles were timed in their ascent from the photographs. Of 10 bubbles so timed, the average velocity was found to be 280 mm/s.

(f) Bubble radius. Of 20 bubbles measured, the average radius on detachment from the jet was 0.242 mm.

4.4, CONCLUSIONS

The experiments described in this chapter show that the general scheme of a metal thread, reacting as it emerges from a capillary opening to produce hydrogen gas, then breaking down into globules of metal protected by a product gas bubble is correct. They do not, however, confirm a 'steady state' situation as outlined in Figure 4.1, which was a reasonable explanation based on a number of non-consecutive photographs. The reaction proceeds, however, in a cycle of physical processes, repeatable, on average, every 26.5 milliseconds. The maximum time for 1 cycle was 33 milliseconds, the minimum 20 milliseconds (Table 4.3). A preliminary 'envelope' of hydrogen gas is in evidence (Fig 4.1, Photograph C), but this is not a permanent feature of the system, since this gas envelope is dynamic, continually forming, flowing into a gas bubble, and then re-forming around the jet.

There appears to be a stable bubble size, which detaches from the metal jet. Since this bubble size is

fairly constant, the bubbles therefore leave the end of the jet at regular intervals. However, some bubbles combine and this fact explains why more than one globule of metal may be found in a single bubble of gas. Occasionally, three or four globules are observed in a hydrogen bubble, indicating a more complicated combination of bubbles.

Presumably, in these experiments, a very rapid inital reaction occurs, as the jet emerges from the capillary, followed by a more subdued reaction, as the jet is enclosed in a gas envelope. The envelope may contain water vapour as well as hydrogen, and the reaction between sodium/potassium and water vapour will occur. Because metal is continually flowing and pushing gas away from the capillary, and due to the cyclic nature of the process, varying lengths of metal jet are visible unprotected by hydrogen gas.

Increases or decreases in the reaction rate are not detectable photographically when dilute solutions of acid or alkali are substituted for water. The difference is marked, however, when 5.5 Molar H_2SO_4 is used.

C H A P T E R V

R A T E S O F R E A C T I O N

5.1 INTRODUCTION

The apparatus and techniques described in Chapter 3 were used in a series of experiments to determine the rate of reaction of liquid NaK with liquid water at various temperatures. The results are divided into two areas:-

(i) Reaction at the jet $\begin{cases} Na_{(l)} + H_2O_{(l,g)} \\ K_{(l)} + H_2O_{(l,g)} \end{cases}$

(ii) Reaction in the bubble $\begin{cases} Na_{(l)} + H_2O_{(l,g)} \\ K_{(l)} + H_2O_{(l,g)} \end{cases}$

The subscripts (l,g) for water indicate that it is not possible to specify the reaction conditions at any one time, in that water vapour is inevitably generated from liquid water during the course of the reaction. NaK entering the water may immediately be covered by an invisible envelope of vapour, vapourisation of the water occurring due to the heat of the reaction. Reaction in the bubble may be due, in fact, to water vapour contained within the product gas bubble, but the photographic experiments show that metal globules do make frequent contact with the gas/water interface.

The results of these experiments may be expressed

in the form water height vs. extent of reaction. Extrapolation to zero water height then gives a value for the extent of reaction at the jet (which travels horizontally), while the gradient of the graph gives a value for the extent of reaction per unit distance of travel. The general system is depicted in Figure 5.1. using the results of Dowling.[49] Here, a certain quantity of alloy is injected, and the proportion of this metal which reacts increases with increasing length of passage (water height) through the water.

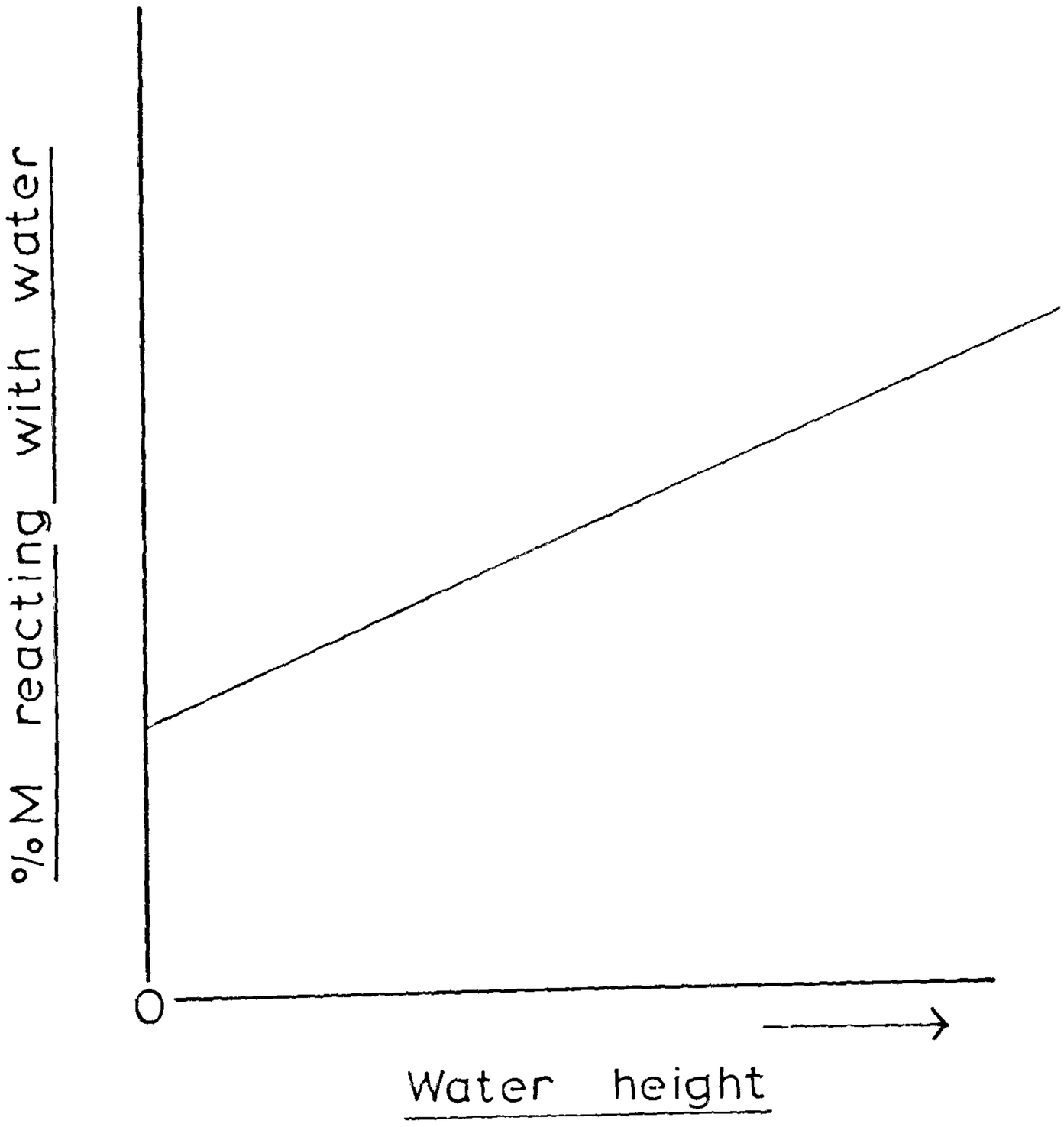

Fig. 5.1. PROPORTION OF ALLOY REACTING IN VARIOUS WATER HEIGHTS

This is the basic behaviour under these conditions, but the results are open to considerable extension and refinement, namely in that the reactions of the two components of the alloy are separable.

The reaction rate at the jet will be calculated on the assumption that the bulk of reaction takes place when the metal thread has no visible hydrogen gas protection. Later results will show this to be a reasonable assumtion. Consider Figure 5.2. The

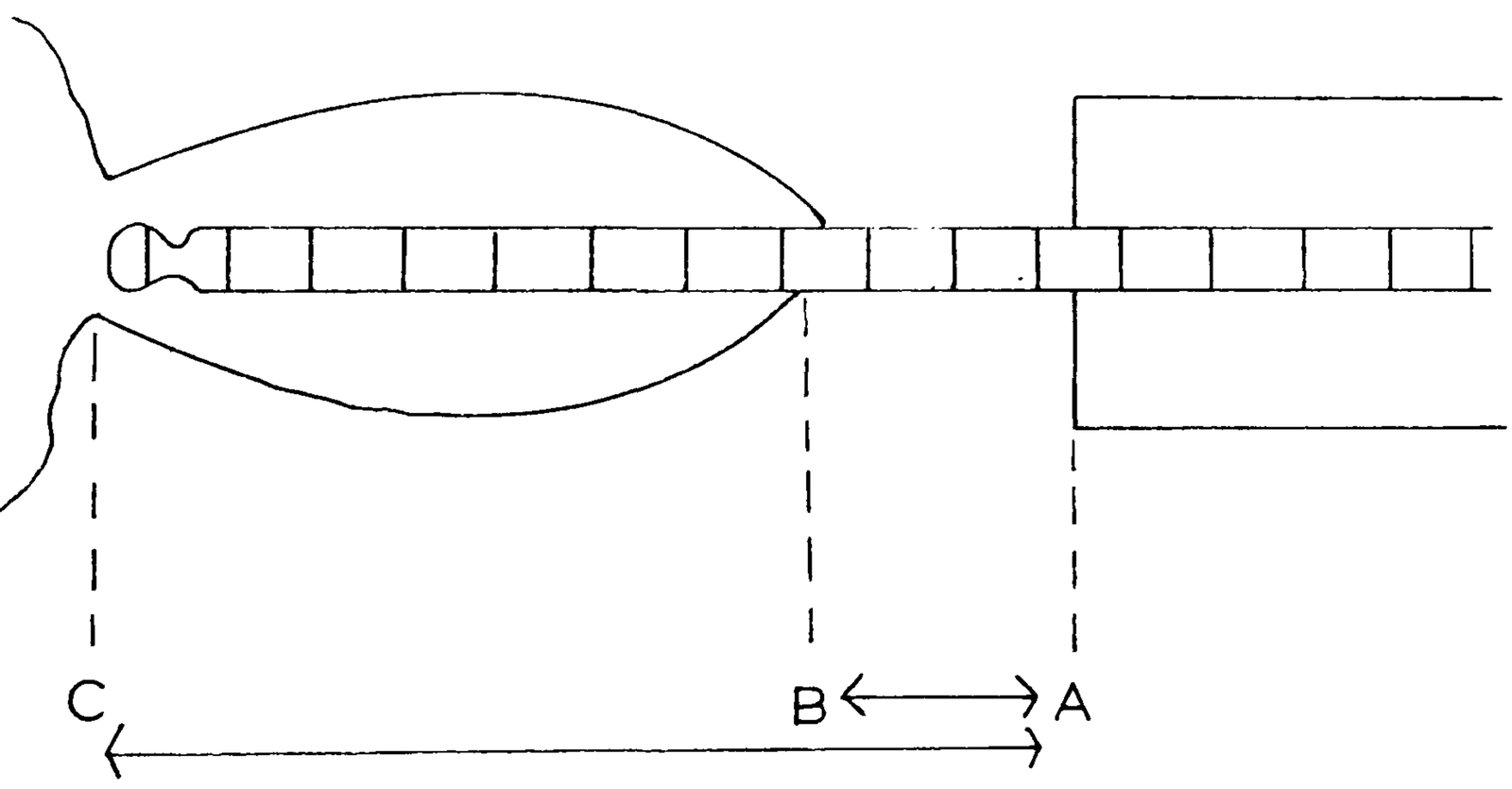

Fig. 5.2. REACTION AT THE JET

result of extrapolating reaction extent vs. distance travelled will be a value that represents the reaction taking place between (A) and (C), the total length of horizontal travel. The surface area measurements, and therefore the rate of reaction calculation, will assume that all the reaction takes place in the region (A) to (B).

5.2 SEPARATION EXPERIMENTS AT 20°C

5.2.1. Initial Results

The results of the first set of separation experiments are shown in Table 5.1. and Figure 5.3. The graph shows that:-

(a) The relationship between the percentage of metal reacting and water height is linear below approximately 100 mm.

(b) At 20°C, a higher proportion of the potassium in the alloy reacts than the sodium.

(c) 4.7% of the sodium in the alloy, and 11.0% of the potassium react at zero height i.e. at the jet.

(d) The gradients of the graphs are, Na, 0.31% per mm. and K, 0.29% per mm.

Reaction rates were calculated for each of the two metals using the above results when combined with the data in the following sections.

TABLE 5.1. RESULTS OF SEPARATION EXPERIMENTS AT 20°C

Height of water (mm)	%Na found in water	%K found in water
30	13.8	18.7
40	17.0	22.5
49	17.9	22.0
60	24.1	29.3
70	25.0	31.5
80	29.0	34.8
90	33.0	37.9
100	36.1	38.9
125	40.4	42.9
150	45.7	47.9
175	46.1	48.0
200	49.7	51.9
225	56.1	60.6
250	64.8	65.9

The average alloy composition in these experiments was 56.9 mole % Na.

FIG. 5.3 % of metal reacting vs. water height at 20 °C

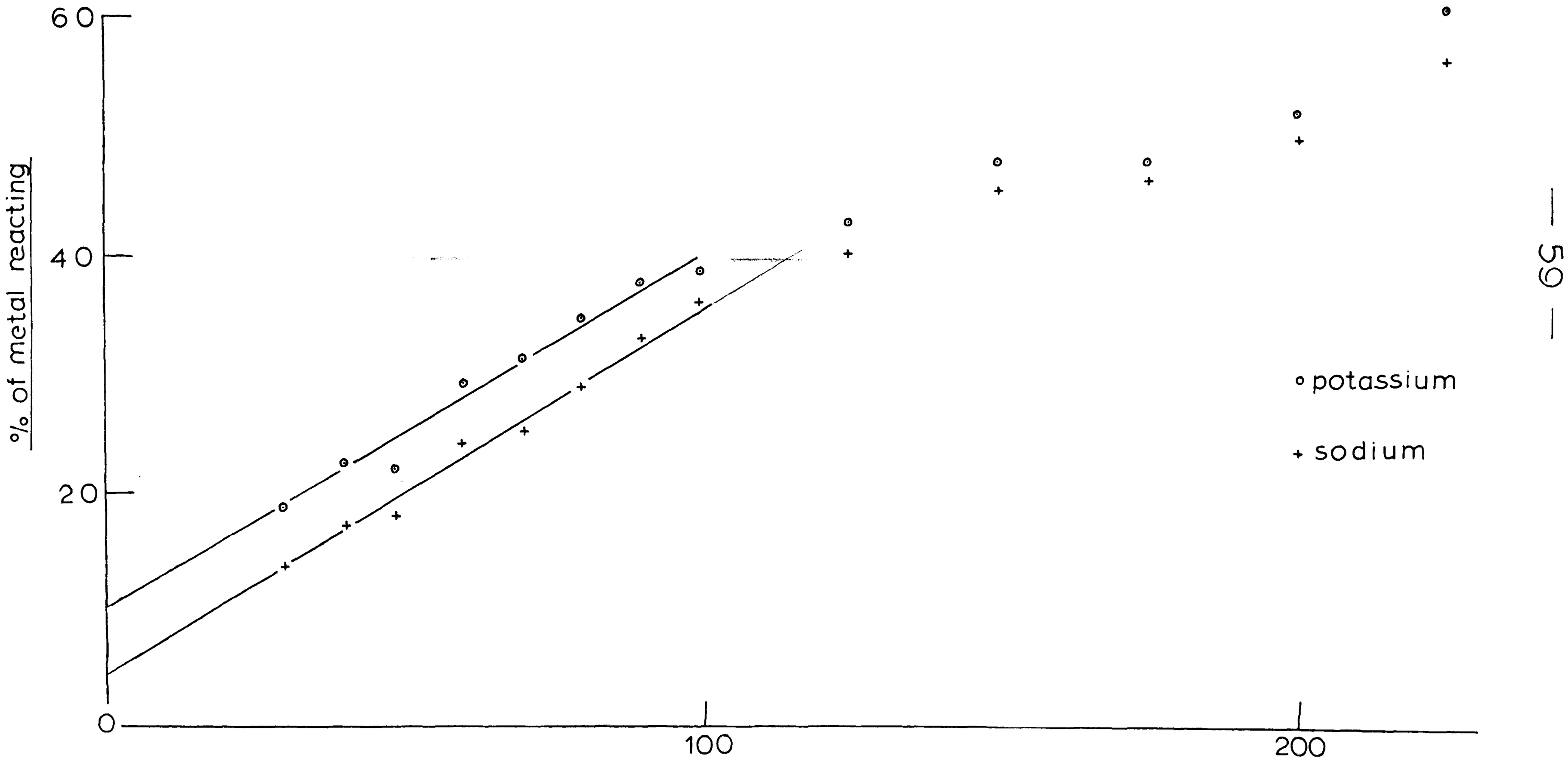

5.2. 2, Surface area of the metal.

(a) At the jet.

From photographs, the average lenth of exposed metal thread was 0.42 mm. This gave a surface area of $2\pi r\ell$ where ℓ =0.42 mm. and r = 0.05 mm. The surface area exposed at any instant of time was therefore 0.132 mm^2. The surface area of each of the two metals in the surface of the alloy was calculated as follows. Assuming that the metal surface contained a random arrangement of sodium and potassium atoms, the proportion of the surface covered by each metal should be a function of the alloy composition, and also the ratio of the areas occupied by individual sodium and potassium atoms. Condider a solid metal. In a B.C.C. unit cell, the number of atoms occupying 1mm^2 of surface can be shown to be $\sqrt{2}/a^2$ in the 110 plane and $1/a^2$ in the 100 plane, where a is the unit cell dimension. *
The value a = 4.29×10^{-8} mm for sodium, and 5.25×10^{-8} for potassium.[52] These figures give the following values.

B.C.C. Na(110), 7.7×10^{12} atoms/mm^2

B.C.C. Na(100), 5.4×10^{12} atoms/mm^2

} average 6.6×10^{12}

B.C.C. K (110), 5.1×10^{12} atoms/mm^2

B.C.C. K (100), 3.6×10^{12} atoms/mm^2

} average 4.4×10^{12}

* See Appendix 1

The same space relationships will not apply precisely to the metals in the liquid state, but the ratio of the numbers contained in $1mm^2$ of solid, 6.6 : 4.4 = 3 Na : 2K will apply to liquid NaK to a first approximation. The surface area factors are therefore Na, 2/5 and K, 3/5. In an alloy of composition 56.9% Na/ 43.1 % K by moles, the relative surface areas will therefore be Na : K, 56.9 x 2/5 : 43.1 x 3/5. Sodium occupies 46.8% of the surface, and potassium 53.2 %. The area determined, 0.132 mm^2 can therefore be said to consist 0.0618 mm^2 covered by sodium, and 0.0702 mm^2 covered by potassium.

(b) In the bubble.

The surface area of the metal was calculated indirectly in the following way. Every second, 20 mg of alloy are injected into the water. Since the NaK composition is 43.7% sodium by weight (56.9% by moles), this weight represents 8.74 mg of sodium and 11.26 mg of potassium. Of these metals, 4.7% of the sodium and 11.0% of the potassium react before reaching the bubble. Therefore in every second, $8.74 - (4.7 \times 8.74 \times 10^{-2}) = 8.33$ mg of sodium and $11.26 - (11.0 \times 11.26 \times 10^{-2}) = 10.03$ mg of potassium enter the bubbles as globules of alloy. 40 globules of metal enter the bubbles in one second (from Chapter 4). The total volume of the alloy in these 40 globules is 18.36/d where d is the density of the alloy, 0.894 mg/mm^3. [53] The volume of each globule is therefore 18.36 / (0.894 x 40), which equals 0.513 mm^3. The surface area of a sphere, volume 0.513 mm^3 is 3.10 mm^2. Therefore, each globule of metal contains, on formation, 0.208 mg of sodium (sodium entering bubbles per second /40) and 0.251 mg of potassium (10.03/40), and has a

surface area of 3.10 mm^2 on average. By a similar calculation as applied in part (a), the composition of the alloy reaching the bubbles is 58.5 mole% Na, and sodium atoms can be said to occupy 48.4% or 1.50 mm^2 and potassium 51.6% or 1.60 mm^2 of surface.

5.2.3, Time of Reaction

(a) At the jet.

This can be calculated directly from the flow rate, assuming that this value is the same at all points along the jet.

(b) In the bubble.

The rate of bubble rise at 20° C, from photographs was found to be 280mm/s. However, this value cannot be used in the rate calculations due to certain complications. The rate quoted was measured for spherical bubbles over a distance of less than 10 mm. Bubbles of the radius measured (0.242 cm.) are known to distort from sphericity and assume elliptical shapes after a short distance of travel, and this fact has been noted in these investigations (Photograph B, 4.3.1). The motion of these elliptical bubbles is considerably slower than spherical bubbles. Their motion has been described mathematically by Miyagi.[54] The motion over a distance z is given by equation 5.1.

$$\frac{1}{k}\, dv.\, \frac{d^2z}{dt^2} = gdv - \varnothing \left(\frac{dz}{dt}\right)^2 \qquad (5.1)$$

d=density of water, v=bubble volume, t=time

k and ϕ are coefficients of resistance to flow depending on the size of the bubbles, and can be calculated from the empirical formulae 5.2 and 5.3 which were determined by experiment. r is the radius of the bubble.

$$k = 0.054/r^2 \qquad (5.2)$$

$$\phi = (1.6r - 0.118 + \sqrt{0.49r^2 - 0.167r + 0.0142})^2 \qquad (5.3)$$

The solutions to Equation 5.1 are plotted as curve A in Figure 5.4. This curve applies to air bubbles in water at 18°C, and shows the variation in bubble velocity with bubble radius. For bubbles of radii 0 - 0.15 cm bubble velocity varies approximately linearly with radius. However, since both the buoyancy effect, producing an upward force on the bubble, and the resistance effect, producing a drag or downwards force, depend on r^3, a critical radius is reached, at which the velocity is a maximum. This critical radius is between 0.16 and 0.17 cm, shown as a broken line on Figure 5.4. Above this value, the velocity falls to a constant velocity of about 23.0 cm/s at 18°C. In adapting these figures to the present work, certain assumptions must be made:-

(i) The difference between the terms (d water - d air) and (d water - d hydrogen) is negligible. The buoyant force, F_B, depends upon the difference in densities of the liquid and the gas as shown by Equation 5.4.

FIG. 5.4. Variation in bubble velocity with bubble radius

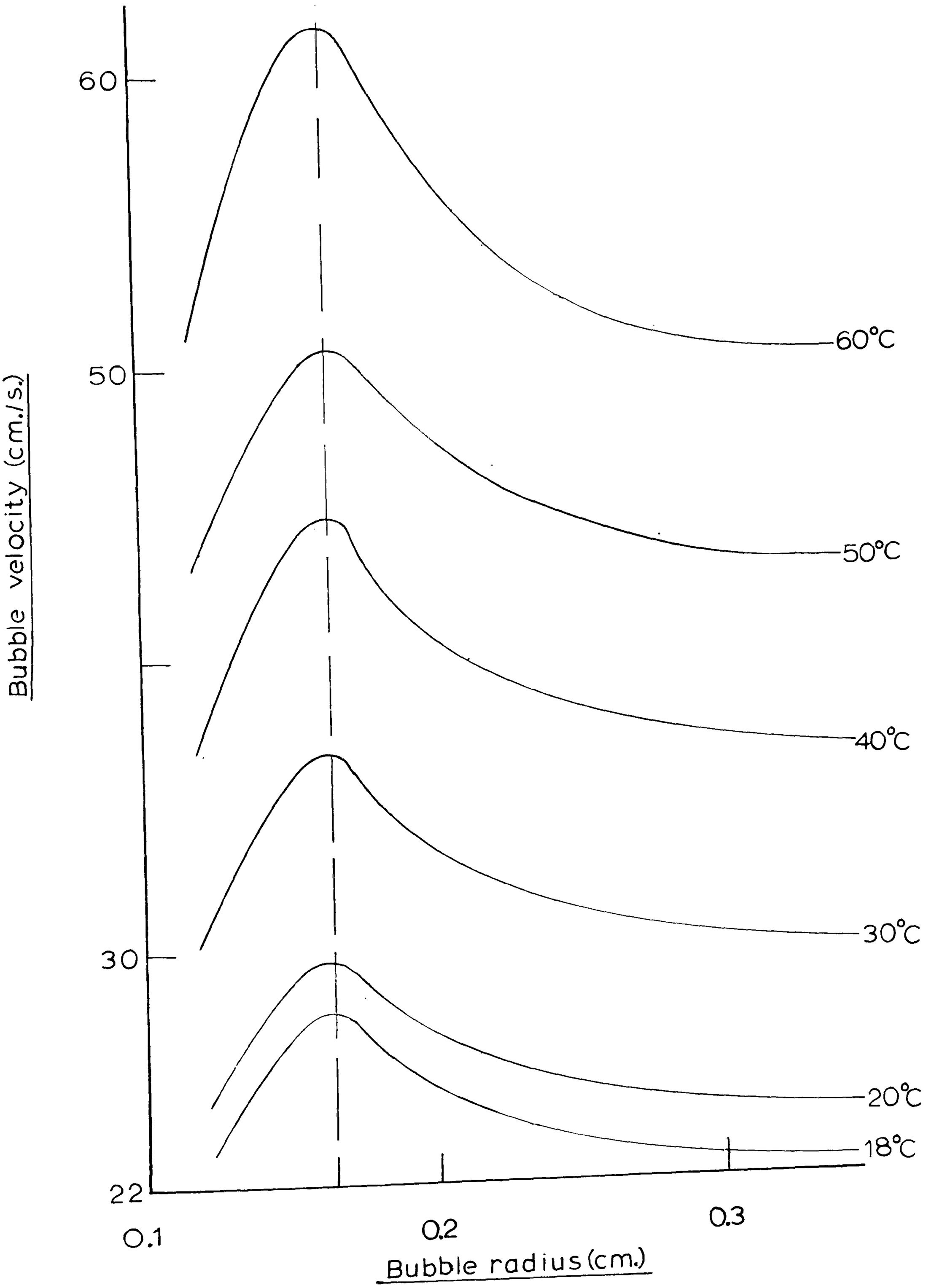

$$F_B = \frac{4}{3} g \ (d \text{ liquid} - d \text{ gas}) \ r^3 \qquad (5.4.)$$

(ii) Bubble velocities correspond to those read from the right hand (i.e high radius) side of Figure 5.3. This is the section of the graph where increasing radius has minimum effect on bubble velocity. In these experiments, initial bubble radii were all in the range 0.22 - 0.26 cm. (Section 4.3.2. (f)), and these radii increased substantially over short distances of travel due to reaction of the metal globule within the bubble to produce more gas.

(iii) At elevated temperatures, bubble velocity rises with the ratio d/u where u is the viscosity of the liquid. This assumption arises from analogy with small, spherical bubbles studied by Allen. [55].

Figure 5.4 gives that rate of bubble rise, for larger diameter bubbles, at 18°C, to be 23.0 cm/s. By means of the calculation outlined in (iii) above, the velocity at 20°C is 24.3 cm/s. This is smaller than the measured rate of 28 cm/s for reasons already stated. Since the velocity of bubble rise is known, and the gradient of the graph (Fig 5.3) is in the units moles reacting/mm, multiplication of these figures should give the units moles / second x 10^2 for the rate calculations.

5.2.4. The rate calculation

Reaction rates were calculated for each of the two

metals, in each of the two stages of the reaction.

(a) At the jet.

Of the 8.74 mg of sodium entering the water every second, 4.7% reacts over a surface area of 0.0618 mm. The reaction rate is therefore:

$$\frac{4.7}{10^2} \times \frac{8.74 \times 10^{-3}}{23.0} \times \frac{1}{6.18 \times 10^2} = 2.88 \times 10^{-4} \text{ moles/s/mm}^2$$

Similarly for potassium:

$$\frac{11.0}{10^2} \times \frac{11.26 \times 10^{-3}}{39.1} \times \frac{1}{7.02 \times 10^2} = 4.52 \times 10^{-4} \text{ moles/s/mm}^2$$

(b) In the bubble

Of the 20mg of metal entering the water per second, for each millimetre of (initial) bubble rise, 0.31% of the sodium (0.027 mg) and 0.29% of the potassium (0.033 mg) react. This represents 1.17×10^{-6} moles of sodium and 8.44×10^{-7} moles of potassium. Since 40 globules of metal are produced every second, 2.92×10^{-8} moles of sodium and 2.11×10^{-8} moles of potassium react per globule per millimetre rise. The rates of reaction become, for sodium :

$$2.92 \times 10^{-8} \times 243 \times \frac{1}{1.5} = 4.73 \times 10^{-6} \text{ moles/s/mm}^2$$

Similarly for potassium:

$$2.11 \times 10^{-8} \times 243 \times \frac{1}{1.6} = 3.20 \times 10^{-6} \text{ moles/s/mm}^2$$

5.3 SEPARATION EXPERIMENTS BETWEEN 20°C AND 60°C

In order to investigate the effect of temperature on reaction rate, and derive an apparent activation energy, experiments were carried out over a temperature range of 20–60°C. It had already been established (Section 5.2) that a plot of percentage of metal reacting against water height was linear below 100 mm. Therefore, two standard heights of water below this value (35 mm and 67 mm) were chosen. The results are shown in Table 5.2 and Figures 5.5 and 5.6. The points marked at 20°C on both of these graphs were read from Figure 5.3.
Values of the quantity of metal reacting were selected from Figures 5.5 and 5.6 at 30, 40, 50 and 60°C. These values were then used to construct the straight lines of per cent metal reacting vs. height of water shown in Figure 5.7. The two heights are shown as broken lines on this graph. The data used in the construction of these lines, and the results of the construction are shown in Table 5.3.

TABLE 5.2 RESULTS OF SEPARATION EXPERIMENTS BETWEEN 20 and 60°C

Temperature (°C)	Height (mm)	% Potassium reacting	% Sodium reacting
26.0	35	27.4	20.0
30.0	35	38.4	31.2
35.0	35	33.1	26.9
41.0	35	38.2	31.9
47.0	35	43.6	38.8
52.0	35	46.0	45.4
55.0	35	56.3	53.6
60.5	35	52.9	50.3
31.5	67	41.8	34.8
35.5	67	43.1	34.5
40.0	67	53.3	47.2
45.0	67	54.8	49.7
50.0	67	56.4	51.0
54.5	67	70.3	68.4
59.0	67	70.3	70.3

FIG. 5.5 % of sodium reacting vs. temperature

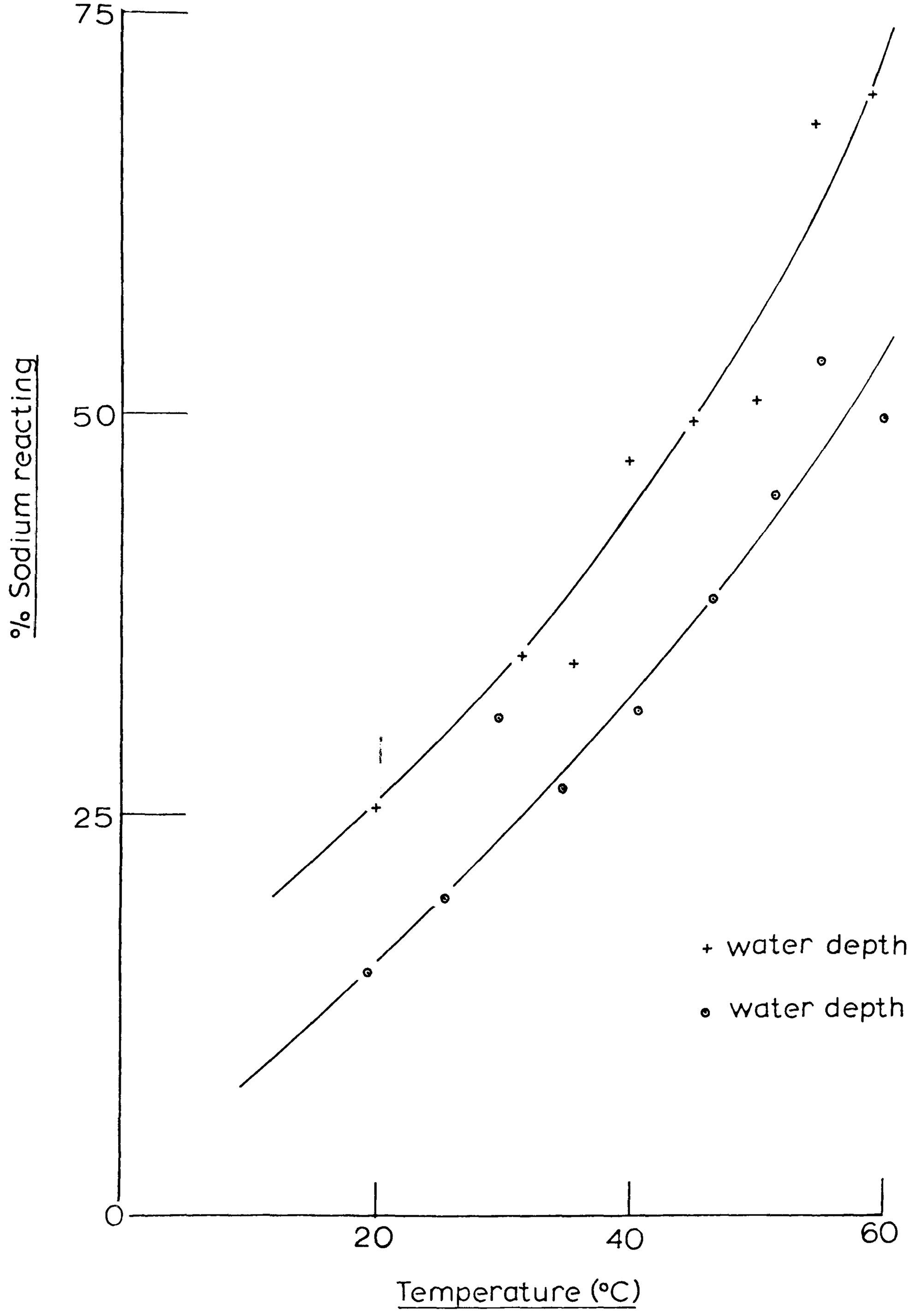

FIG. 5.6 % of potassium reacting vs. temperature

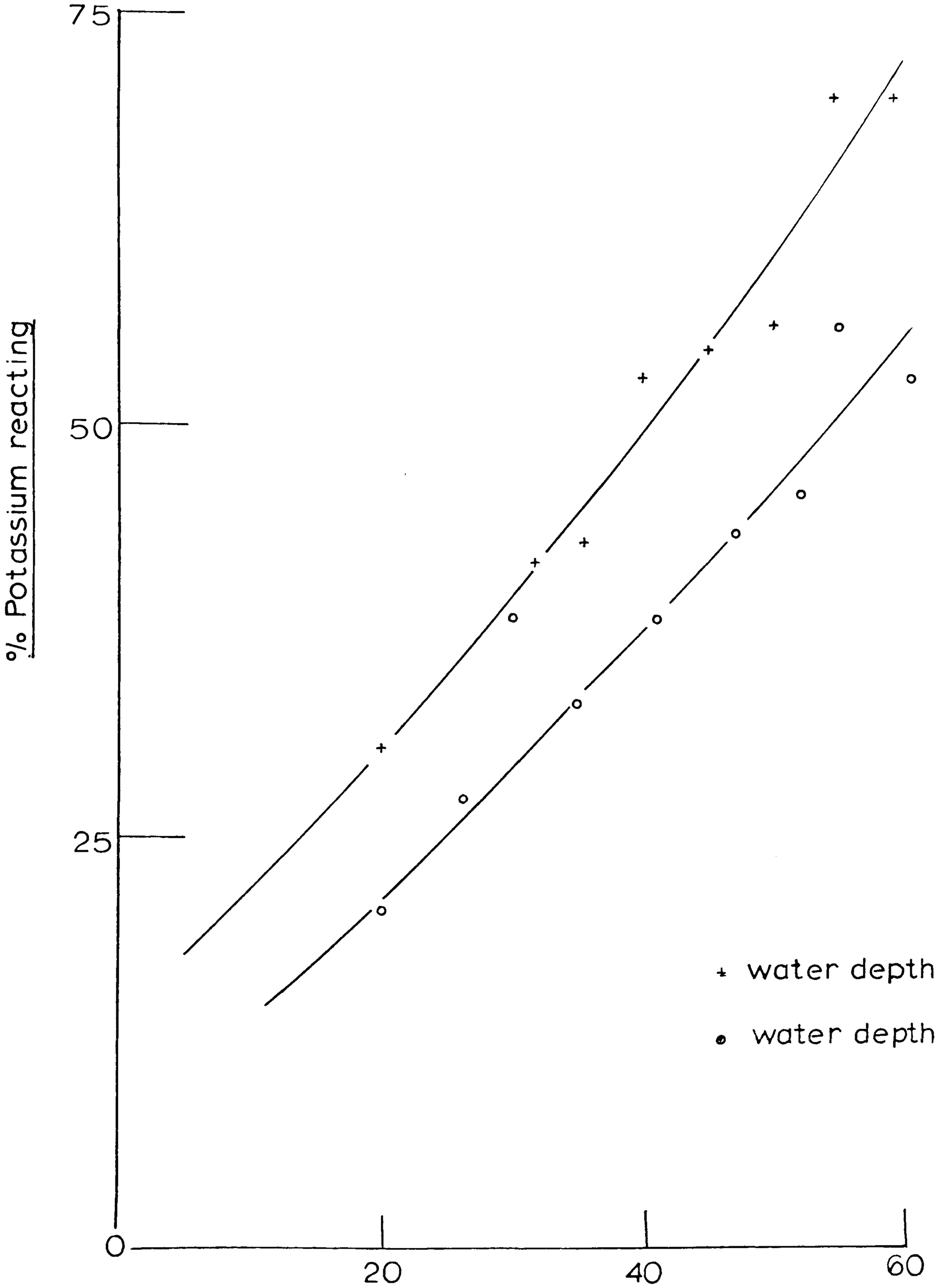

FIG. 5.7 Construction lines for the calculation of reaction rates

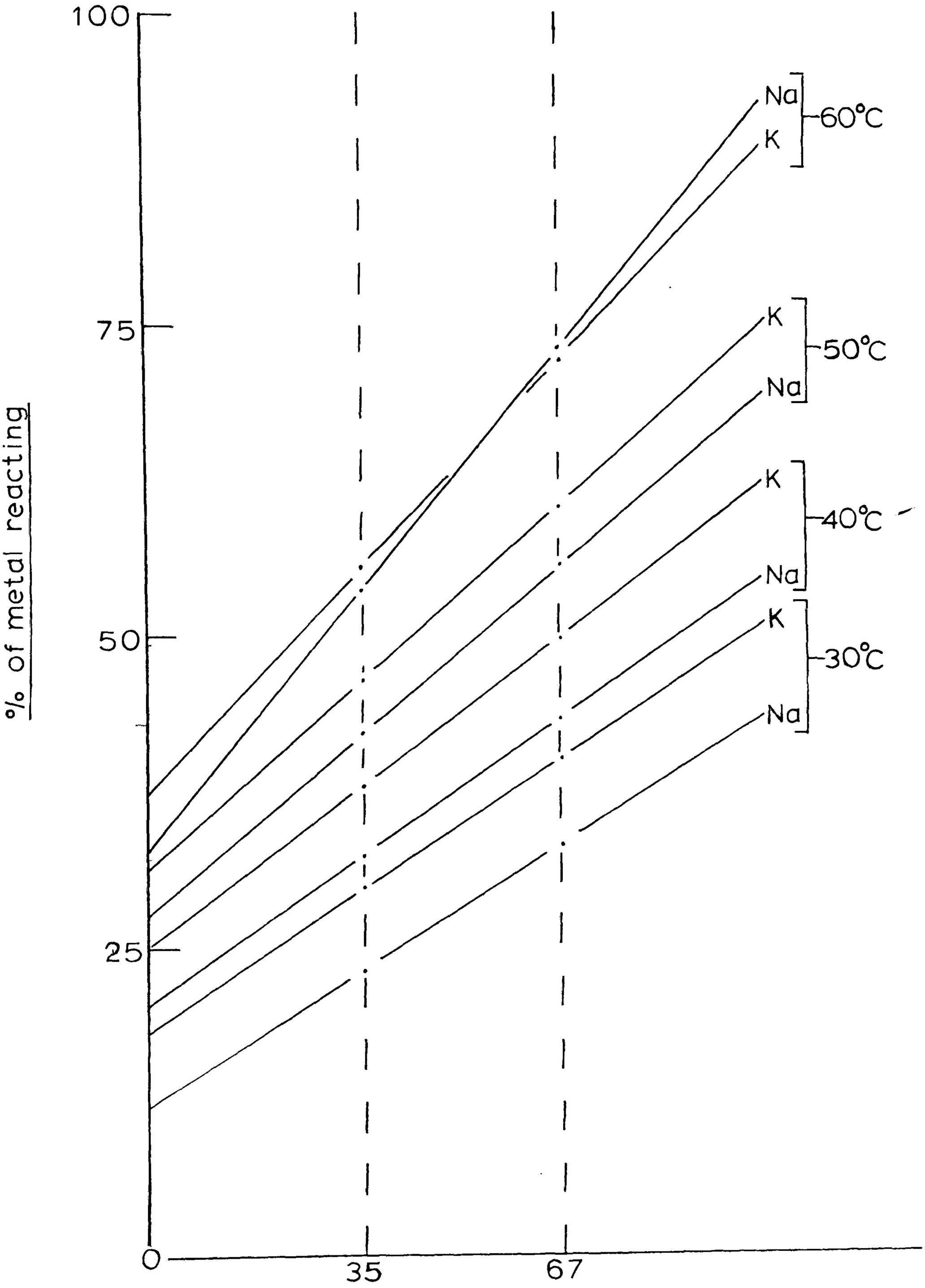

TABLE 5.3 PERCENTAGE OF METAL REACTING AT VARIOUS TEMPERATURES

METAL	TEMP C	VALUES OF % METAL REACTING (from Figures 5.5 and 5.6)		RESULTS FROM CONSTRUCTION (Fig. 5.7)	
		Height =35mm	Height = 67mm	% Metal reacting at jet	% Metal reacting per mm travel
Sodium	30	23.4	33.2	12.8	0.306
Sodium	40	32.3	43.2	20.5	0.341
Sodium	50	42.2	55.8	27.6	0.425
Sodium	60	53.9	73.2	32.9	0.603
Potassium	30	29.4	39.8	18.4	0.325
Potassium	40	37.9	49.6	25.0	0.366
Potassium	50	46.4	60.2	31.4	0.431
Potassium	60	55.3	71.8	37.3	0.516

In order to calculate reaction rates from these data, a similar procedure to that described in Section 5.2 was employed. However, since no photographic data were available for experiments above 20°C, two assumptions were made:-

(i) That the liquid metal thread exposes 0.132 mm^2 of surface to the water at water temperatures up to60°C (as it did at 20°C)

(ii) That this thread breaks up into 40 gas-encased globules of metal per second at these temperatures (as it did at 20°C).

The total surface area in all cases was 0.132 mm^2 (assumption (i)). At 20°C this area could be broken down into 0.0618 mm^2 occupied by sodium and 0.0702 mm^2 by potassium. Since the NaK composition in these experiments was the same as that for the experiments in Section 5.2 these surface areas of individual metals apply to the experiments at temperatures 30,40,50 and 60°C. However, the surface areas of the metals in the form of metal globules, in the second stage of the reaction, will vary with increasing temperature for two reasons. Firstly, more metal reacts at the jet. Thus, less metal is available for the globules which are consequently smaller, since the same number are produced at all these temperatures (assumption (ii)). Secondly, the NaK composition in the globules varies, since the proportion of sodium and potassium reacting at the jet are different for each temperature.

The surface area calculations were carried out by the following steps:-

(a) The volume of metal in one metal globule (v) is given by Equation 5.5.

$$v = \frac{20 - a - b}{40d} \quad mm^3 \qquad (5.5)$$

where d = alloy density in mg/mm^3

a = mass of sodium reacting at jet per second = % Na reacting x 8.74 mg.

b = mass of potassium reacting at jet per second = % K reacting x 11.26 mg.

(b) The surface area of one metal globule (s) is given by Equation 5.6

$$s = \sqrt[3]{36v^2} \qquad (5.6)$$

(c) The mole% of sodium in the alloy forming the metal globules is given by Equation 5.7.

$$\text{Mole\% Na} = \frac{(8.74 - a) \times 100}{23.0\left[\left(\frac{8.74 - a}{23.0}\right) + \left(\frac{11.26 - b}{39.1}\right)\right]} \qquad (5.7.)$$

(d) The percentage of the surface covered by each of the two metals therefore becomes:

$$\text{\% covered by Na} = \frac{\text{mole \% Na x 2/5 x 100}}{(\text{mole\% Na x 2/5}) + (\text{mole \% K x 3/5})}$$

and likewise for potassium. The fractions 2/5 and 3/5 are the surface area factors to take into account the disparity in the atomic sizes. These factors have been

explained in Section 5.2.2.

The surface areas of the individual metals, from these calculations and the values in Table 5.3 become:-

Temperature (°C)	30	40	50	60
Surface area of 1 globule (mm^2)	2.93	2.76	2.60	2.46
Area of sodium per globule (mm^2)	1.42	1.33	1.25	1.19
Area of potassium per globule (mm^2)	1.51	1.43	1.35	1.27

The same time factor was used in the calculations of the jet reaction rate at these higher temperatures as at 20°C. The factor for the 'bubble stage' of the reaction was the velocity of the bubble, and the appropriate values were read from Figure 5.4. They were:-

30°C	40°C	50°C	60°C
30.2 cm/s	36.8 cm/s	43.7 cm/s	51.0 cm/s

The reaction rate calculations (see Section 5.2.5) yielded the results presented in Table 5.4.

TABLE 5.4. REACTION RATES FOR M + H_2O AT VARIOUS TEMPERATURES

	Rate at jet (moles/s/mm^2 x 10^4)	Rate in bubble (moles/s/mm^2 x 10^6)
Sodium (30°C)	7.85	6.18
Sodium (40°C)	12.57	8.96
Sodium (50°C)	16.92	14.12
Sodium (60°C)	20.17	24.55
Potassium (30°C)	7.56	4.68
Potassium (40°C)	10.28	6.78
Potassium (50°C)	12.91	10.05
Potassium (60°C)	15.33	14.92

5.4. DISCUSSION

The conclusions from this series of experiments may be summarised as follows:

(a) The rate of reaction at the jet stage is approximately 100 times that in the 'bubble' or 'hydrogen protected' stage. Moreover, the rate determined for the reaction at the jet represents a lower limit for the process $M_{(l)} + H_2O_{(l)}$ since the reactants may be separated by either an invisible film of water vapour, product gas, or a solid hydroxide film on the metal, which is in dynamic equilibrium with the surrounding solution. Figure 5.8 shows this possibility.

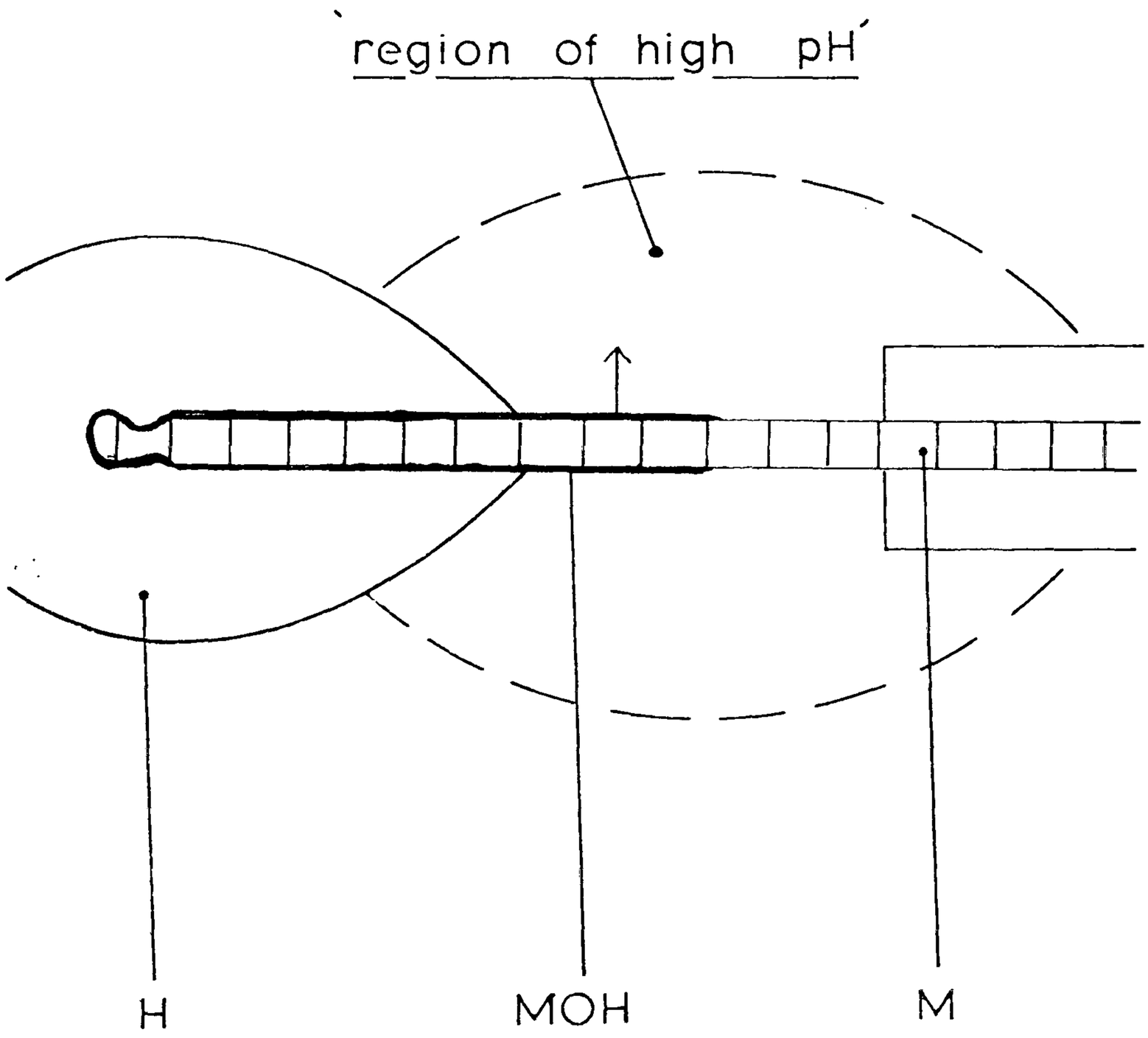

Fig. 5.8. THE ENVIRONMENT OF THE METAL JET

The hydroxide is continually dissolving, producing a region of high pH around the jet, and the solid film barrier continually reforms due to the continued reaction of the metal. The effect of changing the product from hydroxide to a less soluble salt will be examined in Chapter 7.

(b) The rate of reaction for the bubble stage is also complicated by the interference of reaction products i.e the hydrogen bubble. Moreover since the reaction of the metal in the bubble may be that of $M_{(l)} + H_2O_{(g)}$, plus a contribution from $M_{(l)} + H_2O_{(l)}$ as the globule comes into contact with the bubble walls, the values determined for this part of the system represent an upper limit for the former process.

Clearly, these solid and gaseous reaction products have a marked effect on the overall reaction rate. Further details of the effect of hydrogen are investigated in Chapter 8.

(c) The difference between the reaction rates of sodium and of potassium with water are small in both stages of the reaction (compare the upper and lower halves of Table 5.4). Although a higher proportion of the potassium in the alloy reacts than is the case for sodium (11.0%K, 4.7%Na at the jet at 20°C), each mole of potassium, however, has a much larger surface area assigned to it, so that results in terms of moles/s/mm^2 break down to approximately the same values for each metal.

(d) Reaction rates increase at elevated temperatures. There is no immediately apparent why this should be so, since the temperature of the metal itself is likely to be several hundred degrees higher than the bulk water temperatures,[45] and an increase in water temperatures of a few tens of degrees should have an insignificant effect. For some reason, therefore, heat from the metal is prevented from being transmitted to the surrounding liquid water,

but when this is heated externally, a rise in reaction rate is noted.

According to Equation (5.8), the Arrhenius equation[56],

$$K = A\exp(-E^{\ddagger}/RT) \qquad (5.8)$$

a plot of $\log_{10}$ against the reciprocal of the absolute temperature should yield a straight line of slope $-E^{\ddagger}/2.303R$ where $E^{\ddagger}$ is the temperature independent activation energy for the reaction, and R the gas constant. For first order alkali-metal gas reactions, Herold[57] has defined an expression for the absolute rate constant, Kabs, in order to compare the rates of reaction of the alkali-metals in widely differing systems. This expression appears as Equation (5.9). dv/dt is the change in volume, reduced to S.T.P., with time during the reaction.

$$\text{Kabs } (cm^3(\text{S.T.P.})s^{-1}.cm^{-2}\ Pa^{-1}) = \frac{dv}{dt} \times \frac{1}{s} \times \frac{1}{p} \qquad (5.9)$$

s is the surface area in cm^2, and p is the pressure in Pascals. With the assumption (since the rates of reaction in this chapter are defined in terms of disappearance of metal) that 1 mole of sodium ≡ 1 mole water in this reaction, and that 1 mole of water occupies 22451 cm^3 at S.T.P., values of Kabs were calculated for the results in Table 5.4. These values are presented in Table 5.5.

Figure 5.9 shows the Arrhenius plot for these reactions. In general, fairly good straight lines were obtained, particularly for the reactions in the bubble. The lines yielded the following activation energies:-

TABLE 5.5 VALUES OF K_{abs} FOR THE REACTION M + $H_2O_{(l,g)}$

Metal	Situation	Temp (°C)	$\frac{1}{T} \times 10^3$ (K^{-1})	K_{abs}	$Log_{10}K_{abs}$
Sodium	Jet	20	3.413	6.38×10^{-3}	-2.195
Sodium	Jet	30	3.300	1.74×10^{-2}	-1.760
Sodium	Jet	40	3.195	2.79×10^{-2}	-1.554
Sodium	Jet	50	3.096	3.74×10^{-2}	-1.427
Sodium	Jet	60	3.003	4.47×10^{-2}	-1.350
Potassium	Jet	20	3.413	1.00×10^{-2}	-2.000
Potassium	Jet	30	3.300	1.68×10^{-2}	-1.775
Potassium	Jet	40	3.195	2.28×10^{-2}	-1.642
Potassium	Jet	50	3.096	2.86×10^{-2}	-1.544
Potassium	Jet	60	3.003	3.40×10^{-2}	-1.469
Sodium	Bubble	20	3.413	1.05×10^{-4}	-3.979
Sodium	Bubble	30	3.300	1.37×10^{-4}	-3.863
Sodium	Bubble	40	3.195	1.99×10^{-4}	-3.701
Sodium	Bubble	50	3.096	3.13×10^{-4}	-3.505
Sodium	Bubble	60	3.003	5.44×10^{-4}	-3.264
Potassium	Bubble	20	3.413	7.09×10^{-5}	-4.149
Potassium	Bubble	30	3.300	1.04×10^{-4}	-3.983
Potassium	Bubble	40	3.195	1.50×10^{-4}	-3.824
Potassium	Bubble	50	3.096	2.23×10^{-4}	-3.652
Potassium	Bubble	60	3.003	3.31×10^{-4}	-3.480

FIG. 5.9 Arrhenius plot for the reactions of NaK with water

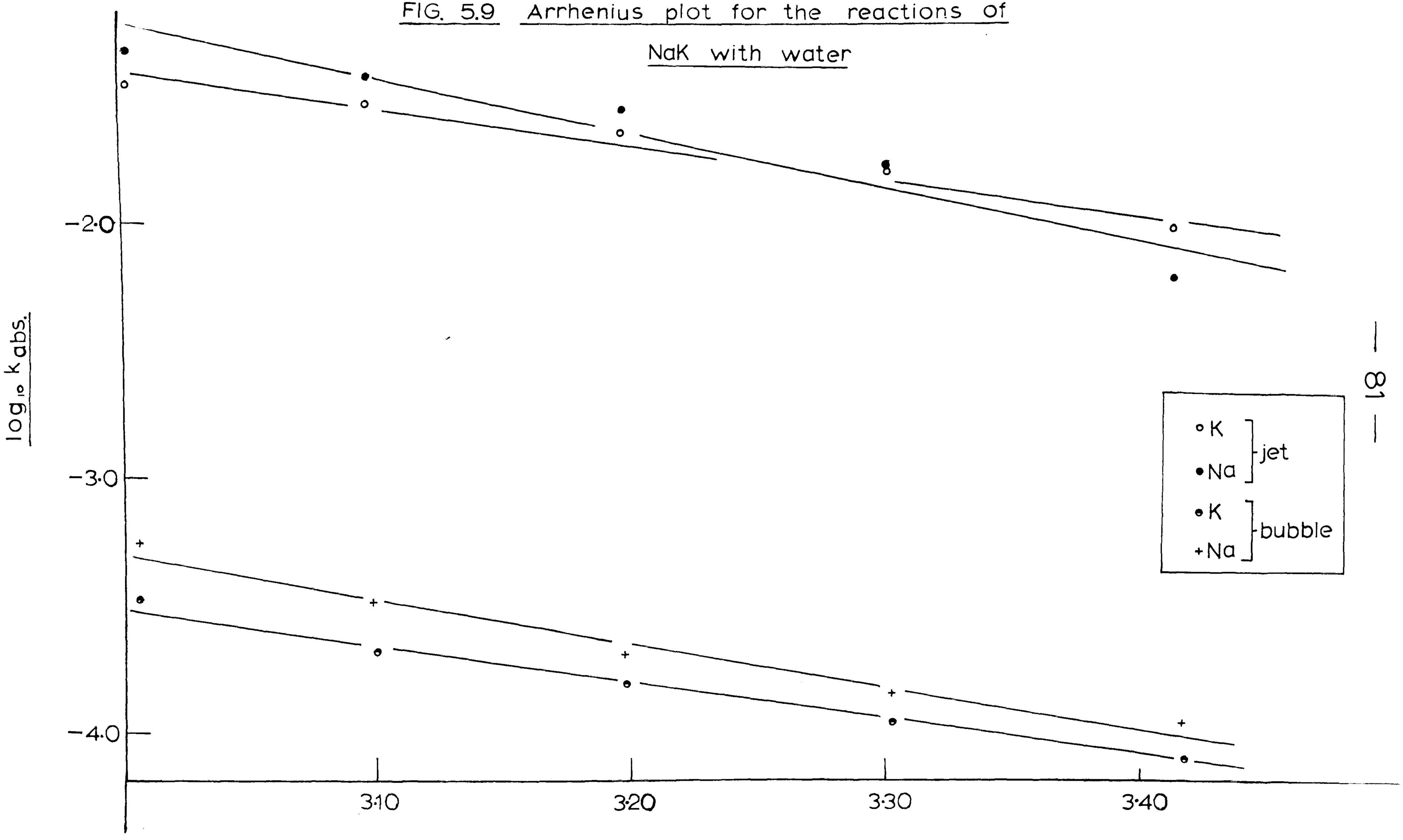

Na (jet) - 38.29 KJ/mole

Na (bubble) - 33.03 KJ/mole

K (jet) - 24.89 KJ/mole

K (bubble) - 27.28 KJ/mole

These results were obtained over a fairly limited temperature range due to the limitations of the apparatus and method. However, they show that the activation energy for the reaction of potassium with water, in both stages of the reaction, is less than that for sodium, as might be expected. A full comparison of these values with previously reported activation energies for alkali-metal / water reactions appears in Chapter 10.

C H A P T E R V I

THE REACTION OF LIQUID SODIUM WITH LIQUID WATER

6.1. INTRODUCTION

The experiments described in Chapter 5 provide a picture of the physical processes occurring during an alkali-metal / water reaction, as well as some rate data for the reactions of sodium and potassium individually. However, complications arose in the calculations of the surface area of metal exposed to water. The treatment described in Section 5.2.2. assumes an ideal solution i.e. that there is no preferential enrichment in the surface of the alloy of either the sodium or potassium, and that the bonds between Na - Na, Na - K and K - K are all approximately equivalent in strength. Employing sodium alone as the liquid metal reactant should remove this assumption and perhaps justify the assumptions made for the alloy rates.

Most liquid metal fast breeder reactors employ liquid sodium as the coolant, and so the reaction between un-alloyed sodium and water may be of more interest practically.

NaK was originally chosen as the alkali-metal reactant in the present work mainly because no external heat is needed to keep it molten. In order to investigate the reaction of sodium, the procedures and apparatus outlined in Chapter 3 had to be considerably modified. It was, of course, found necessary to heat not only the metal, prior to injection, but also the injection apparatus, and in particular, the 0.1 mm. capillary attachment. The new procedures and apparatus are described in the following sections.

6.2 APPARATUS

The reaction vessel was similar to the one shown in Figure 3.3 except that the adaptor on the sidearm (A) was changed to a B 14 socket, to take account of the larger barrel diameter of the modified injection apparatus.

The liquid metal injector is shown in Figure 6.1. The design is basically the same as before, with the inclusion of a gas by-pass (B) and a heating jacket. The heating agent employed was dry oil, capable of withstanding temperatures of about 200°C without smoking. This was pumped from a heated reservoir through rubber tubing by means of a peristaltic liquid pump. Oil from the jacket outlet was returned to the reservoir. All tubing, and the heating jacket itself were lagged with cotton wool and refrasil.

The maximum flow rate of oil, with 10 mm (internal diameter) thick walled rubber tubing was approximately 2000 mm^3 per second. With this flow rate, and an oil temperature of 175°C at the reservoir, the temperature at point A (Figure 6.1) was in the range 120 - 130°C after a period of 10 minutes flow. To allow the thick walled capillary glass section to thoroughly heat up to above the melting point of sodium (97.8°C), heating was continued for two hours prior to liquid sodium injection.

6.2. PROCEDURE

The oxide-coated surfaces of sodium were cut away under an argon atmosphere. Cut into cubes, of approximate dimensions 50 mm., the metal was quickly transferred to the injector barrel. A continous flow of argon swept the

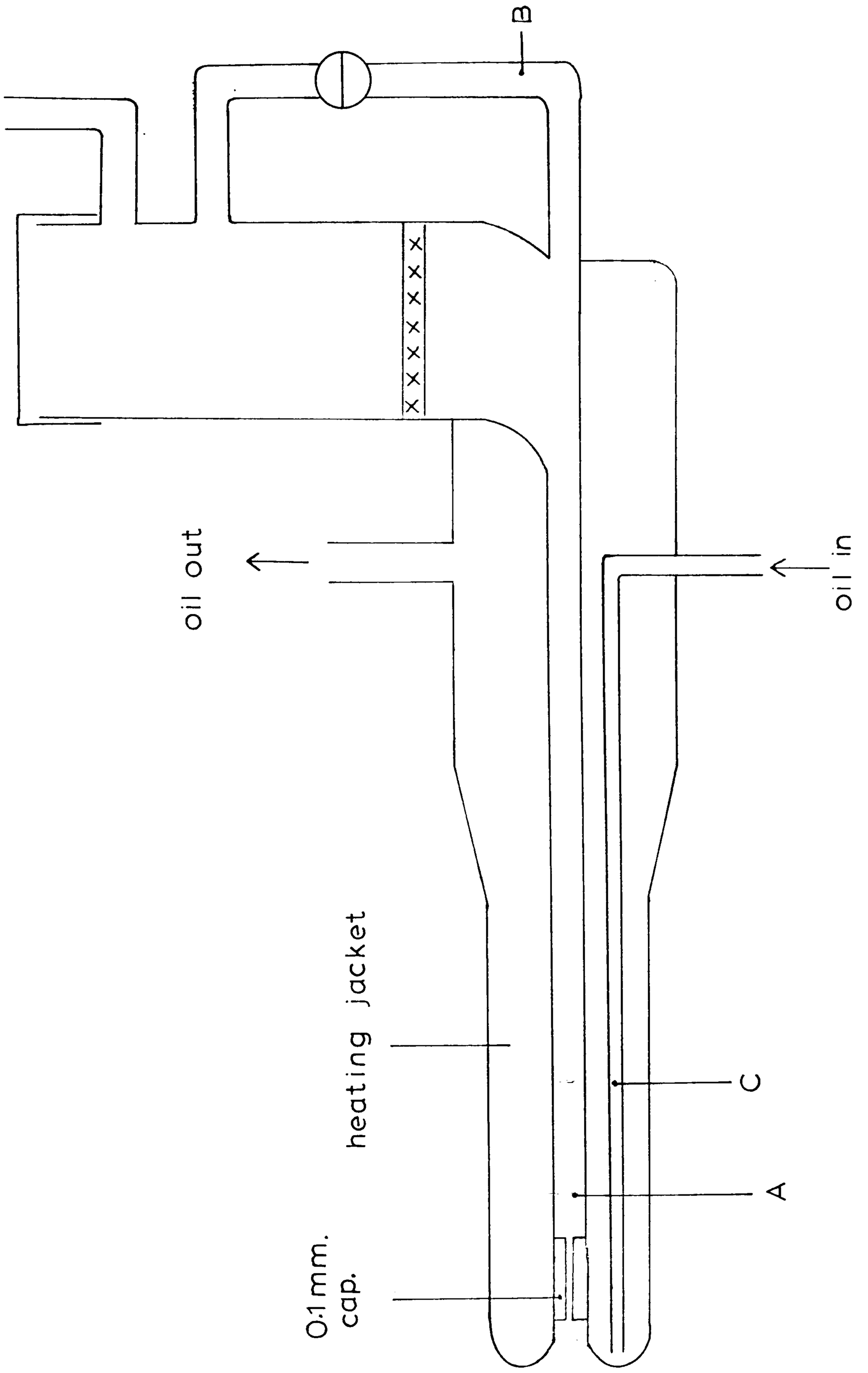

FIG. 6.1 The liquid sodium injection apparatus

injector. This was then sealed with a tightly fitting rubber septum cap, and the argon pressure increased to 69 KPa. The argon by-pass tap was kept open while the metal in the injector barrel was heated externally by either heating tapes at 400°C or a bunsen flame. A bunsen burner was preferred for this task, since direct, local heating was needed to free occasional metal blockage below the sintered glass filter. When molten, the metal rested on the filter until the gas by-pass was closed. The metal then flowed, as with NaK, through the filter and into the pre-heated narrow section of the injector, and thence to the capillary, all oxide and other impurities being left on the filter.

The procedure from then was identical to that described in Section 3.5.

Heating of the injector indirectly also led to heating of the bulk water, at a rate of approximately 5°C per hour, depending upon the depth of water being used. External stirring, using a magnetic flea and rotating magnet, was therefore necessary in order to minimise thermal gradients in the system. Injections were carried out when the water temperature, measured by a thermocouple junction and recorded on a chart recorder, reached 30°C. As with injections of NaK, no significant temperature rise in the bulk water was noted during or immediately after injection of the metal, which generally lasted between one and five seconds. Injection of the metal was halted usually by blockage of the capillary rather than shortage of metal. The external stirring was halted during metal injections, in order to avoid water turbulence.

6.4 INITIAL RESULTS

Preliminary experiments were recorded on video tape. Observation of the area around the liquid metal jet was difficult due to the focusing of the camera, and also because of the nature of the injector. It was necessary, for technical reasons, for the heating jacket around the capillary to protrude further into the water than the capillary opening (see Figure 6.1.). This was to ensure that the thick walled capillary could be heated to the desired temperature. However, the extension of the heating jacket in this way tended to obscure the area where the metal first entered the water.

Despite these drawbacks, it was possible to observe a situation similar to that previously described i.e. a liquid metal jet entered the water. It was surrounded by an envelope of hydrogen. The jet broke up into metal globules which moved vertically through the water, each one 'trapped' in its own protective bubble of gas. On the strength of these observations, certain assumptions could be made in the rate calculations.

6.5. RESULTS OF SEPARATION EXPERIMENTS

These results are presented in the same form as previously i.e. percentage of metal reacting compared with height of water column (distance travelled). They are shown in Table 6.1 and Figure 6.2. As before, the graph intercepts the 'y' axis to give an indication of the extent of reaction at zero water height i.e. the reaction

TABLE 6.1. RESULTS OF SEPARTION EXPERIMENTS FOR $Na_{(l)} + H_2O_{(l)}$ AT 30°C.

Water height (mm)	Percent Scdium reacting
24.0	35.06
30.0	26.00
32.5	28.50
40.0	32.20
53.0	36.10
66.0	42.15
75.0	49.20
86.0	46.00

FIG. 6.2 % of sodium reacting vs. water height at 30 °C

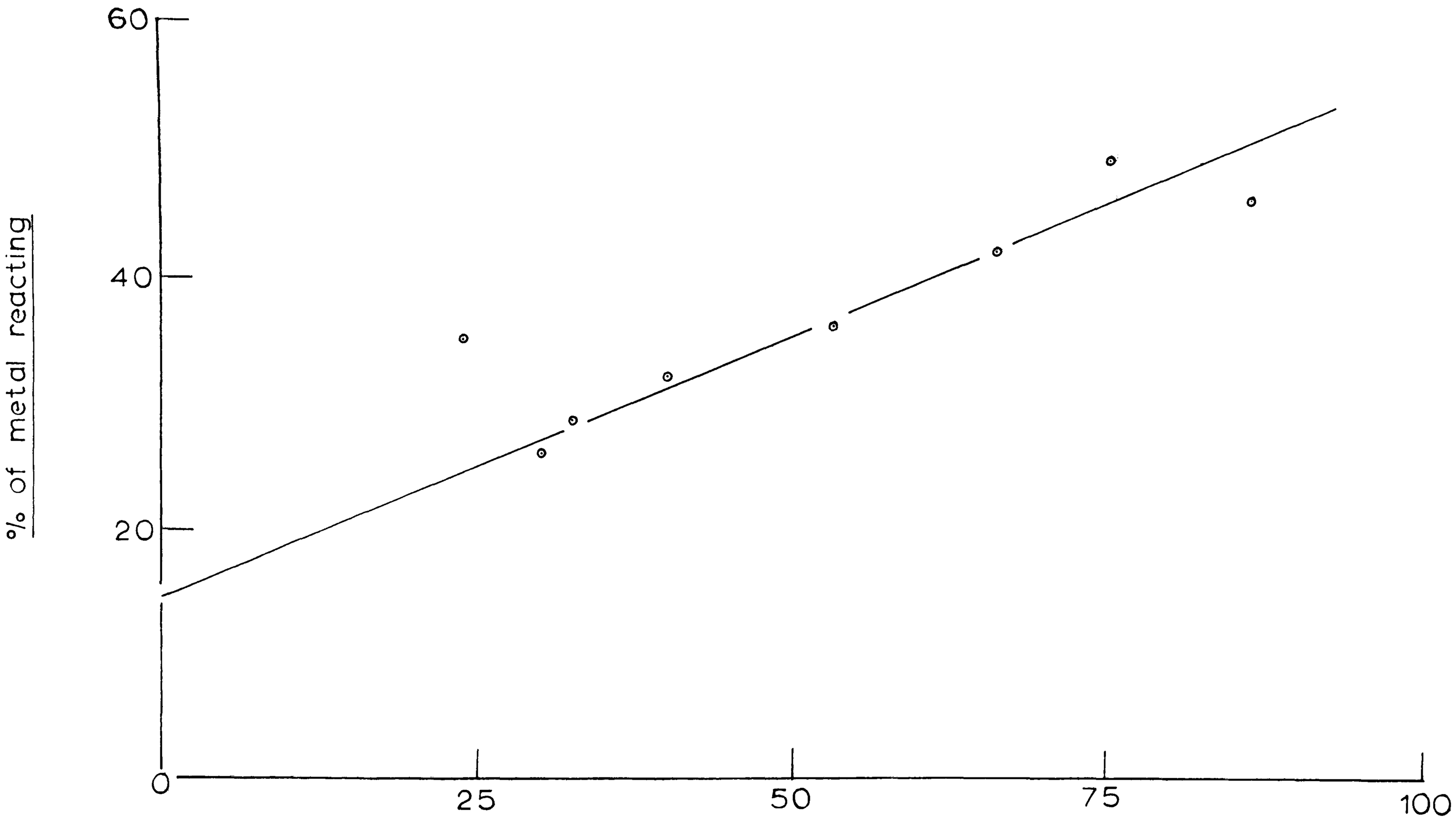

at the jet. The intercept from the graph is at 14.2% metal. The graph also seems to be linear within the range of column heights used i.e below 100 mm, with a gradient of 0.423% per millimetre travel.

Since no photographic measurements were available (in fact, none were possible due to the nature of the apparatus), the following assumptions were made in the rate calculations:-

(a) That the metal flow rate was 20 mg/s. A comparison of densities ($Na_{(100)}$, 0.927g/cm^3, and $NaK_{(20)}$, 0.984 g/cm^3) indicates that, to a first approximation, this is justified.

(b) That the surface area factors are the same as those for NaK + H_2O i.e that on average, 0.42 mm of the liquid metal thread has no visible hydrogen gas protection, and that the thread breaks up into 40 globules of metal every second.

(c) That the rate of bubble rise at 30°C is 30.2 cm/s i.e that the bubble radius is greater than 0.17 cm.

Calculation of reaction rates now follows a similar pattern to that outlined in Section 5.2.

Reaction at the jet. 14.2% of the 20 mg of sodium entering the water every second reacted at the jet over a surface area of 0.132 mm^2. The reaction rate is therefore:-

$$\frac{14.2}{100} \times \frac{20 \times 10^3}{23.0} \times \frac{1}{0.132} = 9.67 \times 10^{-4} \text{ moles/s/mm}^2$$

Reaction in the bubble. Each of the 40 globules formed in one second contains $20 - \left(\frac{14.2}{100} \times 20\right)$ or 0.429 mg of sodium. The volume of such a $\frac{}{40}$ globule is 0.463 mm^3.

A sphere with this volume has a surface area of 2.895 mm^2. For each millimetre of bubble rise, 0.423% of the injected sodium reacts. This represents 8.46×10^{-2} mg. of sodium, or 2.115×10^{-3} mg per bubble. The rate of reaction is therefore:-

$$\frac{2.115 \times 10^{-6}}{23.0} \times 302 \times \frac{1}{2.895} = 9.59 \times 10^{-6} \text{ moles/s/mm}^2$$

6.6 CONCLUSIONS

In many respects, the reaction resembled that for NaK with water:

(a) The reaction could be separated into two parts, that at the jet, and that in the bubble.

(b) Of the metal injected, a small proportion (14.2%) reacted immediately at the jet.

(c) The reaction rate at the jet was approximately 100 times faster than that in the bubble.

Because of these similarities, it is possible to conclude that the general picture applies to all the alkali-metals in reactions of this type with water, regardless of the initial temperature of the metal up to the melting point of sodium (97.8°C)

It is interesting to compare the rate of reaction of sodium alone, and when it is alloyed with potassium. The relevant rates are shown in Table 6.2. The general order of these reaction rates are the same. There is however, a small but real difference in that the rate of reaction for un-alloyed sodium is slightly higher.

TABLE 6.2. RATES OF REACTION OF $Na_{(l)}$ AND $Na(NaK)_{(l)}$ WITH WATER AT 30°C

Reaction	Rate (moles/s/mm^2)
$Na_{(l)} + H_2O_{(l)}$ (jet)	9.67×10^{-4}
$Na(NaK)_{(l)} + H_2O_{(l)}$ (jet)	7.85×10^{-4}
$Na_{(l)} + H_2O_{(l,g)}$ (bubble)	9.59×10^{-6}
$Na(NaK)_{(l)} + H_2O_{(l,g)}$ (bubble)	6.18×10^{-6}

A possible explanation for this lies in the tendency of the two metals to form a compound in NaK. The compound in question, Na_2K, appears in the phase diagram at about 33 mole%K.[50] Although this is an incongruently melting compound of low thermal stability, breaking down into α and liquid at 7°C, perhaps this compound still persists in the liquid, the more so at low temperatures, and reduces the reactivity of the sodium component of the alloy.

6.7. SOME PRACTICAL CONSIDERATIONS

The original system for high temperature injections employed an injector similar to the one depicted in Figure 6.1 but without the directional glass jet (C). Although temperatures reached 160°C in certain parts of the injector barrel, the temperature towards the end (i.e near the capillary) did not rise above 80°C. Due to the thick (4mm external diameter) walls of the capillary attachment, it was estimated that a temperature of 120°C would be needed in the part of the injector barrel close to the capillary to keep the centre of the capillary above the melting point of sodium. This thermal gradient was accentuated by the cool flow of argon which passed through the centre of the capillary. Hence the greatest single difficulty in these experiments was blockage of the capillary by solid metal. This could only be overcome by extending the heating jet right up to the end of the capillary, and by prolonged heating of the injector before injection was attempted.

C H A P T E R V I I

REACTIONS OF NaK WITH AQUEOUS SOLUTIONS OF ACIDS, ALKALIS AND SALTS

7.1. INTRODUCTION

It has been reported that, in the reaction between the alkali-metals and water, the metals react not only with water molecules, but also with hydrogen ions (Equations 2.14, 2.15, 2.16) even at low hydrogen ion concentrations.[39] It is likely, therefore, that the rate of reaction between a liquid alkali-metal thread and water is sensitive to pH, an increase in the concentration of H_3O^+ producing a corresponding increase in reaction rate. It has already been noted (experiment 10, Chapter 4) that the reaction between 5.5 Molar H_2SO_4 and NaK is vigorous, more so than that between water and NaK, yet still controllable using the present system. The reaction between NaK and acid solutions in the second, or 'hydrogen protected', stage of the system should also be subject to the same influences of pH since the bulk of the reaction in this stage is likely to occur when globules of metal contact the gas/liquid interface. Changes in reaction rate may also be attributed to the nature and concentration of the anions. If the rate determining step is the rate of dissolution of the product layer, and this again applies both to reaction at the jet and reaction in the bubble, then the nature of the product film is critical. Substitution for water by dilute mineral acids has the effect of producing simple alsali-metal salts, most of which are less soluble than

sodium and potassium hydroxides. The absolute solubility of these salts may have a bearing, then, on reaction rates, although, strictly speaking, it is the rate of dissolution which is important.

The purpose, then, of the experiments described in this chapter is to investigate some aspects of the reaction $M_{(l)} + H_3O^+_{(aq)}$, and to determine the importance of the products on the rate of reaction.

7.2. NaK + H_2SO_4 SOLUTIONS - RESULTS

The procedures and apparatus described in Chapter 3 were used, and a series of experiments were carried out in which solutions of sulphuric acid were substituted for water. The argon pressure again was 69 KPa. Capillary diameters were in the range 0.1 - 0.2 mm; the composition of the alloy was in the range 40 - 50 mole% sodium, and all these experiments were carried out at 20°C. A standard water depth of 80 mm was chosen, and the sulphuric acid solutions were over the range 0 - 6.30 Molar.

The results are presented in the terms 'percentage of metal reacting with the solution', and are divided into two parts, one set for each of the two metals in the alloy. These results are reproduced in Table 7.1. Although the points on Figure 7.1. represent both sodium and potassium results, the curve is that for the total metal reacting in the alloy i.e. % Na + % K.

TABLE 7.1. THE PERCENT OF METAL REACTING WHILE TRAVELLING 80MM THROUGH SOLUTIONS OF SULPHURIC ACID AT 20°C.

Acid concentration (moles/litre)	% Na reacting	% K reacting
0	29.0	34.8
0.38	34.5	30.6
0.76	30.1	29.6
1.13	21.5	21.7
1.50	26.4	22.4
2.25	18.5	15.9
3.08	22.9	18.9
3.40	22.6	21.5
3.80	29.2	26.1
4.32	25.2	23.1
4.80	55.2	52.5
5.25	57.8	60.9
5.80	81.5	84.0
6.30	79.6	86.5

FIG. 7.1 The percentage of metal reacting with 80mm. of H_2SO_4 solutions at 20°C.

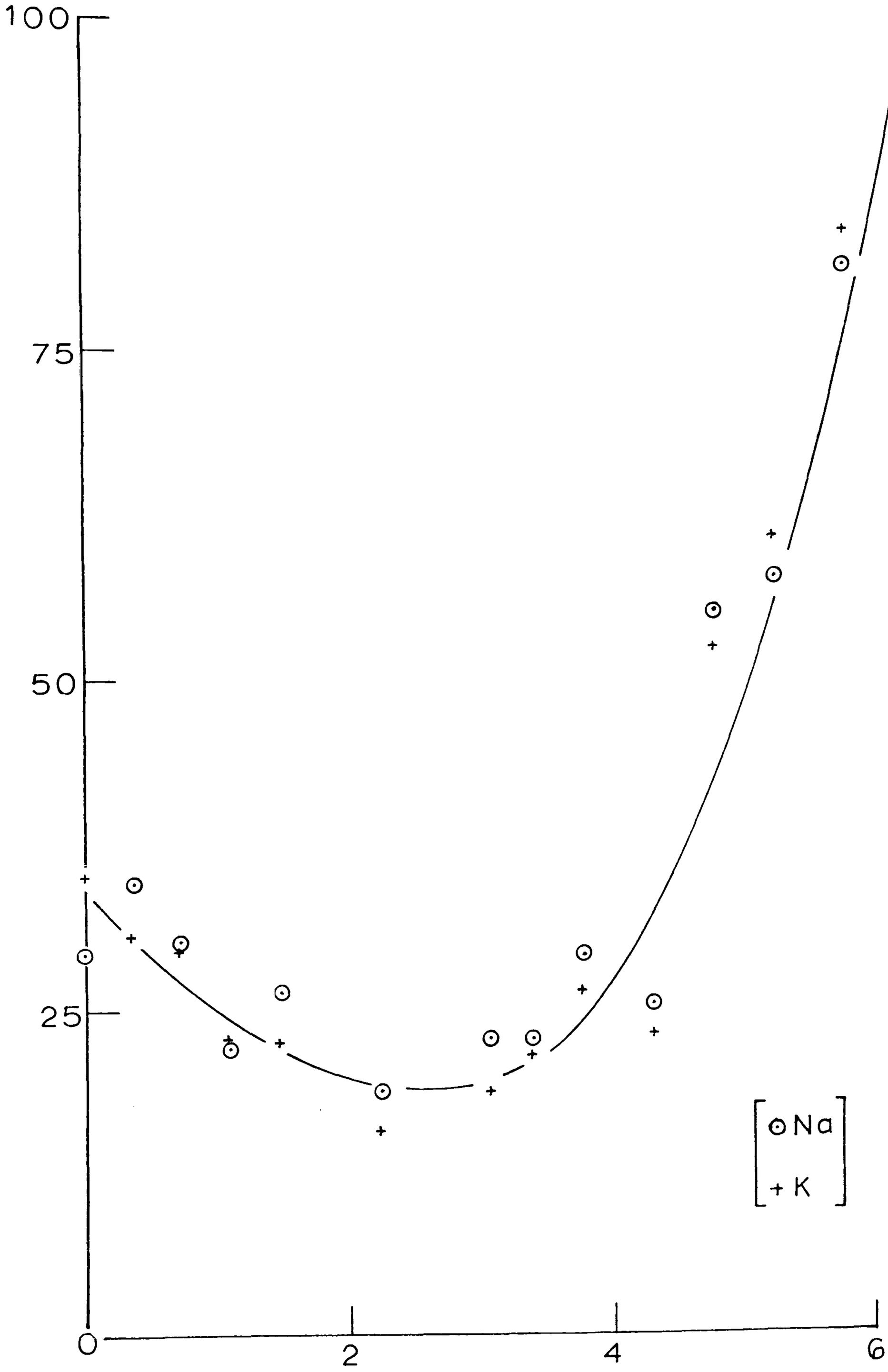

These results will be discussed in full in Section 7.7. However, on preliminary examination, they, show, perhaps surprisingly, that substitution of water by dilute mineral acid does not give rise to an immediate increase in reaction rate at low concentrations. The results found for solutions of concentration below approximately 4 Molar (8 Molar in H_3O^+) are actually lower than those found for water at the same distance travelled (80 mm) and the same temperature (20°C). A general trend is evident in which the results lie on a curve, with a minimum point at approximately 2.5 Molar. The later results (acid concentration > four Molar) are higher than those for water. The final two experiments in this section (5.80M and 6.30 M) were extremely violent, with water turbulence, rapid heating of the vessel and contents and a burning of metal globules within their protective bubbles. Experiments using acid concentrations above 6.30 Molar were therefore not attempted.

It was suspected from these results that the products of the reaction, sodium and potassium sulphate, had bearing on the reaction rate due to the formation of a product film less soluble than sodium or potassium hydroxide. The solubility of NaOH in water at 20°C is 27.25 moles/litre, that of sodium sulphate, Na_2SO_4, 0.13 moles/litre. The corresponding values for potassium are 19.96 and 0.60 moles/litre respectively.[58]

These results were the only ones obtained in the present work in which, in some cases, the proportion of sodium reacting in the alloy was greater than that of potassium.

7.3. NaK + VARIOUS ACID SOLUTIONS - RESULTS

7.3.1. The solubility data

The object of the experiments described in this section was to determine the effect of product solubility on the reaction rates of alkali-metal/water reactions. There were uncertainties in the selection of acids, however, according to the solubilities of their sodium and potassium salts. For example, the injection of sodium at 20°C, into Molar hydrochloric acid results not only in a neutralisation of the bulk medium (2g of sodium into 500 ml of 1.0 M.HCl will reduce the acid concentration to approximately 0.8 M) but the local conditions in the vicinity of reaction may well be very much lower in acid concentration. Thus it is not clear whether to consider the solubility of the product salt in Molar, in 0.8 Molar, or in even less acidic solutions. Secondly, the use of sodium - potassium alloy gives rise to two salts in solution. Data on systems such as NaX - KX - HX - H_2O have not been determined for many of the simple anions (X) at one temperature.

Compromises were therefore necessary. Firstly, the independent variable chosen was the solubility of metal salts in water at 20°C. Secondly, the average solubility of the salts of sodium and potassium was calculated and related to the extent of the total reaction, that is the percentage of metal reacting, not the percentages of sodium and potassium reacting. It is not reasonable to look at the extent of reaction of, say, sodium in NaK with hydrochloric acid, and relate this value to the solubility of sodium chloride. The solubility data used for the relation between the extent of reaction (percent of metal reacting) and solubility of the product (NaX, KX) are shown in Table 7.2.

TABLE 7.2 SOLUBILITIES OF SODIUM AND POTASSIUM SALTS IN WATER AT 20°C (MOLES/LITRE)[58]

Anion	Sodium	Potassium	Average
OH^-	27.25	19.96	23.61
CH_3COO^-	5.67	26.05	15.86
I^-	11.92	8.67	10.29
Br^-	8.84	5.46	7.15
NO_3^-	10.35	3.13	6.74
Cl^-	6.13	4.59	5.36
SO_4^{2-}	0.13	0.60	0.37

They show that the average solubilities of the sodium and potassium salts are in the order OH^- > CH_3COO^- > I^- > Br^- > NO_3^- > Cl^- > SO_4^{2-} .

7.3.2. Preliminary experiments

Pliminary experiments were carried out by injecting NaK into the above mentioned acids in the concentration range 0 - 1.5moles/litre, and a solution height of 50 mm. The results of these experiments are collected in Table 7.3.

Generally, these results do not serve as a precise guide to the difference in reactivity between the various acids. This is probably due to two factors. Firstly, the solution height is too small to allow much reaction, and therefore differences in reactivity will only become apparent when the metal is allowed to travel further. Secondly, any differences may well occur at higher acid concentrations than 1.50 Molar, if the sulphuric acid behaviour (Fig 7.1) is duplicated, but shifted to higher acid concentrations. The experiments in this section were therefore used as a guide to further experiments, after the following points had been noted:-

(a) Experiments with all the acids HCl, HNO_3, HBr, HI and CH_3COOH could be carried out safely, at least at concentrations of less than 1.50 Molar. All of these NaK injections behaved, outwardly at least, in much the same way as injections into water.

(b) As the concentration of any acid was increased no marked increase in reaction rate was noted. On the contrary, except for acetic acid, a decrease in the percentage of metal reacting was observed,

TABLE 7.3. PERCENTAGE OF SODIUM AND POTASSIUM REACTING WITH DILUTE SOLUTIONS OF SIMPLE ACIDS (COLUMN HEIGHT 50 mm) AT 20°C

Water		
Na	17.8	18.1
K	22.3	22.2

HCl	0.009M	0.14M	0.21M	0.49M	0.70M	1.11M	1.20M
Na	19.5	16.1	16.4	13.1	15.5	12.6	12.2
K	21.4	23.4	22.5	18.7	23.2	17.0	17.4

HBr	0.01M	0.14M	0.20M	0.38M	0.49M	0.83M
Na	14.9	16.5	14.5	13.8	9.5	9.9
K	22.9	18.3	19.2	17.0	10.0	15.8

HNO_3	0.21M	0.42M	0.49M	0.85M
Na	16.3	11.9	9.5	7.4
K	18.2	14.3	10.0	11.2

HI	0.11M	0.20M	0.94M	1.50M
Na	17.9	17.2	14.3	15.6
K	23.8	24.1	18.5	17.4

CH_3COOH	0.49M	0.63M
Na	34.0	40.2
K	36.4	47.3

particularly noticeable in the case of nitric acid.

(c) A marked increase in the reaction rate of NaK occurred when acetic acid (0.63M) was substituted for water. It should be noted that potassium acetate is by far the most soluble salt listed in Table 7.2.

7.3.2. More concentrated acids: 4 Molar

Experiments were carried out using 4.0 Molar solutions of the acids at a solution height of 80mm. Differences in reaction rate for different acids, it was believed, would be more apparent at higher concentrations, and also when the metal was allowed to travel further. Five experiments were carried out using each of the acids CH_3COOH, HI, HBr, HCl and HNO_3. The results of these experiments are collected in Table 7.4.

Since the alloy compositions in these experiments were close to each other at 50 ± 3% Na, an average of the values for sodium and potassium in the last column of Table 7.4. gives a value for the total of metal which reacts with acid. The averages are compared with the solubilities (from Table 7.2.) of the acid salts. The correlation is shown in Figure 7.2.

The results show the importance of product solubility on reaction rate, and clearly indicate that these products have more effect on the rate than a severe decrease in pH at these concentrations (4.0M), since all of the results, except those for acetic acid, are less than those obtained for water under the same conditions. The aspect of product solubility will be investigated further in the next section.

TABLE 7.4. PERCENT OF SODIUM, POTASSIUM, AND TOTAL METAL REACTING WITH 4.0 MOLAR SOLUTIONS OF ACIDS (COLUMN HEIGHT 80 mm.) AT 20°C.

HBr	Na	14.0	14.6	13.9	14.1	14.3	14.2 ∓ 0.3
	K	16.6	16.8	18.2	18.1	18.1	17.6 ∓ 0.7
	Total						15.9 ∓ 0.7
HCl	Na	12.3	13.9	15.2	14.1	17.4	14.6 ∓ 1.7
	K	16.8	17.8	18.3	17.1	16.2	17.2 ∓ 0.7
	Total						15.9 ∓ 1.7
CH_3COOH	Na	32.6	30.4	27.3	28.3	26.6	29.0 ∓ 2.2
	K	37.6	35.0	30.2	31.5	38.0	34.5 ∓ 3.1
	Total						31.8 ∓ 3.1
HI	Na	20.2	20.0	21.6	18.9	17.4	19.6 ∓ 1.4
	K	22.0	22.0	21.8	19.4	18.2	20.7 ∓ 1.6
	Total						20.2 ∓ 1.6
HNO_3	Na	12.6	13.8	14.9	12.0	12.5	13.2 ∓ 1.1
	K	14.2	15.1	17.3	13.7	14.7	15.0 ∓ 1.2
	Total						14.1 ∓ 1.2

FIG. 7.2 The correlation between reactivity and product solubility

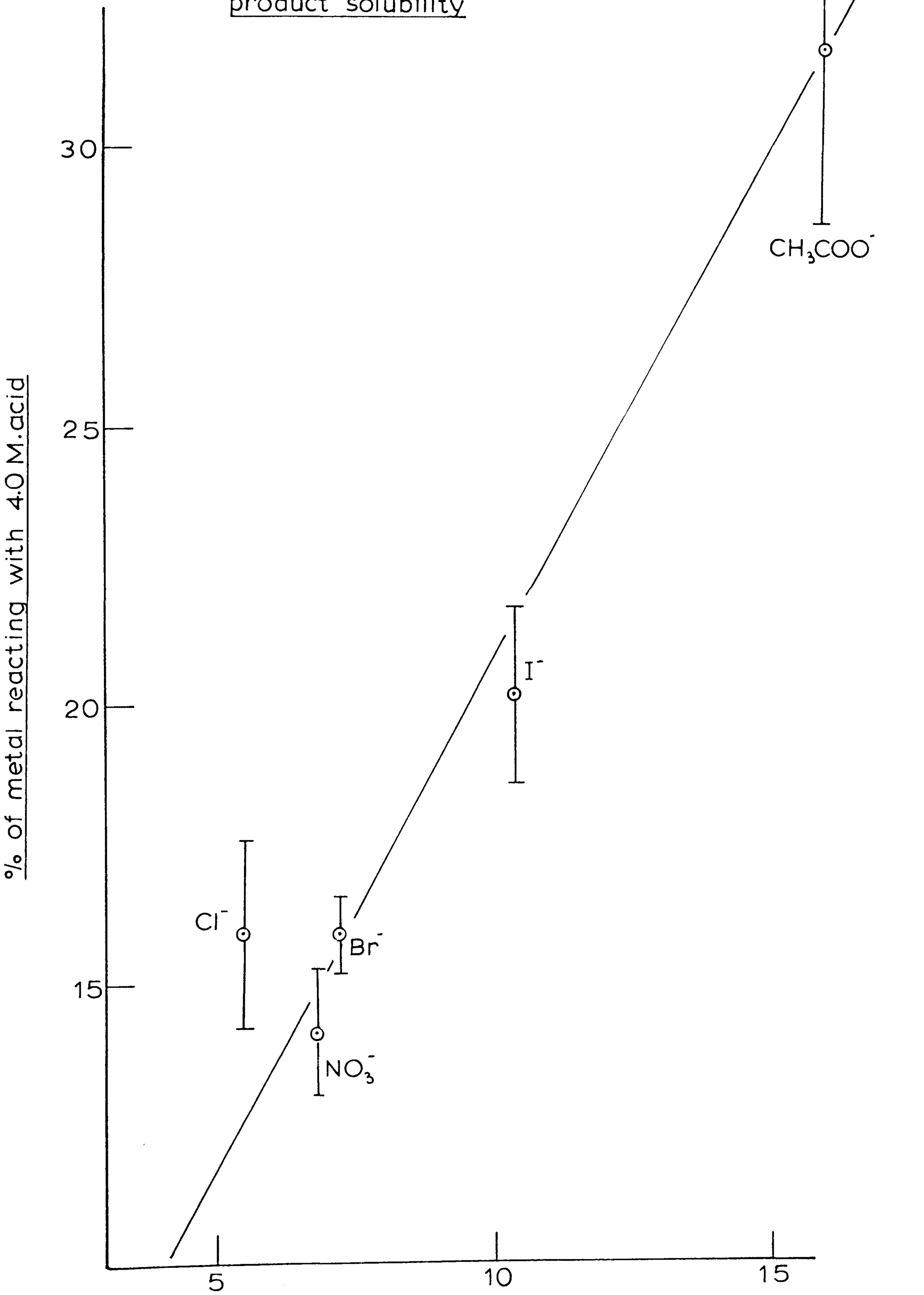

7.4 PREVENTION OF PRODUCT CRYSTALLISATION

Halstead has investigated the solubility of potassium sulphate in water and solutions of sulphuric acid, and the effect on solubility of the inclusion of the impurity ions Fe^{2+}, Fe^{3+} and Cr^{3+}. These impurities were present in the form of their sulphates. He found that whereas ferrous ion (Fe II) impurities had little effect on solubility, the ions in the +3 oxidation state had the effect of preventing the crystallisation of potassium sulphate. With as little as 0.3 g Fe^{3+} / 100 g of solution, for instance, stable solutions at more than 100% supersaturation could be produced. The maximum effect occurred at concentrations of 0.07g Fe^{3+} / 100 g of water.

Enhanced reaction rates would certainly result from the prevention of product crystallisation if the conclusions from Section 7.3 are correct. This was put to the test. Solutions of ferric and ferrous ions in various concentrations of sulphuric acid were made up from the salts $Fe_2(SO_4)_3$ and $FeSO_4$. Injections of NaK were carried out under the same conditions as those described in Section 7.2 - capillary diameter 0.1 to 0.2 mm, argon pressure 69KPa, temperature 20°C, and alloy composition 40 - 50 mole % sodium.
The results, in terms of the percentage of metal reacting in 80mm of solution, are presented in Table 7.5. The effect of doping with Fe^{3+} is shown in Figure 7.3, and with Fe^{2+} in Figure 7.4. In both diagrams, the curve for H_2SO_4 solutions (from Figure 7.1) is reproduced for comparison.

The control experiments (Fe^{2+} doping) are all reasonably close to the original curve, although some of the values, in the one to two Molar region, are higher than those for undoped solutions. The points fall closest to the original

TABLE 7.5 PERCENTAGE OF SODIUM AND POTASSIUM REACTING WITH SOLUTIONS OF SULPHURIC ACID (80mm) DOPED WITH Fe^{3+} AND Fe^{2+} IONS AS THEIR SULPHATES AT 20°C.

Acid concentration (M)	%Na(A)	%Na(B)	%K(A)	%K(B)
0.18	35.4		33.4	
0.36	27.0		25.7	
0.55	34.6		33.3	
0.92	64.0	28.3	64.4	37.6
1.28	64.7		65.0	
1.83	59.3	31.7	50.1	23.1
2.38	21.3		20.2	
2.75	20.1	21.9	18.3	18.4
3.67	18.2	10.1	22.3	10.8
4.59	58.6		60.6	
5.50	75.4	57.5	85.7	64.0

(A) solutions contain 1.2 $Fe_2(SO_4)_3$ / 500 ml solution

(B) solutions contain 2.6 Fe SO_4 / 500 ml solution

FIG. 7.3 Percentage of metal reacting with 80 mm. of H_2SO_4 solutions doped with Fe^{3+}

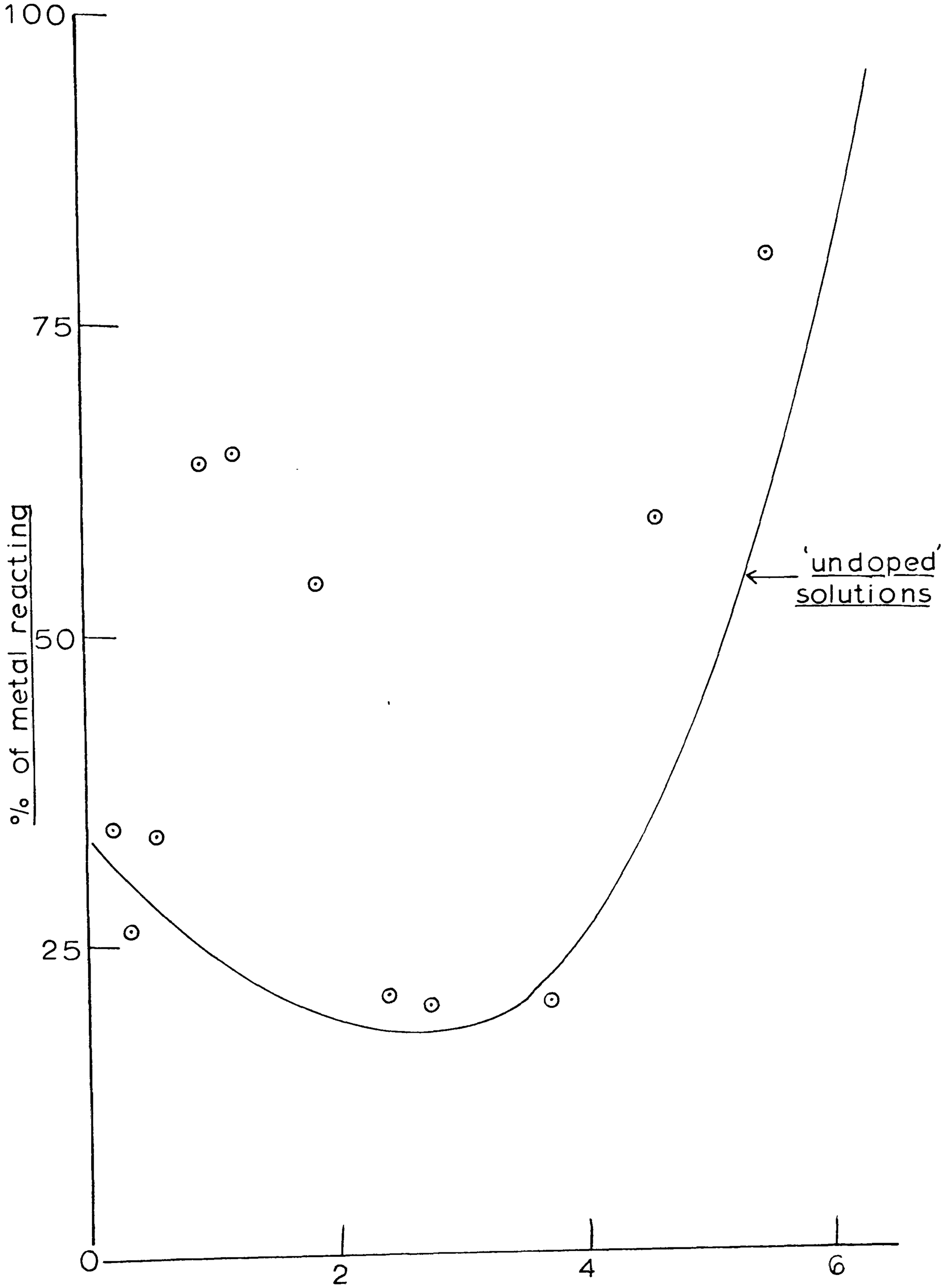

FIG. 7.4 Percentage of metal reacting with 80 mm. of H_2SO_4 solutions doped with Fe^{2+}

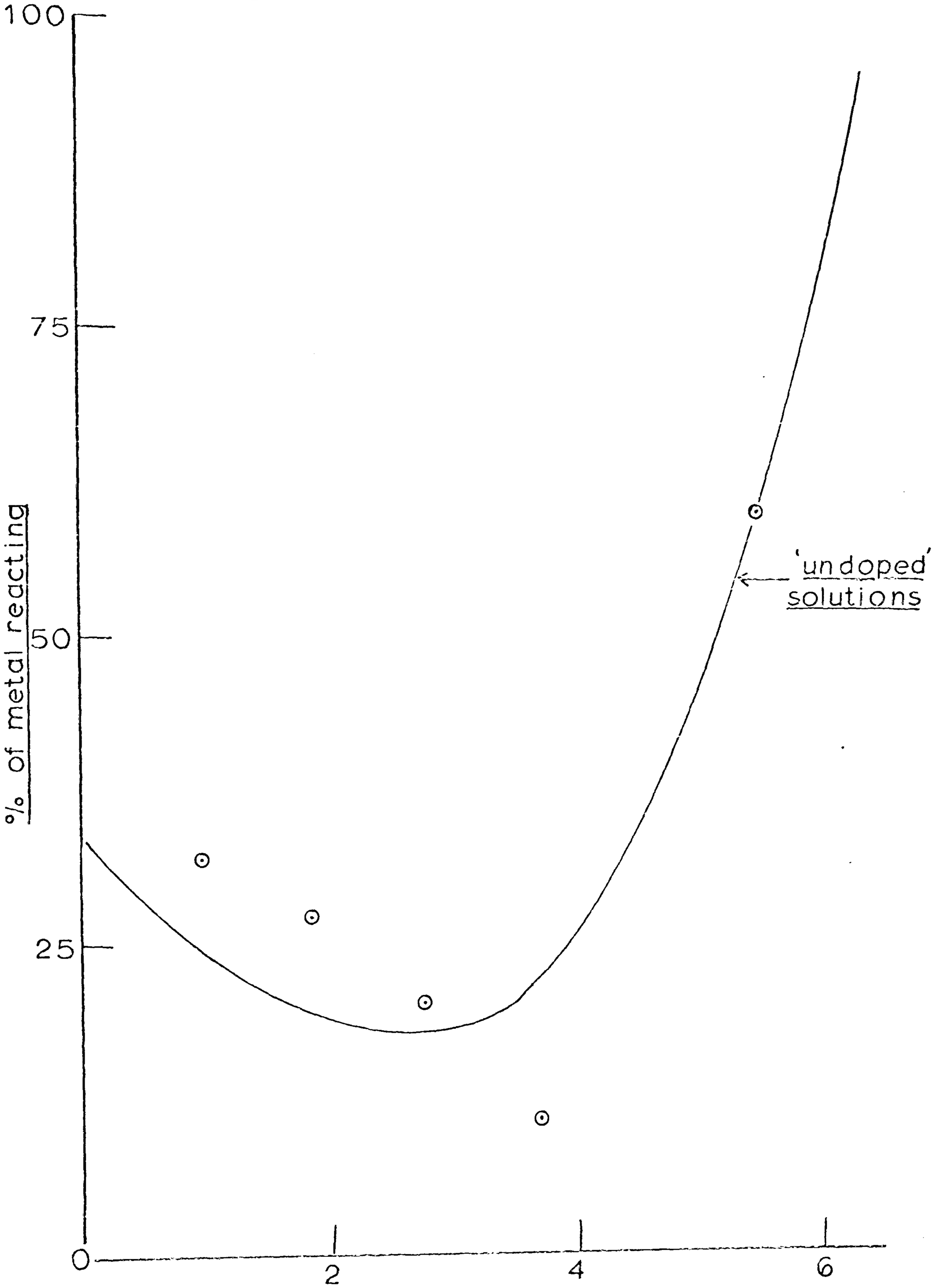

curve at the minimum point.

There is some evidence of enhanced reactivity with the addition of Fe^{3+} ions to the solution, but this is confined to a small region of concentration, between one and two Molar strength. Definite, but relatively less enhancement occurred for two experiments at high acid concentration (4.59 and 5.50 M).

Although, then, some differences appear, the scatter of these results renders them inconclusive. However, the five experiments showing reaction rate enhancement (0.92M, 1.28M, 1.83M, 4.59M and 5.50M) provide more evidence to suggest that products interfere with the reactants, and that this is an important feature of this system.

7.5 ANION REDUCTION BY THE METAL

In the reaction of NaK with solutions of sulphuric acid, there was some evidence that the metal was reducing the sulphate ion. This occurred particularly in the vicinity of the jet at high sulphuric acid concentrations, where yellow sulphur could be seen drifting away from the metal.

In a reaction carried out using 5 Molar H_2SO_4 saturated with mercury (II) sulphate, a dark suspension of mercury sulphide floated up through the water column to rest at the water/oil interface, indicating production, during the reaction, of hydrogen sulphide. The metal then, is responsible for the reduction of sodium and potassium sulphates to sulphur in the 0 and -2 oxidation states.

This reduction was examined quantitatively at various acid concentrations.

7.5.1. Experimental Procedure

A system was arranged by which all of the injected metal reactedwith the water. This entailed modification of the separation vessel (Figure 3.3), which was increased in height to allow a solution height of 400 mm. The oil layer was omitted from the system. Preliminary tests showed that, with water, all of the injected metal reacted while travelling through this distance i.e. no metal globules arrived at the water surface, and no smoke was released from the surface into the argon atmosphere.

After metal injection, the aqueous solution was flushed with argon, flowing at approximately 5000mm^3 per second, through tap D (Figure 3.3) i.e. from the bottom of the vessel. The gas was passed from the top of the vessel (tap C) through two dreschel bottles, each containing 100 cm^3 of acetic acid containing lead acetate. Lead sulphide was precipitated from the hydrogen sulphide in the argon carrier, and this continued to deposit for a period of two hours, verified by continual replacement of the dreschel bottle solutions. The gas flush was continued for a further two hours. The precipitate was collected on a grade-2 sintered glass filter, and analysed gravimetrically. The solution in the reaction vessel was analysed for sodium and potassium content by atomic emission techniques as before.

7.5.3 Results

The results are presented in Table 7.6. The fourth line from the top shows that the alloy composition for each experiment was in the range 40.5 - 44.1 mole % sodium. The quantity of metal injected was fairly low and constant for the series of eight experiments. The results are presented in terms of the number of moles of sulphide deposited per mole of alloy (sodium + potassium) reacting with the water. Again, however, the figure does not represent the total reduction, since sulphur was again produced in the vicinity of the jet during experiments 4 - 8.

Figure 7.4 shows the results in graph form. It shows that there is no sulphide production in reactions with acid solutions of less than 4.27 Molar. Production rises dramatically above this concentration. It was not possible to use higher concentrations of acid for the reasons stated in Section 7.2, so it is not known whether the extent of this reduction continues to increase at higher concentrations, or whether a maximum value is reached.

TABLE 7.6 THE REDUCTION OF SULPHATE DURING INJECTIONS OF METAL INTO SULPHURIC ACID SOLUTIONS

Experiment	1	2	3	4	5	6	7	8
Acid concentration (moles/litre)	3.66	4.04	4.59	4.72	4.95	5.33	5.89	6.47
Mass of lead sulphide precipitate (g)	0	0	0	0.1995	0.1627	0.2714	0.3890	0.2989
Moles of Metal ($\times 10^2$) — Na	-	-	-	1.450	0.800	1.275	1.725	1.125
Moles of Metal ($\times 10^2$) — K	-	-	-	2.125	1.013	1.688	2.437	1.550
Moles of Metal ($\times 10^2$) — Total	-	-	-	3.575	1.813	2.963	4.163	2.675
Mole % sodium in alloy	-	-	-	40.5	44.1	43.0	41.5	42.1
Moles of sulphide from 1 mole metal ($\times 10^2$)	0	0	0	2.333	3.309	3.827	3.906	4.669

production in solutions of sulphuric acid

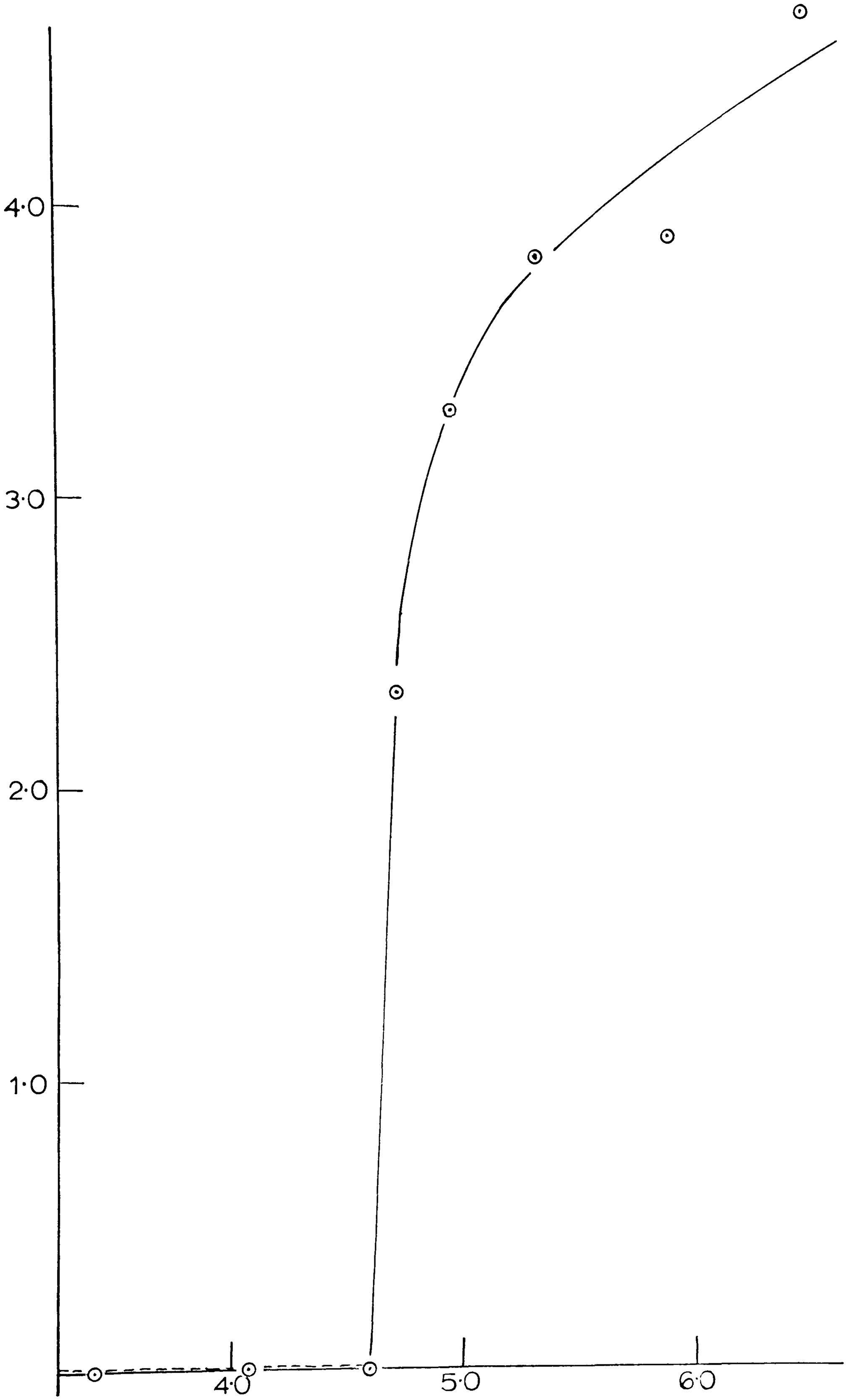

7.6. REACTIONS IN SOLUTIONS OF pH > 7

Solutions of ammonia in water were employed as the reaction media in order to avoid the complications of metal ions, particularly Na^+ and K^+ in both the reaction and the analysis. Experiments were carried out using the standard conditions already described, and the results, again, are in the form 'percentage of metal reacting' in a standard solution height of 80 mm. They are presented in Table 7.7.

Table 7.7. PERCENTAGE OF METAL REACTING WITH 80mm OF AMMONIA SOLUTIONS AT 20°C

$[NH_4OH]$ /litre	1.01	1.81	3.63	4.54	5.44	6.35	7.23
% Na reacting	24.3	24.7	25.6	24.9	22.8	25.2	23.6
% K reacting	29.8	33.3	30.5	33.4	34.2	30.8	30.3

Comparing these values with those for water, which are sodium, 29.0% and potassium, 34.8%, it can be seen that the increase in alkalinity has far less effect than an increase in acidity of the medium. There is some spread in the results, but no real, positive, increase or decrease in reactivity occurs at these concentrations.

Saturated solutions of potassium hydroxide ($\simeq$ 20 moles/litre at 20°C) were prepared and three experiments carried out. The quantity of sodium reacting in each was

20.6%, 24.2% and 21.8%, average 22.2%. This value represents a real drop in the extent of reaction. Concentrated hydroxide solutions decrease the rate, therefore, by about 7% (from 29.0% in water). The salts KOH /NaOH were precipitated in the reaction vessel during the course of the these reactions.

7.7. DISCUSSION

The results in this chapter are presented in terms of 'percentage of metal reacting in a given solution height. They are not, therefore, rates, but the values represent a contribution from each of the rates at the jet and from within the bubble. Conditions, also, were not exactly identical. Small variations in capillary diameters (changing marginally the surface areas of the liquid metal jets) and in the alloy composition, may explain the scatter in some of the results. This latter effect will not be particularly important, since it seems that the rate of reaction of sodium does not change significantly when sodium metal is substituted for the alloy (Section 6.6) i.e. the composition of the reacting metal is relatively insignificant. Another factor in the rate calculations was the velocity of bubble rise. This might be expected to vary marginally as solutions of acids replace water, due to the differences in viscosity and density. For these reasons, a number of results for each series of experiments were necessary.

It should be possible to carry out all the experiments

described in this chapter a number of times, with variation in the depth of water, in order to calculate rates of reaction at each stage, but for the purposes described in the introduction to this chapter, this was not necessary.

It is generally accepted that the reaction between the alkali-metals and dilute mineral acids is more vigorous than that between the metals and water, and under some conditions this may be true for the reason that Equation(7.1) is likely to be more competitive than Equation (7.2). In

$$2Na + H_3O^+ \longrightarrow Na^+ + OH^- + H_2 \qquad (7.1)$$

$$Na + H_2O \longrightarrow Na^+ + OH^- + \tfrac{1}{2}H_2 \qquad (7.2)$$

the present work, however, when the concentration of H_3O^+ in the solution is increased to between 2.0 and 3.0 Molar H_2SO_4 ($[H_3O^+]$ of 4 - 6 Molar), the rate of reaction diminishes, and falls to about two thirds of that for water. The most plausible explanation of this phenomenum is that a relatively insoluble salt is formed, which sets up a dynamic equilibrium with its surroundings i.e. $MX_{(s)} \longrightarrow M^+_{(aq)} + X^-_{(aq)}$. This has already been depicted for the situation at the jet (Figure 5.8). This idea can be extended to the situation of the metal in the bubble (Figure 7.6). As the metal comes into contact with the interior bubble surface, the product layer has to dissolve before intimate contact of the reactants is possible. As the product dissolves, the metal reacts, producing more product. Provided that the rate of solution of the salt increases with its solubility, then the more insoluble

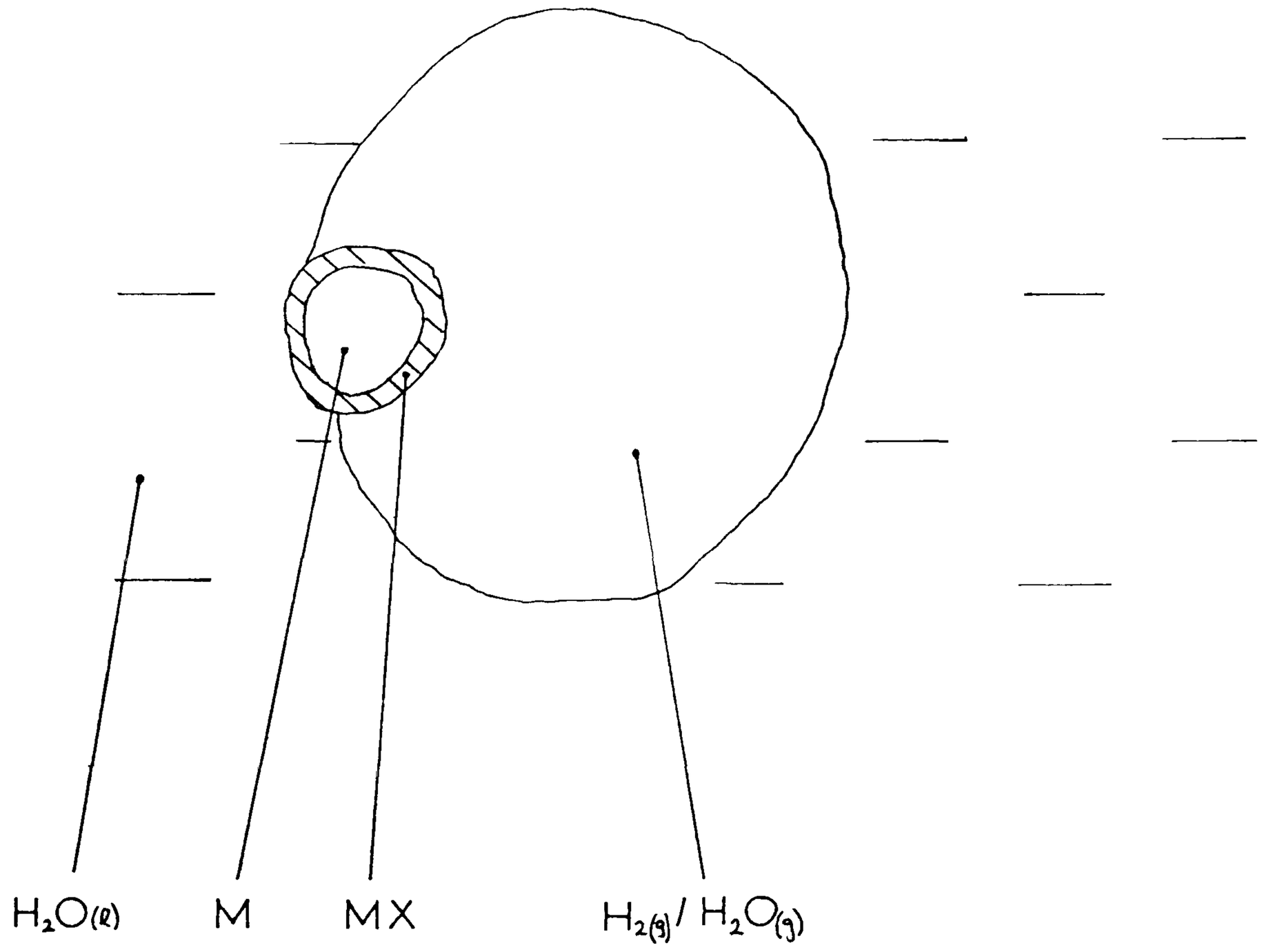

FIGURE 7.6 METAL REACTING IN THE BUBBLE

is the product, the lower will be the reaction rate.

This picture is reinforced by two further experiments. When the solution is doped with Fe^{3+} ions, these prevent ready crystallisation of the product in sulphuric acid. With some experiments carried out with such doped solutions, a rate increase is noted of over 100%. However, rate increases were not noted for all such experiments. Secondly when the product of the reaction is more soluble than sodium or potassium sulphate e.g. metal iodides, the reaction rate is enhanced. A correlation exists, therefore, between salt solubility and reaction rate. The correlation is not straightforward since the rate of reaction in HCl to produce alkali-metal chlorides seems to be too high. Likewise for H_2SO_4, which gives the lowest of all alkali-metal salt solubilities. This acid does not appear in the experiments in Section 7.3.3. since complications arise over which

concentration term to use. Naturally, in terms of salt solubility, the term should be the acid molarity. However, the di-basic nature of the acid, which doubles the hydrogen ion concentration in aqueous solution, may compensate for the lack of solubility of the product, and this may be the reason why these results (from Fig. 7.1. the % of metal reacting at 4.0 Molar) do not fit the solubility/reaction rate correlation.

The real clue that salt solubility is more important, at least at low acid concentrations, is provided by the fact that solutions of acetic acid provide a medium in which the reactivity of NaK is greatly enhanced over that for water. Table 7.2. shows that sodium and potassium acetate are among the most soluble of these alkali-metal salts. The concentration of hydrogen ions is not however, as high as in any of the mineral salts, and this factor therefore makes little contribution. Table 7.8 gives the dissociation constants for the acids employed in the experiments in this chapter.

Moreover, there is no marked effect on the reaction rate when the concentration of hydrogen ions is dramatically reduced, as in the experiments in Section 7.6. , with the addition to the solution of OH^- ions. Some reduction in the rate is evident when the reaction medium is saturated with KOH yet this may simply be another effect of the product film failing to dissolve, or loitering near the reaction site.

The more concentrated is the acid, then, the more pronounced becomes the retarding effect of the insoluble sulphates. However, this trend in loss of reactivity does not continue, but reactivity begins to rise again at higher concentrations, until at concentrations above 6.0 Molar, the reaction is too vigorous to control or measure. As this rise in reactivity begins, there is also evidence that the metal begins to react directly with the product

TABLE 7.8 DISSOCIATION CONSTANTS OF ACIDS AT 25°C

Dissociation	K	pK
$HI + H_2O \rightleftharpoons H_3O^+ + I^-$	3.2×10^9	-9.50
$HBr + H_2O \rightleftharpoons H_3O^+ + Br^-$	10^9	-9.00
$HCl + H_2O \rightleftharpoons H_3O^+ + Cl^-$	10^6	-6.00
$HNO_3 + H_2O \rightleftharpoons H_3O^+ + NO_3^-$	2.3×10	-1.37
$H_2SO_4 + H_2O \rightleftharpoons H_3O^+ + HSO_4^-$	4×10^{-1}	0.40
$HSO_4^- + H_2O \rightleftharpoons H_3O^+ + SO_4^{2-}$	1.26×10^{-2}	1.92
$CH_3COOH + H_2O \rightleftharpoons H_3O^+ + CH_3COO^-$	1.75×10^{-5}	4.76
$H_2O \rightleftharpoons H_3O^+ + OH^-$	10^{-7}	7.00

surrounding it, reducing the SO_4^{2-} anion to elemental sulphur and H_2S.

In gas/metal reactions, the sequence of film growth followed by film cracking and enhanced reaction rates is commonplace.[62] This film cracking occurs when the film of product reaches a certain thickness, and becomes inflexible. Halstead [40] proposes, in experiments described in Section 2.3 that this type of film fracture occurs when a drop of liquid water is released in bulk sodium, after a short period of film formation. The reaction becomes muted during this period, but this is followed by a sudden increase in rate which is attributed to film fracture, which exposes the reactants to each other once more. An explanation of the increase in reactivity at higher acid concentrations in the present work may be that the insoluble product builds up to sucha thickness as to be unstable at a particular concentration. The difference between this case and that mentioned above is that the product, sodium/potassium sulphate is slightly soluble in sulphuric acid and in water. Film growth occurs, then, in a system of dynamic equilibrium. This is illustrated in Figure 7.6. Film growth occurs through 7.6 A, and reaches a maximum at 7.6 B (at this stage, with the metal completely enclosed, reaction occurs between the metal and the product directly), finally cracking at high concentrations at 7.6 C.

The work described in this chapter tends to conform to the principles proposed in Section 2.4 i.e. that a prime factor governing the rates of alkali-metal/water reactions is the degree of mixing of the reactants, or the surface areas of metal and water in contact.

FIG. 7.7 Film formation and breakdown in acid solutions

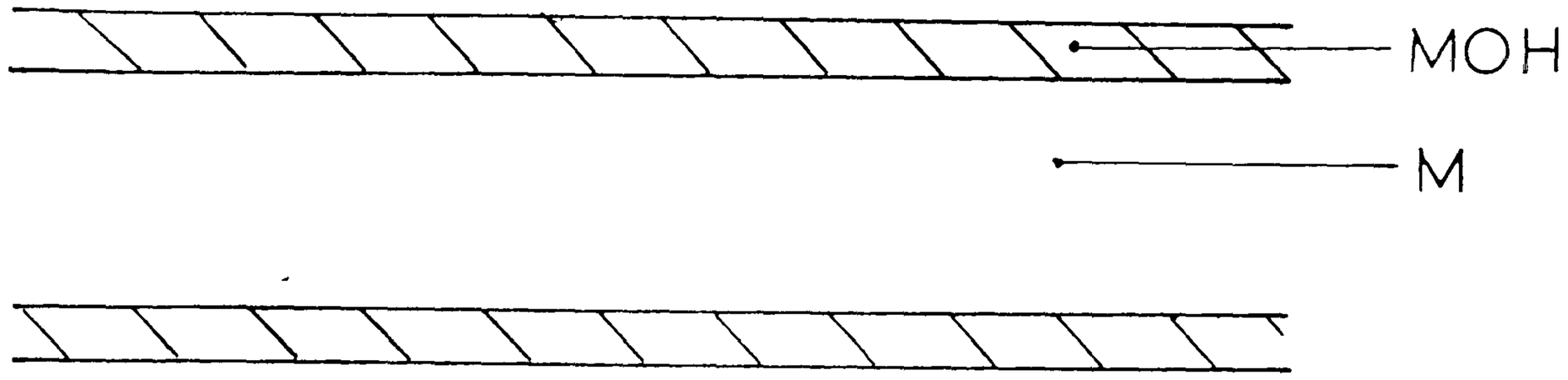

A. [ACID] = 0 — 3.0 M.

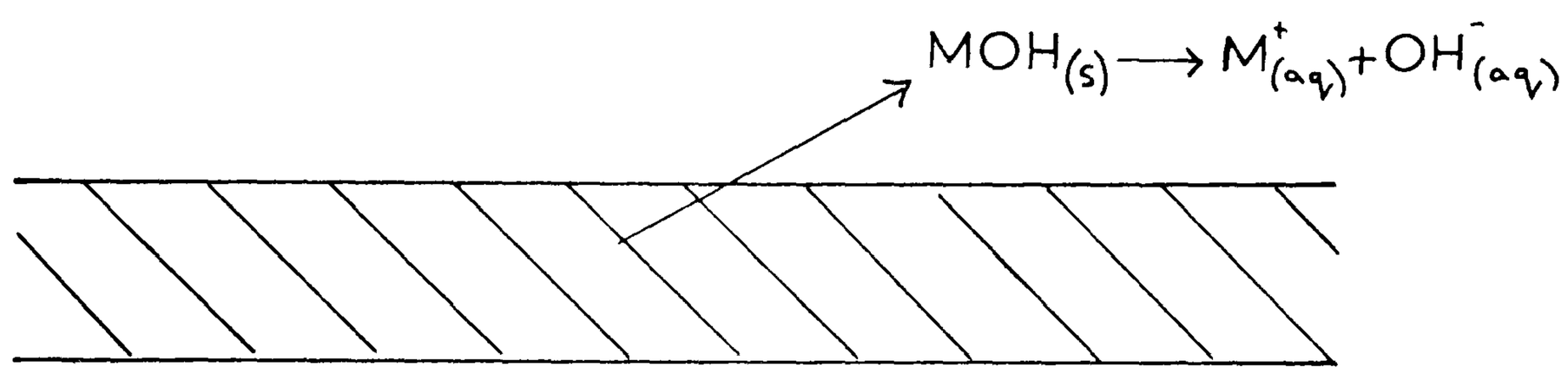

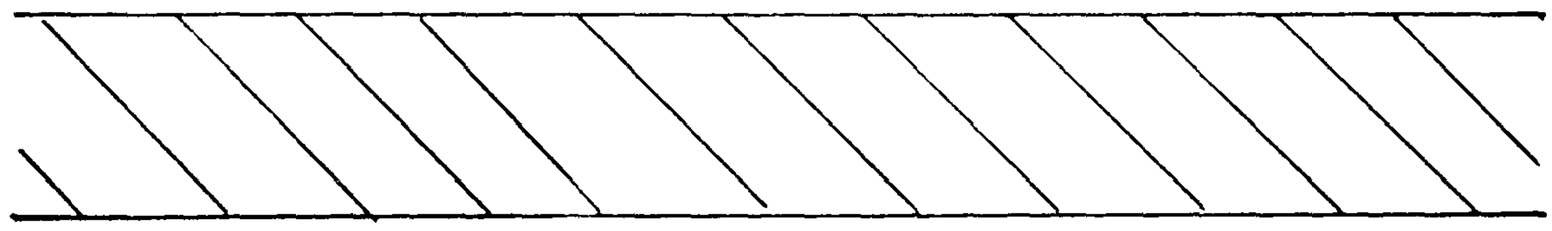

B. [ACID] ≐ 3.0 M.

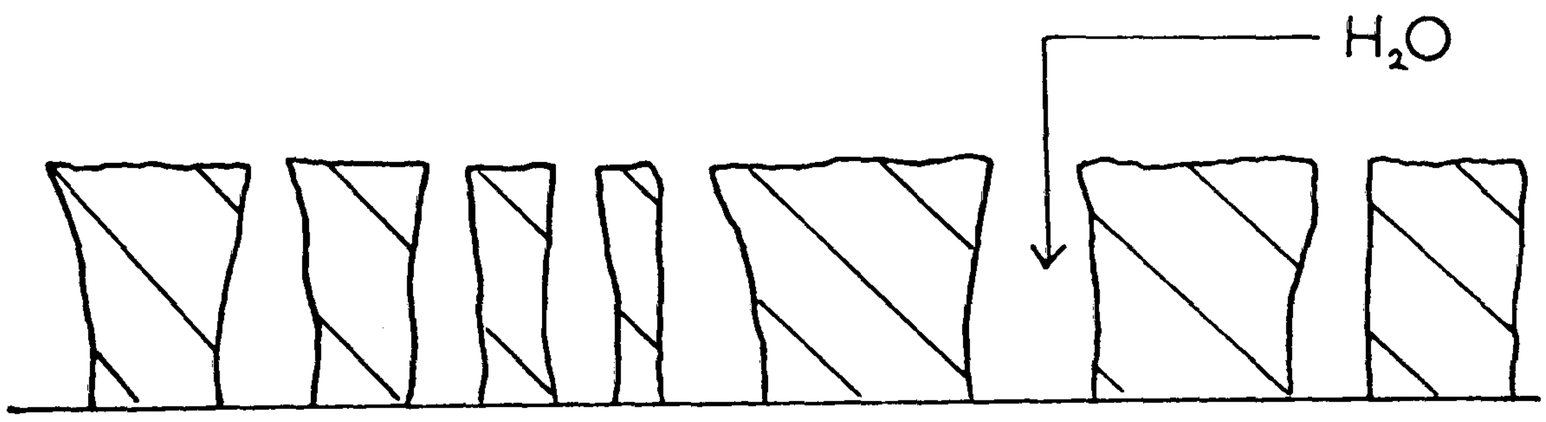

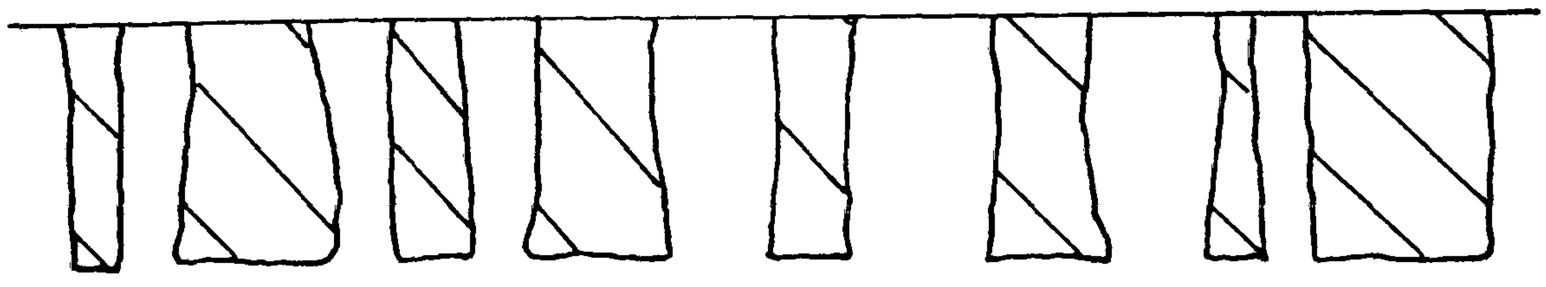

C. [ACID] > 5.0 M.

C H A P T E R V I I I

REACTION STOICHIOMETRY

8.1. INTRODUCTION

The eventual stoichiometry for the reaction between NaK and water is as shown by Equation(8.1). This is the

$$M + H_2O \longrightarrow MOH + \tfrac{1}{2}H_2 \qquad (8.1)$$

overall result, and can feasibly be reached directly, or by a combination of the steps shown in Equations (8.2) and (8.3).

$$2M + H_2O \longrightarrow M_2O + H_2 \qquad (8.2)$$

$$M_2O + H_2O \longrightarrow 2MOH \qquad (8.3)$$

The latter possibility has already been discussed in Section 2.4. Since the reaction rates in the present work rely on the rate of loss of metal, the rates do not distinguish, therefore between the two alternative routes.

Yet a third process can feature, and this is the formation and subsequent hydrolysis of metal hydride, shown by Equations(8.4) and (8.5). Now the conditions at the metal

$$M + \tfrac{1}{2}H_2 \longrightarrow MH \qquad (8.4)$$

$$MH + H_2O \longrightarrow MOH + H_2 \qquad (8.5)$$

jet are conducive to the formation of metal hydrides, which requires high temperatures and high hydrogen pressures. The reaction rate of hydrogen with both sodium[62] and potassium[63] increases, as expected, with increasing temperature. The hydride formed first dissolves in the metal, but saturation and precipitation rapidly follow, since solubility of hydride, is relatively small even at high temperatures. This is shown by Table 8.1.

TABLE 8.1 THE SOLUBILITY OF HYDROGEN IN LIQUID SODIUM[64]

Temperature (°C)	250	300	315	330
Solubility (Wt % H_2)	0.00042	0.0022	0.0052	0.0104

A high pressure of hydrogen increases its rate of reaction with the metal, and the process is generally first order with respect to pressure.

The stability of the hydride is also a function of both temperature and pressure. Generally, high temperatures cause loss of hydride on two counts: thermal decomposition of salt, and increased dissolution in the metal. The inter relationships are best described by a pressure–composition diagram at various temperatures. Consider the first region of the graph (Figure 2.5). This corresponds to the dissolution of hydrogen, as sodium or potassium hydride, in the bulk metal. The second, or 'plateau' region of the graph corresponds to the further reaction of the metal with hydrogen, to produce the non-stoichiometric hydride MH_{1-x}, and this is precipitated when the solution

becomes saturated. Addition of hydrogen to the system now does not result in an increase in pressure, and a three-component region ($M\,H$, MH_{1-x}, $H_{2\,(g)}$) exists. At higher temperatures, the variation in this equilibrium pressure varies according to the general Equation (8.6).[65] A and B are constants

$$\log p = -\frac{A}{T} + B \qquad (8.6)$$

which vary from metal to metal. For sodium the values are A, 5958 and B, 10.47 in the temperature range 500 - 600°C [47].

Although the temperature range in the present work was from 20 to 60°C only, local temperatures at the metal-water interface could have been much higher. Previous reports [10] have indicated large temperature rises (up to 600°C) of alkali-metal jets in contact with moist argon. Temperature rises of this magnitude have been discussed in Section 2.4 in connection with the reverse (water/steam⟶ liquid sodium) process to the one investigated in this work, and the experiments described in Section 5.2 indicate that heat is not quickly communicated away from the metal in the present system. It is not unlikely, then, that the temperature of the alkali-metal jet is in the region of 600°C. In fact, this temperature can be regarded as a minimum for this system.

The conditions, therefore, - high temperature, clean metal jet surrounded by hydrogen - favour the direct reaction between NaK and hydrogen.

The formation of hydride at such a jet has been verified. Dowling[49] used a method of photographic analysis in an attempt to detect this product. By measuring the volumes of two bubbles, one as it left the jet and one a short distance above the jet, he calculated the quantity of hydrogen

produced by hydrolysis of the metal during this distance of travel. Knowing the number of moles of metal reacting in this distance (from the gradient of % metal vs water depth graph) he was able to conclude that simple metal hydrolysis (Equation (8.1)) did not account for enough of the hydrogen which had been produced, and that a contribution from the hydrolysis of metal hydride (Equation (8.5)) would explain the disparity. Note that the reaction (8.5) yields twice as much hydrogen per mole of metal than the reaction (8.1). The metal, therefore, reacted both with water and hydrogen at the jet (Equations(8.1)and(8.4)). Subsequently in the bubble, the hydrolysis of metal was accompanied by hydrolysis of metal hydride (Equations (8.1.) and (8.5))

There are at least two ways in which this may be verified:-

(a) Observation of hydrogen production at the jet. Knowing how much metal reacts at the jet, this can be compared with the quantity of hydrogen produced. This quantity should be less than expected for the total hydrolysis of the metal if, in fact, hydrogen is dissolving in, or reacting with the metal.

(b) Product analysis. Since it has been proposed that the metal hydrides hydrolyse in the 'bubble stage' of the reaction, hydrides are most likely to be found at the metal jet.

Method (a) is the simplest to apply in theory, since it requires information already available i.e. the rate of bubble production and average bubble size at the jet (Chapter 4) and the number of moles of metal reacting at the jet (Chapter 5). There is a drawback, however, due to vapourisation of water in the vicinity of the hot metal jet. The bubbles contain water vapour, and the proportion of hydrogen in this gas mixture cannot be determined.

Method (b) was applied in the present work. Metal

from the jet was analysed for Na(K)H by the method of hydrolysis, the difference in hydrogen production indicating the proportion of hydride in the metal.

8.2. EXPERIMENTAL

The experimental procedure was in two parts, collection of the metal sample, then analysis of the sample for metal hydrides by hydrolysis.

Sample collection was from a modified reaction vessel. This is shown in Figure 8.1. It consisted of a glass reaction vessel, as before, with the addition of a water reservoir at the end of a U-tube, situated above the level of the oil in the vessel, and connected to the bottom of the vessel. The sample vessel was connected through the sidearm (A) above the oil level. The tap (B) allowed the sample vessel to be flushed with argon gas using the gas inlet on the reaction vessel, at the same time as the reaction vessel, prior to metal injection.

The injector, with 0.1 mm capillary attached, was introduced to the vessel in the usual way, and the distance between the capillary opening and the oil layer was arranged to be as small as possible, to reduce hydrolysis of hydride during passage through the water. Argon gas flow through the injector made measurement of this distance difficult. Figure 9.2 illustrates this. The gas continually disturbs the surface, and the water depth through which the gas is passing fluctuates. The water depth through which the metal passed was estimated to fluctuate in the range 0 - 4 mm,

FIG. 8.1 Hydride detection — sampling apparatus

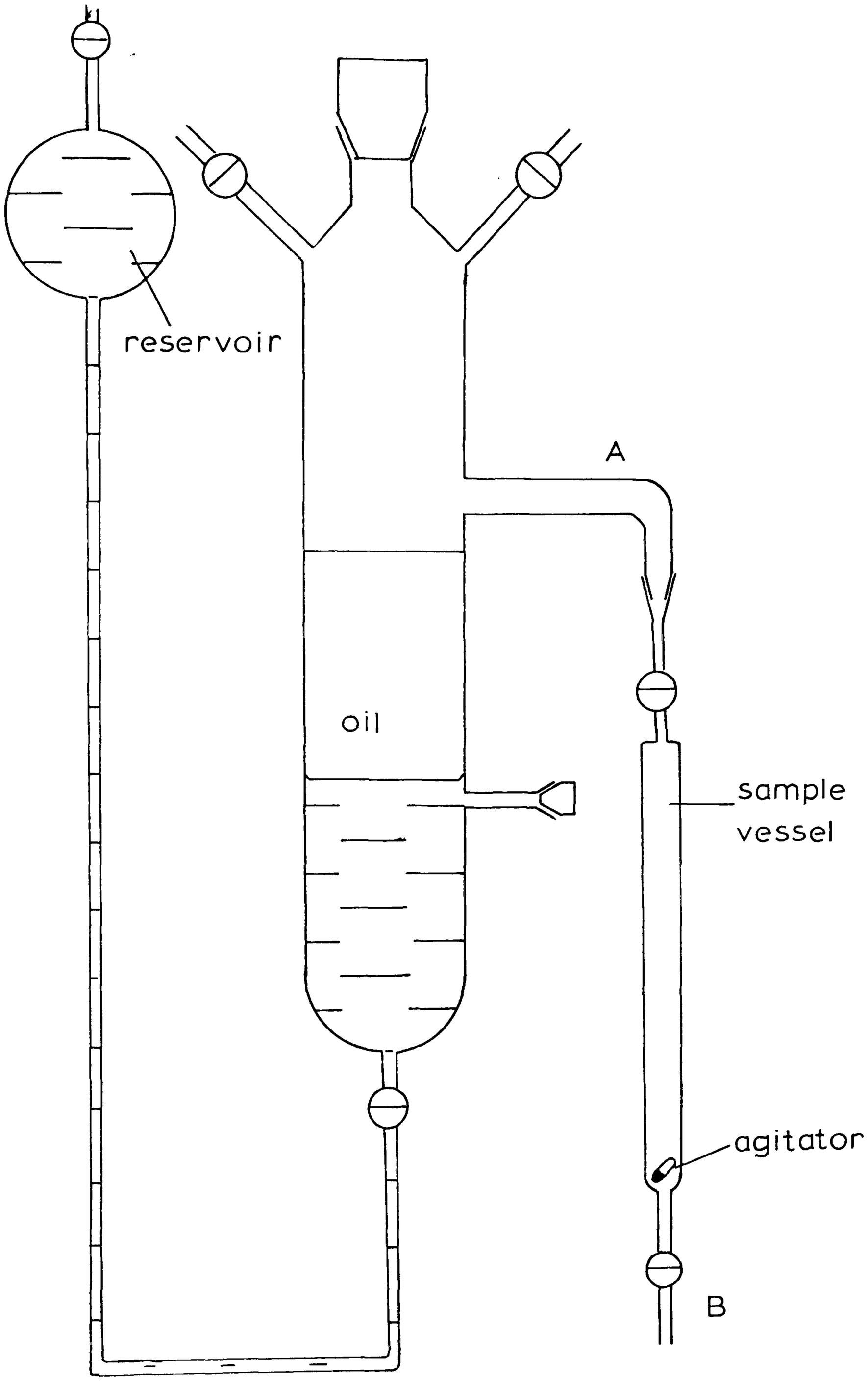

after observation of a metal injection using a telescope with a cathetometer.

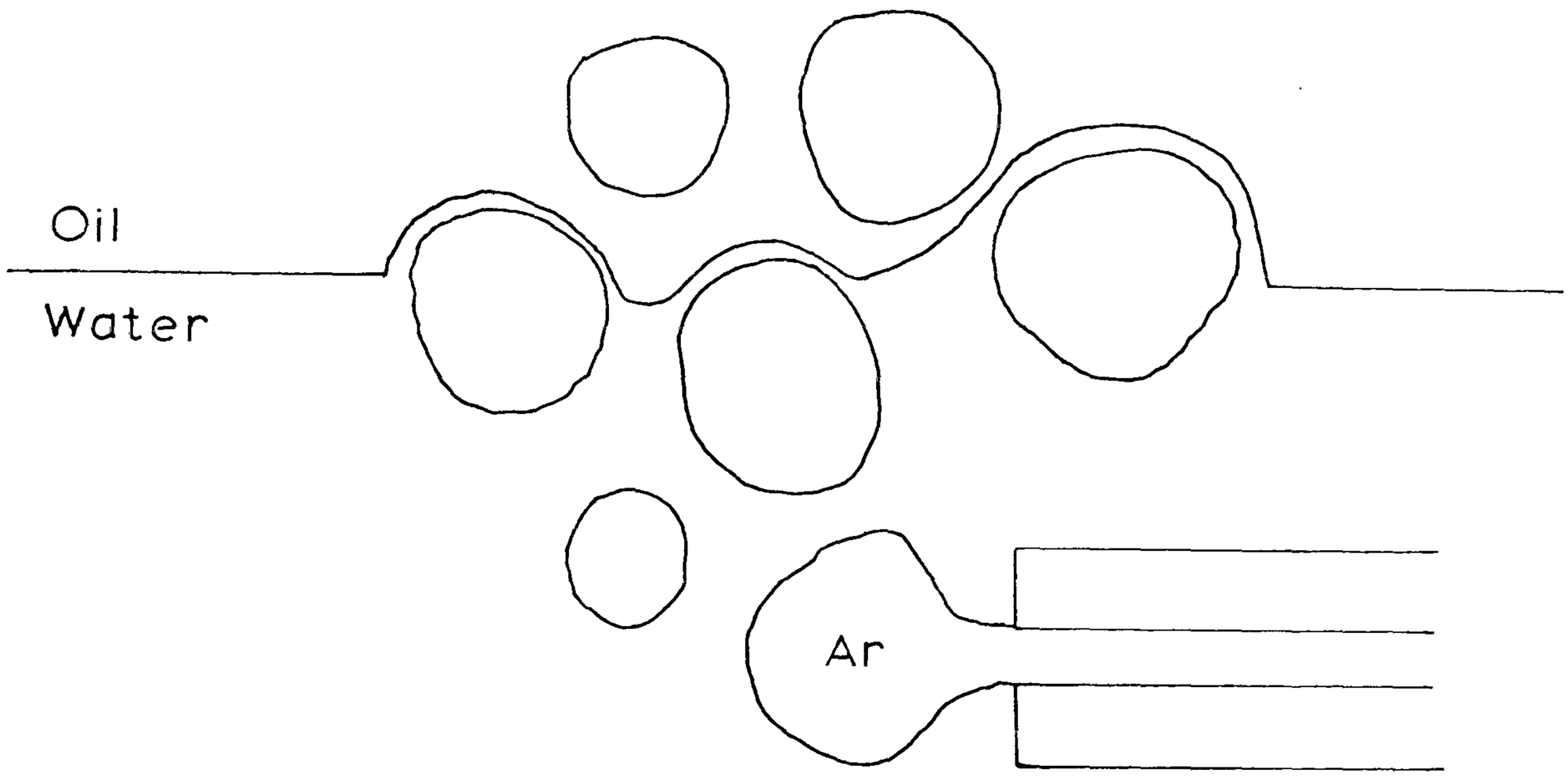

FIGURE 9.2. ARGON FLOW AT THE WATER/OIL INTERFACE

After an injection of metal, the unreacted metal ended up as usual in the form of globules sitting on the surface of the oil. Water was then admitted to the vessel via the U-tube connection. Oil, containing metal from the jet, flowed into the sidearm (A) and thence into the sample vessel. About 20 cm^3 of oil were necessary to fill the sample vessel to half depth, after which the tap was closed and the vessel isolated. The sample vessel was then removed from the reaction vessel, and dregs of oil/metal cleaned out from the section between the tap and the ground glass joint.

Sample analysis was carried out using the vacuum frame shown in Figure 8.3. for measurement of the total hydrogen evolution during hydrolysis. The solutions of

FIG. 8.3 The hydrolysis frame

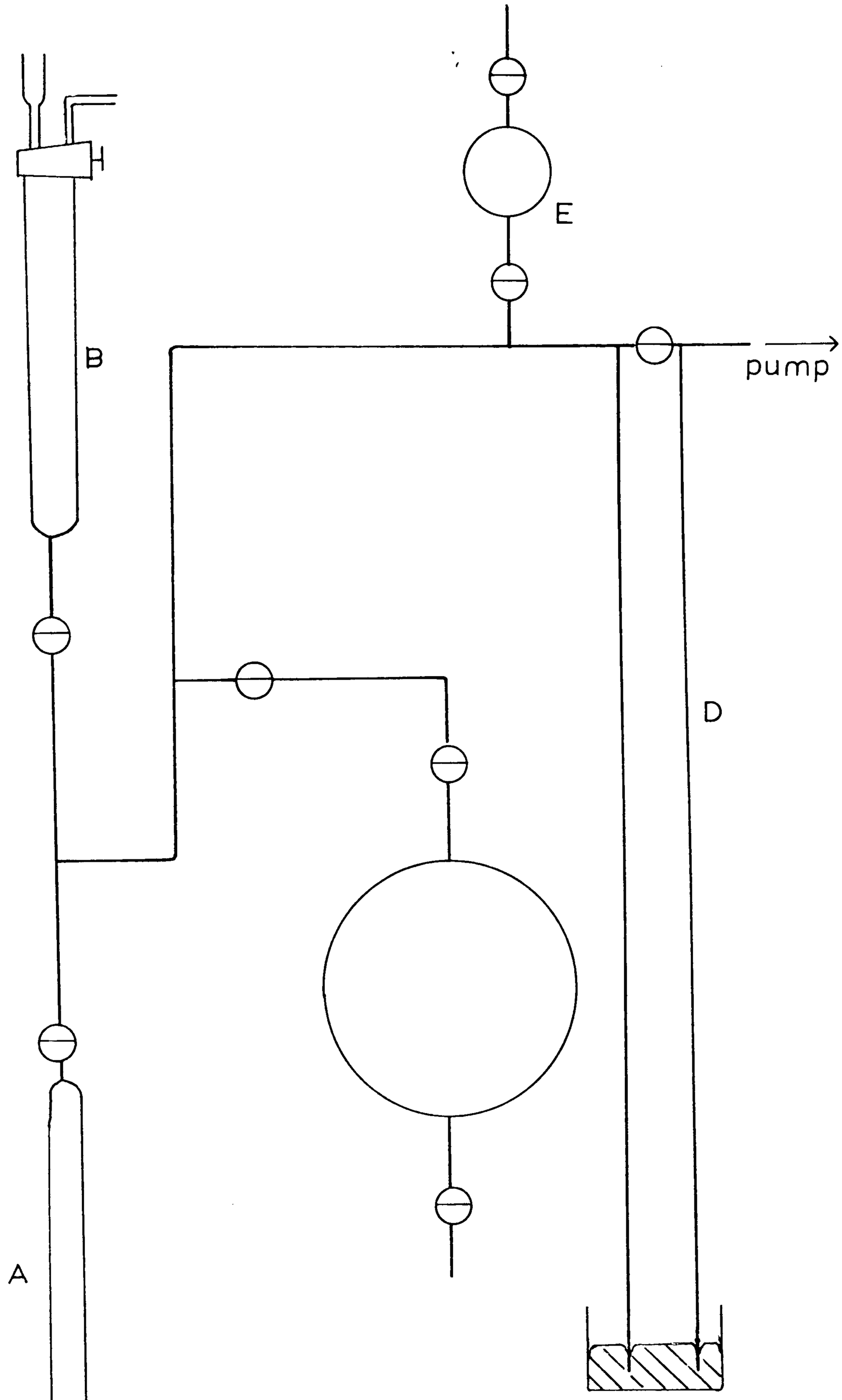

Na^+/K^+ remaining after hydrolysis were analysed by atomic emission techniques.

The analysis vessel (A), containing metal suspended in oil, was mounted beneath the reservoir of the de-aerated water (B). After evacuation of the frame and analysis vessel, the frame was isolated from the pump, and water from the reservoir allowed in, in quantities of one cm^3. Each addition of water was followed by a period of agitation using a magnetic flea as agitator and rotating magnet (C). The hydrogen pressure was monitored on the manometer (D). After agitation for approximately one hour, the manometer level settled, and another 1 cm^3 of water was allowed in. Additions, in total, of 4 - 6 cm^3 were necessary for complete hydrolysis. This was considered to be complete when no change in hydrogen pressure was noted after agitation for an hour. The volume of the gas space in the frame was then calculated from a series of P.V.T. data using the known volume of the bulb (E). This volume was different for each experiment, since the volume of the water + oil in the analysis vessel varied.

The analysis vessel was detached from the frame, and when the layers had separated, the water (lower) layer was run off. More water was introduced, shaken with the oil, allowed to separate and then run off. This process was repeated several times, and finally the water layer was made up to a volume of 500 cm^3 for analysis.

A total of nine experiments were performed. A further series of four were carried out in which the depth of water above the capillary opening was increased to 50 mm.

8.3. RESULTS

Experiments 1 - 9 are for a water depth of 0 - 4 mm, experiments 10 - 13 for a depth of 50 mm. Full details of the analyses are presented in Appendix 2. The essential results are presented in Table 8.2.

The second column is the total quantity of metal ions ($Na^+ + K^+$) found in the sample after hydrolysis. The theoretical quantity of hydrogen produced according to the reaction (Equation (8.1)) during hydrolysis is half of this value. The third column shows the quantity of hydrogen actually produced during hydrolysis. The values in the fourth column were calculated from Equation (8.7).

$$\text{Mole \% of MH in sample} = \frac{2(b - a/2) \times 100}{a} \qquad (8.7)$$

a = moles of metal in sample (column 2)

b = moles of hydrogen produced during hydrolysis of the sample (column 3).

The fraction $(b - a/2)$ represents the excess hydrogen over that resulting solely from metal hydrolysis (Equation (8.1)). This comes from $2(b - a/2)$ moles of metal hydride. A full derivation of Equation (8.7) appears in Appendix 3.

TABLE 8.2 RESULTS OF HYDRIDE DETECTION EXPERIMENTS

Experiment	Moles metal in Sample (a) ($x10^3$)	H_2 released (moles) (b) ($x\ 10^3$)	% Na(K)H in sample
1	5.08	2.54	0
2	8.08	4.73	17.1
3	8.56	4.55	6.3
4	6.12	3.31	8.2
5	8.90	4.95	11.2
6	5.11	2.70	5.4
7	1.43	0.73	1.4
8	8.61	4.42	2.6
9	7.32	3.78	3.3
10	6.48	3.20	-1.2
11	8.72	4.18	-4.1
12	6.22	2.98	-4.2
13	8.99	4.20	-6.5

8.4 DISCUSSION

The results fall into two categories: Experiments 1 - 9 for small travel distances, show the presence of metal hydride. There seems little doubt, therefore, that metal hydride is produced at the jet and is carried away from the primary reaction zone by the unreacted metal globules. The proportion of hydride, however, seems to vary from zero to 17.1% mole % even under constant conditions. Hence only a rough average is obtained. This discrepancy in the results may have a number of causes:-

(a) Variation in the ratio of sodium to potassium in the alloy. At 240°C the rate of reaction of sodium with hydrogen is 1.84×10^{-8} cm^3 s^{-1} cm^{-2} Pa^{-1}, [62] that of potassium is 6.85×10^{-8}, [63] or more than three times as fast. If the metal-hydrogen system in this type of metal-water reaction is not at equilibrium, the above figures would suggest that more hydride would result from experiments in which a potassium-rich alloy was used, then for a sodium-rich alloy. The results, however, do not indicate this. Experiments 1 - 5 employed sodium rich alloys, and 6 - 9 potassium rich alloys (see Appendix 2). There is no noticeable difference between these sets of results.

(b) Variation in the distance travelled. This is the most likely reason for the variation in the results. Maintaining the constancy of such a small head of water from experiment to experiment was difficult. Moreover, the head varied due to turbulence when the metal was injected. The most pertinent conclusion that can be drawn is that Na(K)H is rapidly hydrolysed

immediately after leaving the jet, and since it is likely to be found on the surface of the metal globules, due to its insolubility in the metal, it is preferentially hydrolysed when the globule hits the bubble wall. Therefore, hydride disappears after only a very short distance of travel.

The average value is 6.2%. Since the lowest (zero) and highest (17.1%) results were from the first two experiments performed, where expertise was naturally least, it is not unwise to ignore these, and the average becomes 5.5%. This adjusted value is subsequently used in the reaction rate calculation.

Experiments 10 - 13, over larger distances (50mm) show that all the hydride has been hydrolysed within this short ascent. The values in column 4 are no longer greater than zero. The fact that they are not zero but now negative is very significant. They mean that the positive values for experiments 1 - 9 are probably minimum. This implies that not all of the metal ions which were analysed originated from hydrolysis of metal and metal hydride. Clearly these must have come, therefore, from metal hydroxide. Thus the ascending hydrogen bubble contains not just metal globule covered with hydride, but also some metal hydroxide which may have been responsible for the observed grey colouration on the globules eventually trapped in the oil layer.

From these results, it is proposed that the build-up and subsequent removal of metal hydride is extremely rapid. Figure 8.4 illustrates this. In the jet reaction, M is consumed very rapidly and MH produced. Subsequently, as the bubble rises, M is consumed less rapidly but the surface MH disappears by hydrolysis almost immediately. With a more sophisticated technique, it should be possible to plot points for the curve MH, by minute variation in the water depth, followed by analysis as described above. The

FIG. 8.4 The production and removal of Na(K)H

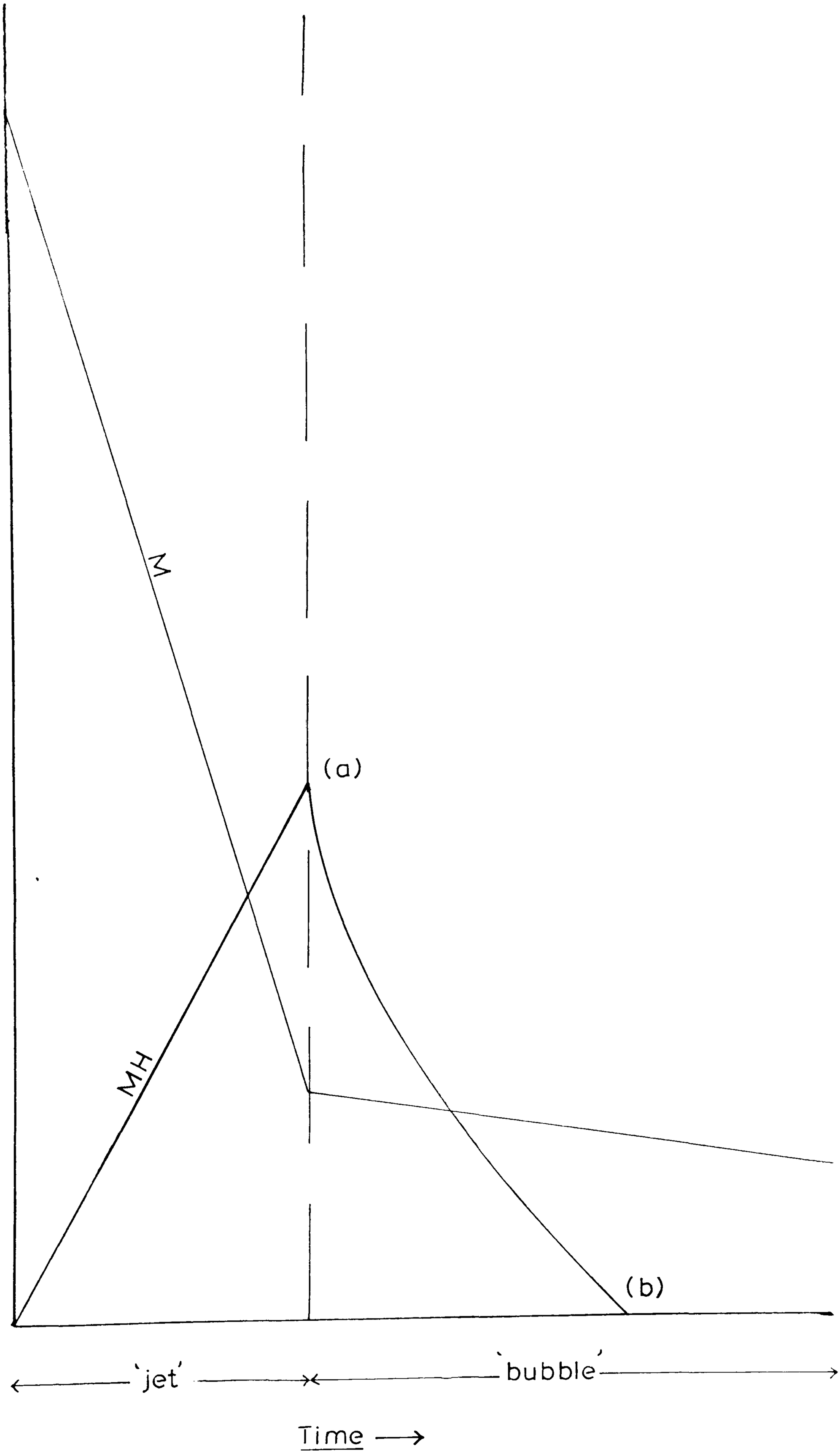

present work places the point (a) at 5.5% of the total metal, and point (b), 0%, at 50 mm travel (0.2 seconds) at the most.

The rate of reaction of hydrogen with the metal (it is not possible to separate the alloy into its two constituent parts as with M + H_2O reactions) is calculated from the knowledge that metal leaving the jet contains approximately 5.5 mole % MH. A similar treatment to that in Chapter 5 (M + H_2O reaction rates) is applied.

The reaction between metal and water was assumed to take place over the surface area of exposed metal A - B (Figure 8.5). In this case, reaction 8.4 can only take

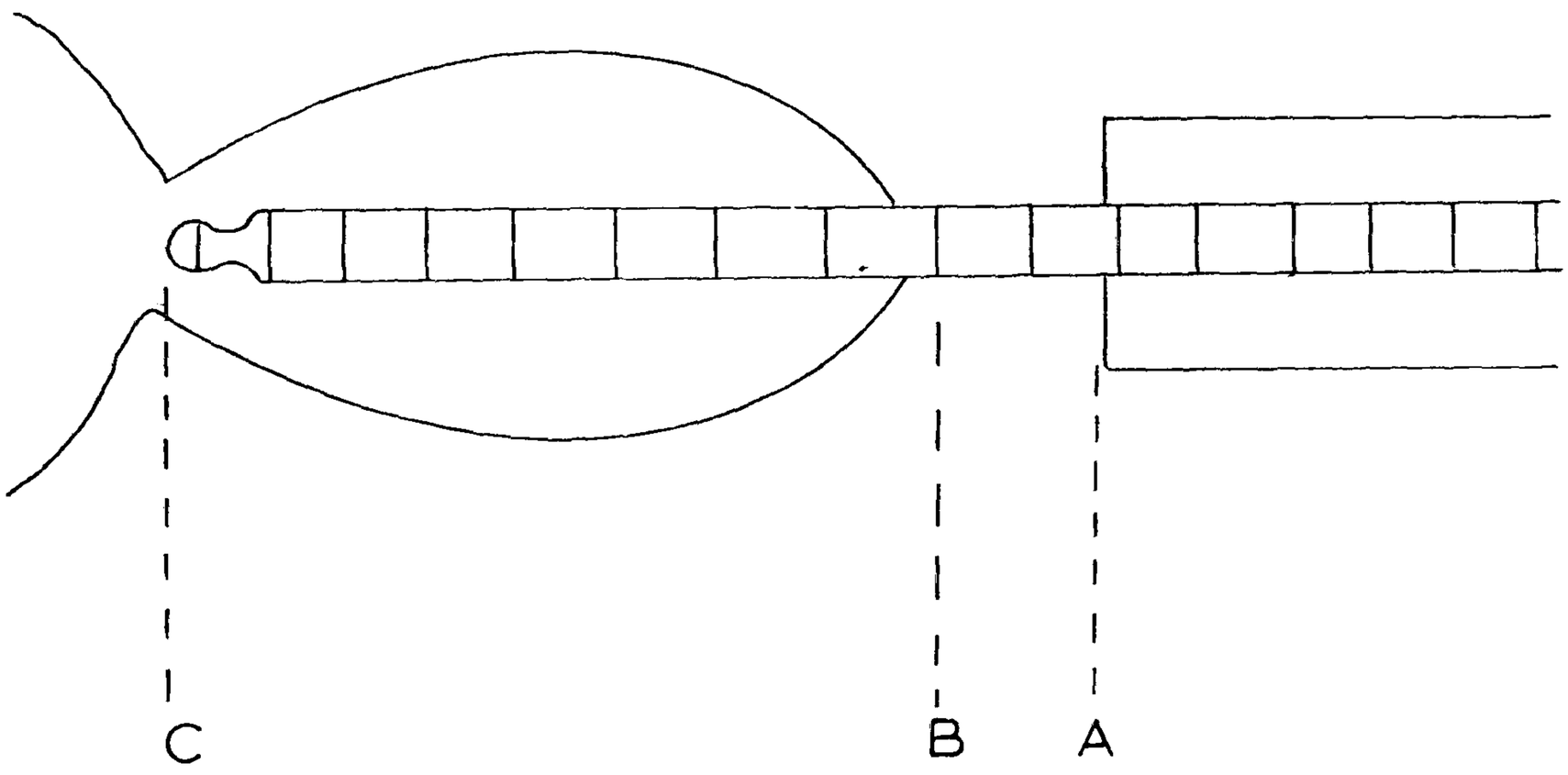

FIGURE 8.5 THE REACTION M+H_2

place in the region BC. The total length AC, from photgraphs, was 3.90 mm on average. This means that the reaction is taking place over a distance of 3.90 - 0.42 = 3.48 mm, 0.42mm being the average distance AB.

Every second, 20 mg of alloy leave the capillary to produce the metal jet. In an alloy of composition 50 mole % sodium, this represents a total of 6.44×10^{-4}

moles of metal. Of this, 11% of the potassium (0.35×10^{-4} moles) and 4.7% of the sodium (0.15×10^{-4} moles) react in the region AB. This leaves $(6.44 - 0.35 - 0.15) \times 10^{-4} = 5.94 \times 10^{-4}$ moles of metal to enter the gas envelope and react with hydrogen. Of this metal, approximately 5.5%, or 3.27×10^{-5} moles react according to Equation (8.4) over an area of $2\pi rl$ or 10.93 mm^2. The rate of reaction is therefore 2.99×10^{-6} moles/s/mm^2 at the bulk water temperatures of approximately 20°C, although the local temperature at the site of reaction may be much higher.

8.5 CONCLUSIONS

1. NaK reacts at the jet to form Na(K)H.

2. The proportion of Na(K)H in the jet metal is 5.5% on average.

3. Na(K)H is captured with unreacted metal in the bubble.

4. Surface Na(K)H hydrolyses rapidly in the ascending bubble.

5. The rate of reaction (Equation (8.4)) is 2.99×10^{-6} moles/s/mm^2 in this system.

C H A P T E R I X

REACTION INTERMEDIATES

9.1 INTRODUCTION

When the alkali-metals are dissolved in certain solvents, blue solutions are observed. The phenomenon was probably first observed in the solvent liquid ammonia.[66] A similar solution arises using the alkyl amines,[67] and with the fused alkali amides and even with fused sodium hydroxide.[68] Wolthorn and Fernelius[69] noted that whereas blue solutions arise on the dissolution of potassium in methyl alcohol, there is no such colour in ethyl alcohol. Extending their work to cover the solvent water, they tentatively suggested a transient blue colour arose during the reaction between potassium and water, and suggested therefore that water be considered a solvent for the alkali-metals, albeit giving a very unstable solution. The source of the blue colouration in these solvents is now established as the solvated electron, which arises from the reaction described by Equation (9.1)

$$M + \text{solvent} \longrightarrow M^{+}_{(\text{solvent})} + e^{-}_{(\text{solvent})} \quad (9.1)$$

This species is regarded as stable in the case of liquid ammonia and the alkyl amines, less so in the case of the alcohols, and much less so in the case of water. As the acidity of the medium increases from ammonia to the alcohols to water, so does the stability decrease.

In the case of water, the accepted reaction path was as shown by Equation (9.2) until the discovery of the

$$M + H_2O \longrightarrow M^+ + OH^- + H \qquad (9.2)$$

hydrated electron. The intermediate in this reaction is the H atom. Molecular hydrogen arises from the secondary combination of this species, as shown in Equation (9.3)

$$H + H \longrightarrow H_2 \qquad (9.3)$$

Bronsted and Kane[70] modified this to take account of hydrogen ions in solution, and slso of the fact that a metal surface consists of positive metal ions and free electrons. For the reaction at a metal surface, therefore, they replaced Equation (9.2) by (9.4). It was not recognised at this

$$M^+ + H_3O^+ + e^-_{(surface)} \longrightarrow M^+ + H_2O + H \qquad (9.4)$$

time that the electron depicted in this equation could exist independently in solution. This was first proposed by Stein and Platzman in in 1952 [71], and is now a recognised feature of the radiation chemistry of water. Two modern reviews [72,73] and a book[74] show the importance of the species, and describe its many and varied chemical reactions.

It was shown, at least in the case of sodium amalgams, by Shaede and Walker,[75] that the hydrated electron is an intermediate species in the reaction between the alkali-metals and water. They recognised the difficulty in distinguishing between $e^-_{(aq)}$ and H atoms due to their similar chemical nature (as very powerful reducing agents) and their interconvertibility, shown by Equation(9.5). By the

$$e^-_{(aq)} + H_2O_{(l)} \longrightarrow H_{(aq)} + OH^-_{(aq)} \qquad (9.5)$$

technique of competition kinetics, however, they showed that $e^-_{(aq)}$ and not H is the precursor of molecular hydrogen.
An efficient scavenger of $e^-_{(aq)}$ is N_2O (Equation (9.6))

$$e^-_{(aq)} + N_2O \longrightarrow N_2 + O^- (\longrightarrow OH) \qquad (9.6)$$

and CH_3OH is known to remove H atoms (Equation (9.7)).

$$H + CH_3OH \longrightarrow H_2 + \dot{C}H_2OH \qquad (9.7)$$

In a reaction between sodium amalgam and water in which the solution contained both nitrous oxide and methanol, nitrogen was the principal product (Equation (9.8))

$$Na(Hg) + H_2O + CH_3OH + N_2O \longrightarrow NaOH + N_2 \qquad (9.8)$$

The comparative reaction rates for the above processes are shown in Table 9.1.

TABLE 9.1. THE REACTION RATES OF HYDRATED ELECTRONS AND HYDROGEN ATOMS[76]

$e^-_{(aq)} + N_2O \longrightarrow$ products	9×10^9 mole^{-1}. s^{-1}
$H + N_2O \longrightarrow$ products	3×10^5 mole^{-1}. s^{-1}
$e^-_{(aq)} + CH_3OH \longrightarrow$ products	10^4 mole^{-1}. s^{-1}
$H + CH_3OH \longrightarrow$ products	2×10^6 mole^{-1}. s^{-1}

Further evidence for $e^-_{(aq)}$ as an intermediate is shown by the effect of cupric ions on the reaction between sodium amalgams and water.[77] With the inclusion of Cu^{2+}, if molecular hydrogen arises from the combination of two hydrated electrons, the relative rate constant would be $k(e^- + e^-) / k(e^- + Cu^{2+}) \simeq 0.3$. If the hydrogen is from the combination of hydrogen atoms, this becomes $k(H + H) / k(H + Cu^{2+}) \simeq 190$. Experimental ratios indicate the former case.

The initial reaction step is therefore described by Equation (9.9), followed by Equations (9.10), (9.11) or (9.12). Note that in the case of (9.11) and (9.12) that the hydrogen atom is still a precursor to hydrogen molecules (Equation (9.3)), but the production of this is not an initial step in the reaction. The rates of these reactions are:-[78] 0.6×10^{10}, 2.06×10^{10} and 16.0 mole^{-1}. s^{-1} for equations (9.10), (9.11) and (9.12) respectively.

$$e^-_{(aq)} + e^-_{(aq)} \longrightarrow H_2 + 2OH^-_{(aq)} \qquad (9.10)$$

$$e^-_{(aq)} + H_3O^+_{(aq)} \longrightarrow H + H_2O_{(l)} \qquad (9.11)$$

$$e^-_{(aq)} + H_2O_{(l)} \longrightarrow H + OH^-_{(aq)} \qquad (9.12)$$

The most likely reaction in water, therefore, is that shown by Equation (9.11). The reaction shown by Equation (9.12) plays a minor role.

9.2 THE OBSERVATION OF $e^-_{(aq)}$ BY SPECTROSCOPY

The absorption spectrum for the species $e^-_{(solvent)}$ is known for many systems. The best understood is that for the solvent ammonia [79], and in this solvent there is a maximum at 1400 nm with an extinction coefficient of 50×10^{-4} M^{-1} cm^{-1}. In water, the spectrum of $e^-_{(aq)}$ has been determined during pulse radiolysis experiments. The results for ice[80] and water at 25°C, [81,82] show a maximum at 715 nm with an extinction coefficient of $1.85 \times 10^{-4} M^{-1} cm^{-1}$. It has been claimed that this spectrum can be observed during the reaction of sodium with water.[83]

Using a similar experimental apparatus to that in Figure 4.2 (reaction vessel modified for photographic

observation) attempts were made in the present study to obtain a spectrum, using a Perkin-Elmer 402 Ultraviolet Spectrometer, in the area of injection. Despite several endeavours, no characteristic peak in the region of 715 nm could be detected. The beam of the spectrometer cut the area shown in Figure 9.1.

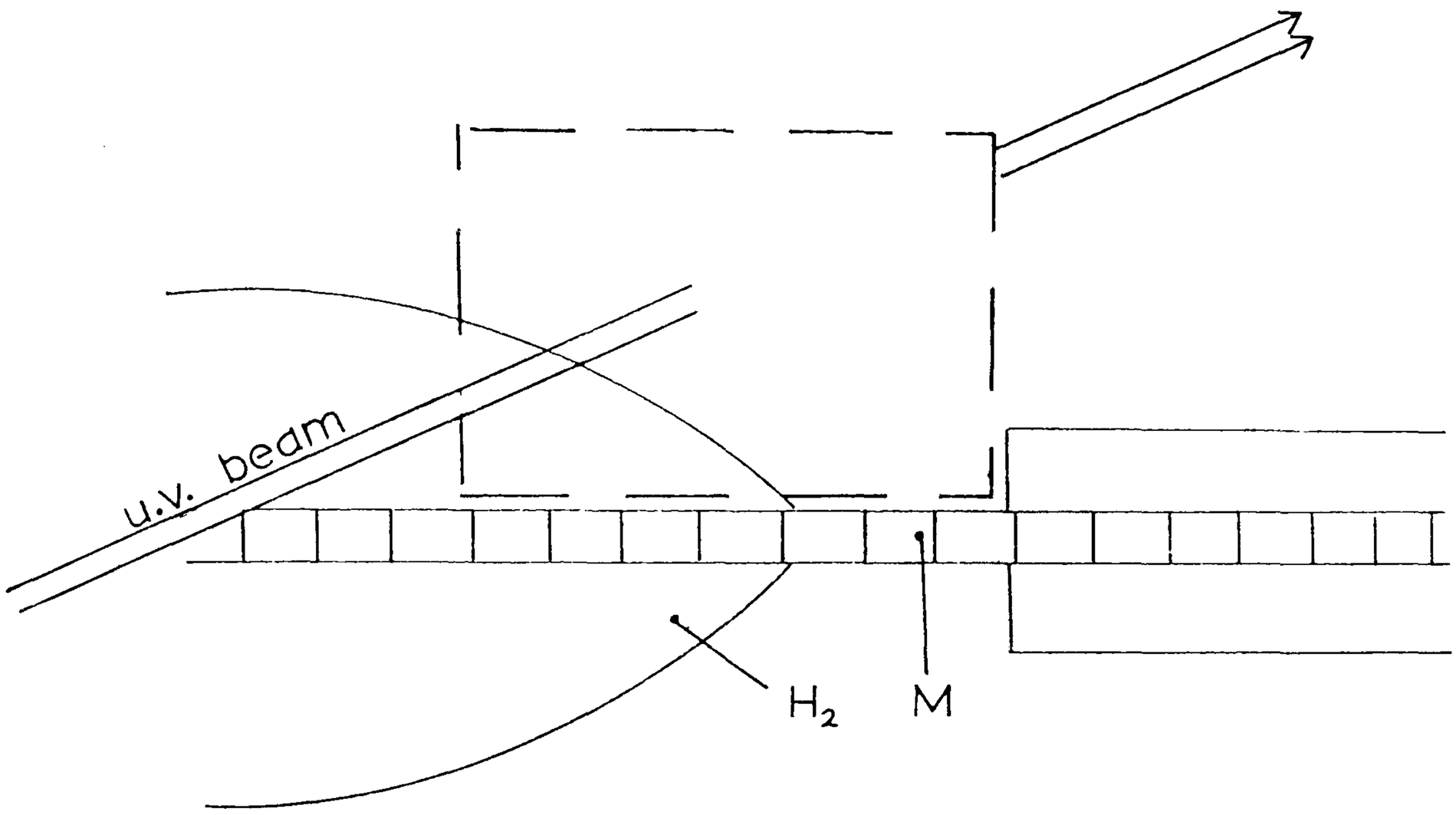

FIGURE 9.1. AREA COVERED BY U.V. SPECTROMETER BEAM

There are obvious difficulties in attempting to record a spectrum of $e^-_{(aq)}$ in this way. The hydrogen envelope is not permanent, but fluctuates, thereby rapidly changing the path length of the radiation. The main problem, however, concerns the concentration of the species in the region observed. In a U.V. spectrum of $e^-_{(aq)}$ produced by pulse hydrolysis, the species are widely separated, minimising their interaction (Equation (9.10)). In the present work,

however, hydrated electrons are produced over a localised region, and are not likely to penetrate into the solution to any great extent.

9.3 VISUAL OBSERVATION

In most reactions between an alkal-metal and water, it seems impossible to prevent the species $e^-_{(aq)}$ from being rapidly removed due to reaction (9.10). Some authors [69,83] have suggested conditions which might enable hydrated electrons to be observed visually. These conditions are:-

(a) The use of low temperature, to decrease the rate of reaction (9.10), and thereby increase the lifetime of $e^-_{(aq)}$.

(b) The use of alkaline solutions, to decrease the rate of reaction (9.11) by reduction in the concentration of H_3O^+.

(c) The use of metal in excess e.g. at the interface between reacting metal and glass.

With these suggestions in mind, some simple experiments were conducted in the Nottingham laboratory. Thus water was poured onto the surface of sodium at -78°C. Reaction occurred, but no blue colour, transient or otherwise, was observed. When the water was allowed to freeze still in contact with the sodium surface, there was no blue colouration at the ice/metal interface. The same result was obtained when NaK was substituted for sodium.

In another experiment, however, in which conditions

(b) and (c) prevailed, but not (a), a blue solution was obtained in a reaction between liquid NaK and water. The situation is shown in Figure 9.2.

(i) A drop of water ran down the length of an open glass tube. The surface of the tube was coated with liquid NaK

(ii) Reaction occurred immediately, with the production of white hydroxide.

(iii) After several seconds, a blue film appeared between the metal and the glass surface. The tube at this stage was very hot, and the hydroxide molten.

This experiment indicated that condition (a) above is not necessary for visual observation of a hydrated electron. In fact, the opposite may be true. The reaction described by Equation (9.10) is likely to be slower at low temperatures, but at higher temperatures, reaction (9.13), the production of solvated electrons, may more than compensate for this.

$$Na(K)_{(l)} + H_2O_{(l)} \longrightarrow Na(K)^+_{(aq)} + e^-_{(aq)} \qquad (9.13)$$

This shows that the situation depicted in Figure 9.3 may prevail. At a particular temperature, x°C, reaction (9.13) becomes faster than reaction (9.10) i.e. the hydrated electron is generated faster than it is consumed.

FIG. 9.2 NaK(excess) + H_2O(l)

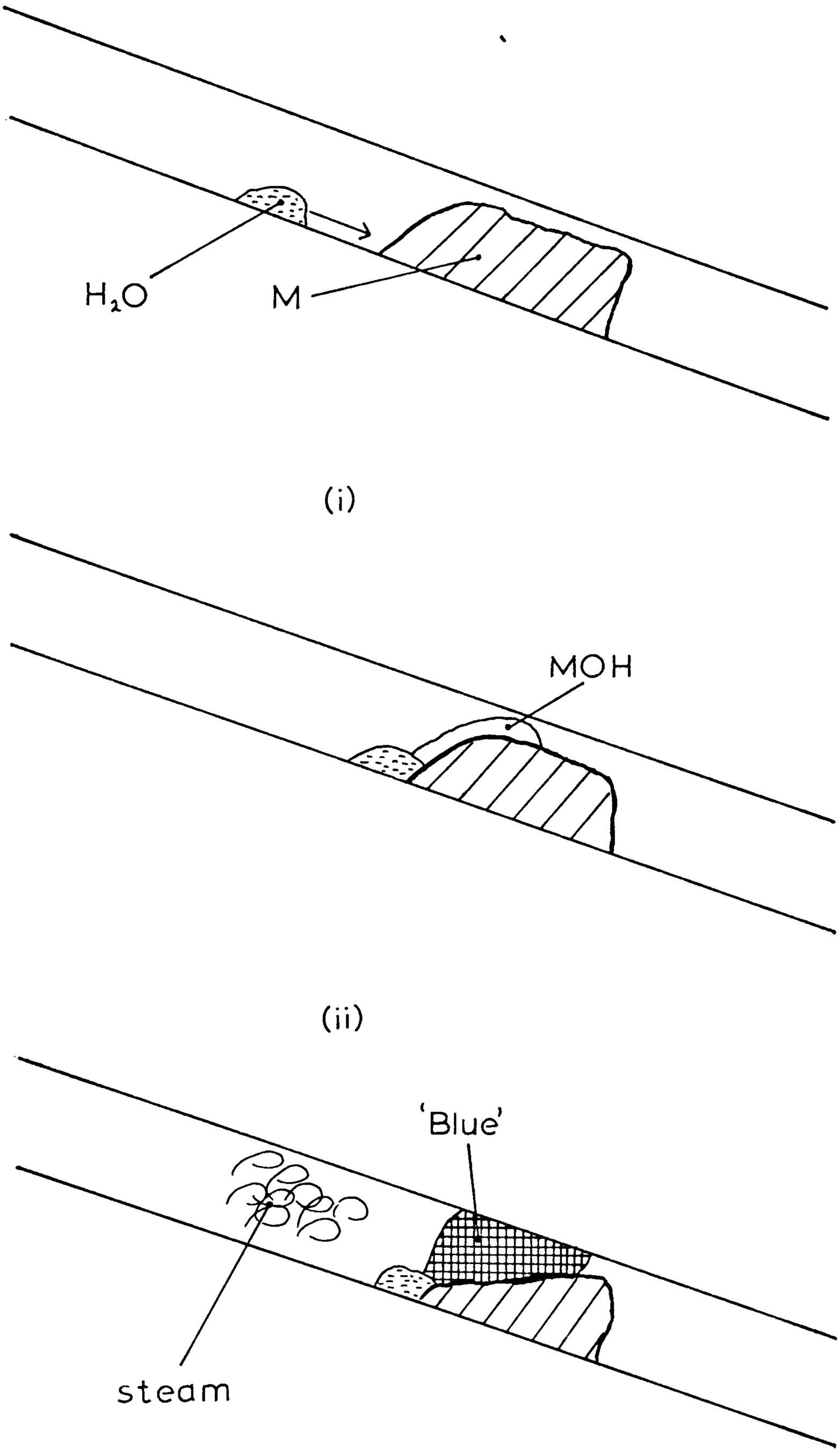

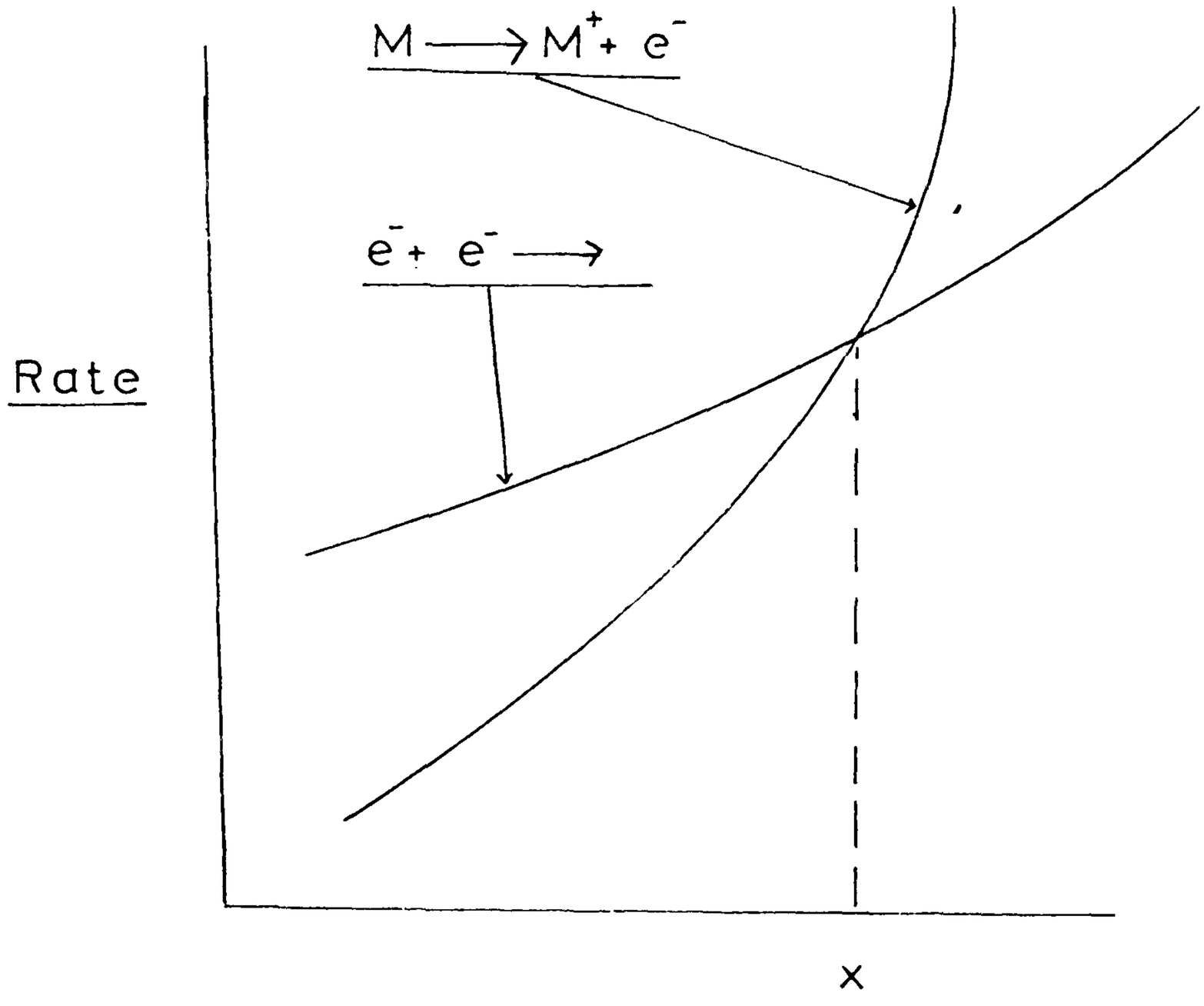

FIGURE 9.3 THE PRODUCTION AND REMOVAL OF $e^-_{(aq)}$, VARIATION WITH TEMPERATURE

This simple experiment showing the remarkably clear blue colouration at the metal surface is extremely significant. It shows that in these liquid metal - liquid water reactions, the hydrated electron is produced and that this species must be incorporated into any postulated reaction mechanism.

The balance of rate of generation and consumption of $e^-_{(aq)}$ appears to be quite criticæl if the blue colour is to be seen. Thus similar experiments with sodium alone, and with potassium alone, did not show the blue colour, possibly due to the fact that the development of high

temperatures does not occur as rapidly in the parent metals as it does in the more reactive alloy.

C H A P T E R X

REVIEW OF THE PROJECT

10.1 INTRODUCTION

The work in this thesis falls into several distinct areas:

(a) The physical behaviour of liquid alkali-metal jets in water.

(b) Rates of reaction of the metals with water, and the activation energies for such reactions. These are in two sections: one for the rates of reaction of the components of NaK and one for those of sodium.

(c) The reaction between the alkali-metals and hydrogen.

(d) The effect on the reaction of additives to the solution.

(e) Aspects of the reaction mechanism in solution.

The results of (a) have already been dealt with in detail. The results from part (b) will be compared with the results obtained by other workers, and with the rates of reaction of other Group I metals. The combined results will be used to propose some ideas on the reaction mechanism.

10.2 COMPARISON OF ACTIVATION ENERGY DATA

A comparison between the published activation energies for the reactions of lithium and sodium with water is shown in Table 10.1. For the reactions numbered 3,4 and 5, the Roman numerals I, II and III refer to the stages of the reaction $Li + H_2O_{(g)}$ described in Chapter 2. For reactions 11 and 12, the numbers (i) and (ii) refer to the situation of the reaction; (i) applying to the jet and (ii) to the bubble, in the present work.

Reactions 1 and 2 were carried out by Dowling. Due to the similarity of the activation energies determined, he concluded that a similar rate determining step may apply to the reactions of water both in the gas and liquid phase.

Reaction 2 is most experimentally comparable with the present work which is depicted by reactions 11 (i) and 12 (i). The present work provides activation energies which are both higher (for Na in NaK) and lower (for K in NaK), than for NaK itself. Intuitively, this is to be expected i.e. the alloy has characteristics in between those of the pure metals. There appear to be certain concentrations, however, e.g. 60 mole% Na which possess unexpected enhanced reactivity and give rise to activation energies which are lower than those for either sodium and potassium alone.[44] No specific data are available, however, for potassium alone with either liquid or gaseous water, so that this claim should be treated with some reservation.

For the reactions of sodium in the condensed phase with water vapour (reactions 6 - 9), the quoted values of the activation energies range from 18.4 to 33.5 KJ/mole, thereby showing a considerable spread. An average value

TABLE 10.1 ACTIVATION ENERGIES FOR M + H_2O REACTIONS

Reaction	E (KJ/mole)	Author	Reference
1. $NaK_{(l)} + H_2O_{(g)}$	38.8	Dowling	49
2. $NaK_{(l)} + H_2O_{(l)}$	35.5	Dowling	49
3. $Li_{(s)} + H_2O_{(g)}$	23 - 26 (II)	Deal and Svec	24
4. $Li_{(s)} + H_2O_{(g)}$	49.0 (I) 32.2 (II)	Irving and Lund	25
5 $Li_{(s)} + H_2O_{(g)}$	96.3 (I) 41.2 (II) 58.6 (III)	Besson and Pelloux	26
6. $Na_{(l)} + H_2O_{(g)}$	33.5	Besson	26,84,85
7. $Na_{(l,s)} + H_2O_{(g)}$	20.9	Cornec and Sannier	28
8. $Na_{(l)} \ddagger H_2O_{(g)}$	30.6	Longton	86
9. $Na_{(s)} + H_2O_{(g)}$	18.4	Longton	86
10. $Na_{(s)} + H_2O_{(l)}$	60.8	Miskinova and Giddin	87
11. $Na(NaK) + H_2O_{(l)}$	38.3 (i) 33.0 (ii)	This work	
12. $(NaK) + H_2O_{(l)}$	24.9 (i) 27.3 (ii)	This work	

is 25.9. The only value quoted for the reaction of liquid water (reaction 10) is 60.8 KJ/mole, and this is considerably greater than the 38.3 and 33.0 KJ/mole obtained in the present work. It should be remembered, however, that these lower values are for a system which must include some water vapour (See Chapter 5). Perhaps the most general feature is that the present values of 38.3 and 33.0 fall between those previously quoted for liquid water (60.8) and water vapour (average 25.9).

10.3 REACTION MECHANISM

Whereas the reaction of water vapour or individual molecules with the alkali-metal surface must involve adsorption, polarisation of the molecule, electron transfer and bond cleavage, the use of liquid water adds a new dimension in that the electron can now be transferred to a group of water molecules to create an electron in a cage thereby spreading the charge over several molecules. This bestows some transient stability since in Chapter 9 some evidence was presented for believing that water could dissolve the alkali-metals through the process of creating a solution of hydrated electrons and metal cations. Due to extreme reactivity of the electron, however, such solutions are not stable. The generation and fate of the electrons are shown by the scheme below.

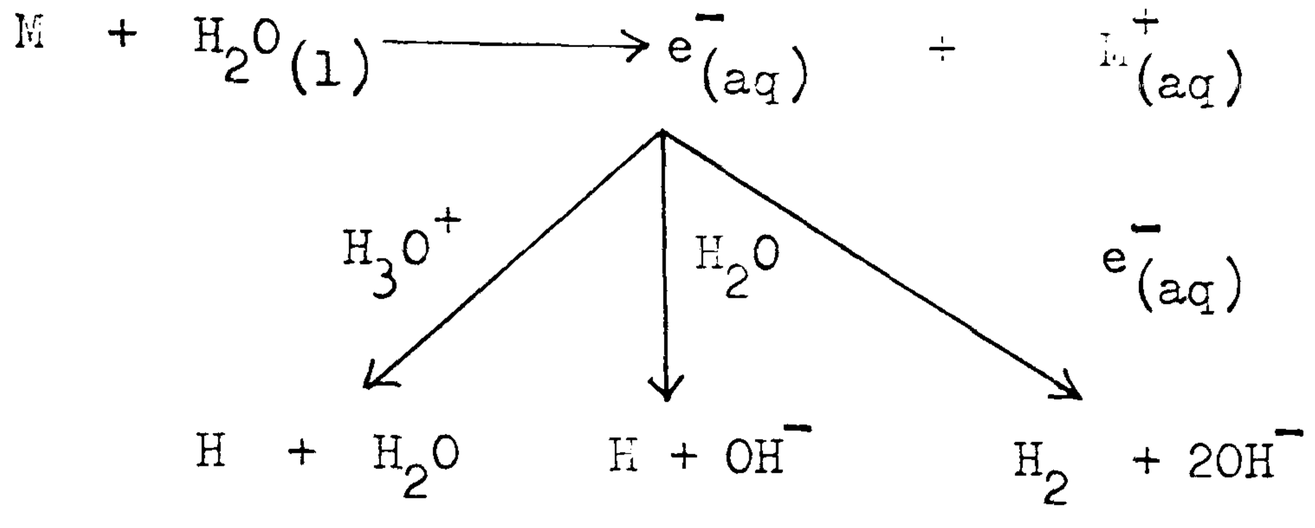

10.3.1 Reaction in solution

A number of points arise on the solution side:-

(1) The reaction of liquid water with NaK in tubes was shown in Chapter 9 to give the characteristic blue colour of the hydrated electron. Thus there is strong justification for invoking this species in the present work. Competition kinetics have also indicated this reaction path for the reaction between dilute sodium amalgams and water.[75]

(2) The nature of the hydrated electron is independent of its mode of generation.[88] The spectroscopic properties of the species are the same with $\varepsilon = 1.84 \times 10^4 M\ cm^{-1}$ at the absorption maximum 715 nm, irrespective of the source.[89] Thus differences in the chemical reactivity of the alkali-metals towards liquid water must be explained by variations in the initial, or dissolution step.

(3) The dissolution step involves loss of an electron from the metal and encapsulation of this electron and metal cation by water molecules. This can be illustrated by the scheme below.

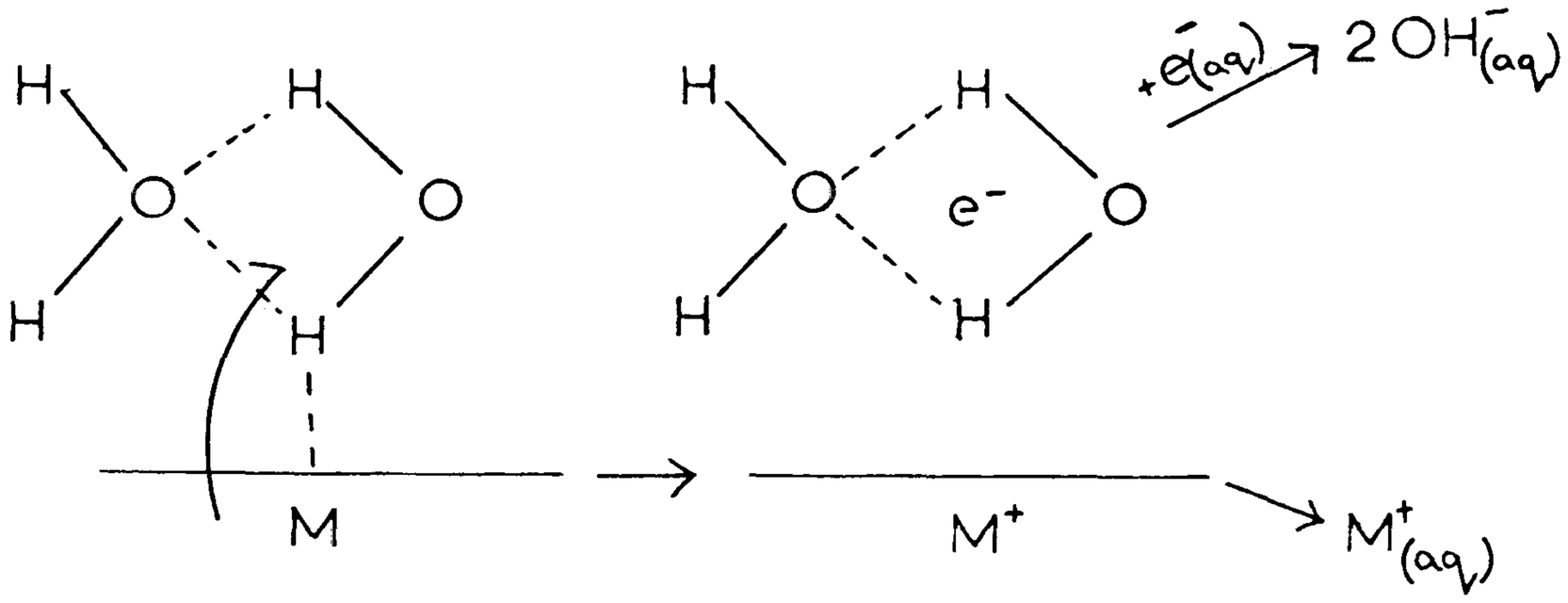

Molecules in liquid water are adsorbed at the metal surface. Electrons are transferred to the hydrogen-bonded liquid creating the caged or hydrated electron which reacts with another such species to produce hydroxide and molecular hydrogen. The electron is thus consumed, the solvated cation remains in solution, and molecular hydrogen escapes unless further contact with the metal is allowed. The slowest and hence rate determining step appears to be adsorption and electron transfer. Adsorption would then be strongest on the heavier metals i.e. caesium, and electron transfer easier for the heavier metals. Adsorption is favoured by suitable M - M spacing and electron transfer, generally, by the atomic size. Whereas it is not clear which spacing is most suitable for adsorption, the ionisation potential and work function decrease down the group, the latter being more appropriate for the bulk metal.

Metal	Li	Na	K	Rb	Cs
Work function KJ/mole	233	220	216	201	174

The dissolution of cations does not appear to be rate determining. Naturally, these must be transferred into solution before further reaction can take place with the second layer of metal atoms. However, this dissolution becomes less energetically favourable the larger the metal ion, and the mobility of metal ions (apart from that of lithium) in water decreases down the group. Since these factors do not vary in accordance with the observed behaviour of the metals (increasing violence of reaction with water with increasing atomic number) the dissolution and removal of cations from the surface is not rate determining.

(4) In practice, the basic processes may be masked by products. Gaseous products prevent the metal from arriving in solution, and with solid salt films the observed rate might well be controlled by the diffusion of metal atoms through the salt towards water molecules. The thickness of the salt film may be governed by its rate of solution in water and also its absolute solubility.

(5) The reaction between $e^-_{(aq)}$ and $e^-_{(aq)}$ gives rise to the observed reaction products directly. The species $e^{2-}_{2(aq)}$ is probably present as a transition state or highly unstable intermediate. This is analogous to the species $e^{2-}_{2(NH_3)}$, its equivalent (stable) counterpart in liquid ammonia.

(6) The reaction of NaK with aqueous acid is more rapid than with pure water at high acid concentrations in the present work. There is evidence (Chapter 7) that when interference from salt films is eliminated or reduced, that the rate is enhanced at low acid concentrations as well. Certainly

the reaction of $e^-_{(aq)}$ with H_3O^+ is approximately three times as fast as that of $e^-_{(aq)}$ with another $e^-_{(aq)}$,[90] but this does not automatically mean that the fate of the solvated electron controls the overall rate. Under acid conditions, the adsorbed species may no longer be a simple water molecule but a hydrated proton, H_3O^+. Adsorption and transfer of an electron to this species is intuitively expected to be both more energetically favourable and rapid. The scheme is illustrated below.

(i) $H_3O^+_{(l)} \longrightarrow H_3O^+_{(ads)}$

(ii) $M \longrightarrow M^+ + e^-$

(iii) $H_3O^+_{(ads)} + e^- \longrightarrow H_2O + H_{(ads)}$

(iv) $M^+_{(surface)} \longrightarrow M^+_{(aq)}$

The hydrated electron does not feature in the above scheme. A significant difference between the reaction of metal with water and acid is the mode of generation of <u>molecular</u> hydrogen. With water, this is the result of reaction of $e^-_{(aq)}$. In acid, atomic hydrogen results both from the above scheme and from the reaction of $e^-_{(aq)}$ with H_3O^+. Another step is therefore necessary to account for the observed formation of hydrogen molecules.

(v) $H_{(aq)} + H_{(aq)} \longrightarrow H_2(g)$

<u>Or</u> $H_{(ads)} + H_{(ads)} \longrightarrow H_{2(ads)} \longrightarrow H_2(g)$

(7) Yet one more reaction appears to be relevant in acid solutions and this is the reduction of anions by the hydrated electron. In the reactions between NaK and concentrated sulphuric acid, both sulphur and hydrogen sulphide were detected, possibly arising from the reaction shown by Equation(10.1). This is a relatively slow reaction

$$e^-_{(aq)} + SO_4^{2-} \longrightarrow \text{sulphite, sulphide, sulphur etc} \quad (10.1)$$

($10^6\ M^{-1}\ s^{-1}$) and hence only becomes important at high concentrations of this anion. In the present work on acids (Chapter 7) it seems probable that the reduction of sulphate must occur directly and not through the solvated electron, since the concentration of sulphate ions in solution was always half that of hydrogen ions (assuming complete ionisation of the acid), and the reaction between $e^-_{(aq)}$ and $H_3O^+_{(aq)}$ is approximately 2×10^4 times faster than Equation (10.1). If sulphate forms a solid layer against the metal, then direct reaction ensues, possibly according to the following Equations (10.2, 10.3, 10.4, and 10.5). Reduction of this nature has been reported in previous work on alkali-metal plus sulphuric acid reactions.[91]

$$Na_2SO_4 + 2Na \longrightarrow Na_2SO_3 + Na_2O \quad (10.2)$$

$$Na_2SO_4 + 2Na \longrightarrow SO_2 + 2Na_2O \quad (10.3)$$

$$Na_2SO_4 + 6Na \longrightarrow S + 4\,Na_2O \quad (10.4)$$

$$Na_2SO_4 + 8Na \longrightarrow Na_2 + 4Na_2O \quad (10.5)$$

(8) The rate of the reaction between $e^-_{(aq)}$ and a water molecule is so slow ($16 M^{-1} s^{-1}$) compared to the other possible reactions that this reaction can effectively be ignored in the reaction schemes.

10.3.2. REACTION AT THE SURFACE

Although the reaction pathway for sodium amalgam + water reactions has been shown to proceed via a hydrated electron, the evidence is not so strong for sodium metal. Using partially deuterated water, the H/D isotope effect in hydrogen evolution from sodium amalgam comes out to be 4.6 0.2 which is consistent with the effect expected for the reaction $e^-_{(aq)} + e^-_{(aq)}$.[92,93] For sodium metal, however, the value is less than 2. Thus in the reaction $Na_{(l,s)} + H_2O_{(l)}$, the possibility of a surface reaction (Equation(10.6)) cannot be excluded, and takes the form of

$$M + H_2O \longrightarrow MOH + H \qquad (10.6)$$

a direct electrophilic attack by the metal atom on the oxygen atom of water. This mechanism has been proposed for the gaseous process between $Li_{(g)}$ and $H_2O_{(g)}$.[94] The reaction at the surface then proceeds with the combination of adsorbed hydrogen followed by desorption of the hydrogen molecule (Equation (10.7))

$$H_{(ads)} + H_{(ads)} \longrightarrow H_{2(ads)} \longrightarrow H_{2(g)} \qquad (10.7)$$

The dissolution step (Equation 10.8) occurs at the end of the reaction sequence.

$$MOH_{(s)} \longrightarrow M^{+}_{(aq)} + OH^{-}_{(aq)} \qquad (10.8)$$

In the case of reactions of the metal with water vapour, the above sequence is likely to apply to all of the alkali-metals. A significant feature is the cleavage of hydrogen-oxygen bonds, this process being responsible for the observed chemiluminescence.[95] The overall reaction is then illustrated by the following steps:-

(i) Dissociative adsorption

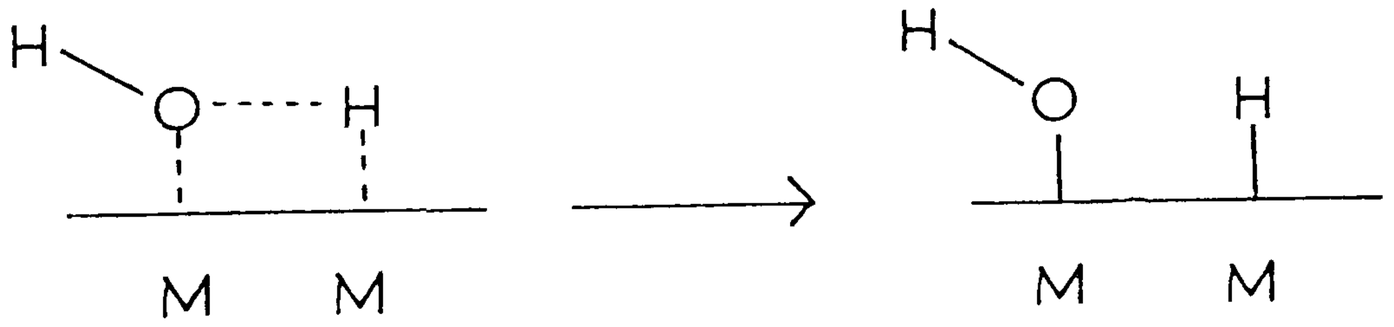

(ii) Reaction of adsorbed hydrogen atoms

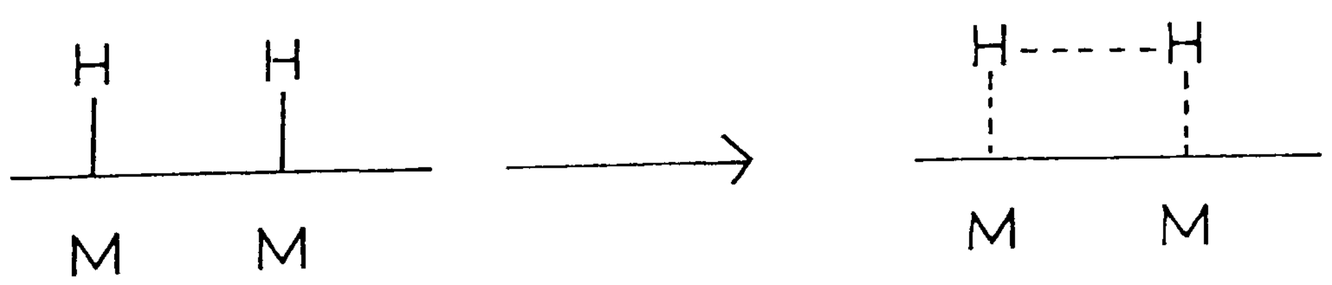

(iii) Desorption of molecular hydrogen

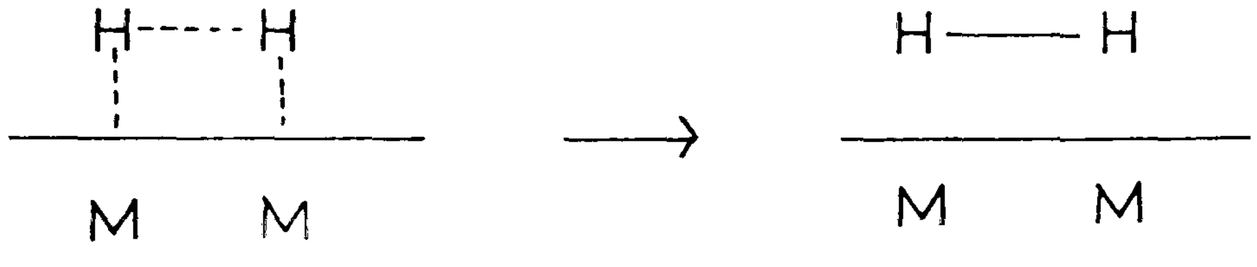

In many ways, this dissociative adsorption of water resembles the reactions of gases with the transition metals e.g. NH_3 is co-ordinated with the metal surface through N and H during dissociative adsorption [96,97] and reactions of alcohols with such metals is accompanied by O H bond cleavage. [98] The adsorption and desorption of hydrogen on an alkali-metal surface can likewise be compared with the same process on transition metals.

Generally, the reaction with water vapour will be inhibited by the presence of a product film. Film cracking may occur, as it does with solid lithium. Until such a stage is reached, however, the rate of reaction will be determined by the rate of diffusion of reactants through the product.

10.3.3. Summary

In the present work, the injection of liquid NaK into water is accompanied by immediate dissolution of the metal in the water to produce hydrated electrons and cations.

The electrons react quickly, one with another, and do not penetrate far into the solution. The build-up of reaction products in the vicinity of the jet may hinder further dissolution. The gaseous product, hydrogen, collects in the vicinity of the jet and forms an envelope around the metal. The hydrogen serves to protect the metal from the liquid water but itself reacts to form hydride. Hydrogen bubbles form around individual globules from the metal jet. Reaction continues within the hydrogen bubble but there is limited contact between the globule and the bubble wall. Within the bubble, reaction between metal and water vapour also occurs, and this is necessarily through dissociation of the water molecule at the metal surface to produce hydrogen atoms without passing through the solvated electron stage. Additional hydrogen is liberated in the bubble by the hydrolysis of metal hydride. Alkali in the water has little effect on the rate since the OH^- ion is not attacked by the solvated electron. Addition of H_3O^+ increases the rate due either to electron transfer to this species at the metal surface, or to the faster reaction of the solvated electron with it. Anions have little effect except when at high concentrations when reduction may occur.

10.4 APPLICATION TO F.B.R. COOLANT CIRCUITS

Fast nuclear reactors using liquid sodium as coolant are designed so that in the event of a leak across the heat exchanger, water or steam is forced into the liquid metal rather than vice-versa, and this, of course, is to avoid explosions associated with the water (excess)-metal reaction. It has been observed on occasions however, that despite

this pressure differential, there is still a backward flow or creep of metal into the water, and this makes the present work relevant to nuclear reactors. The results described in this thesis indicate that:-

(1) A small proportion of metal entering water coolant reacts immediately, but the majority of the metal is encapsulated in hydrogen bubbles which carry the metal a considerable distance from the leak or source of injection.

(2) The rate of hydrogen generation, which may be taken as a measure of the size of a leak, is complicated by hydride formation at the initial metal-water interface followed by hydride hydrolysis in the hydrogen bubble as it travels away from the leak. Thus generation of some molecular hydrogen is transferred to a point well away from the leak. These points may influence the positioning of hydrogen leak detectors. Moreover, the total reaction cannot be monitored by hydrogen pressure surges. This has already been proved for the 'metal' side of a steam generator and now seems to apply to the 'water' side as well. After an initial pressure surge, the further release of hydrogen may be gradual due to the formation and subsequent hydrolysis of sodium or NaK hydride, depending on the coolant. According to Hurd,[99] however, the hydrolysis of hydride is considerably more violent than hydrolysis of metal, thereby inducing a second, delayed pressure surge.

(3) Minor deviations from pH 7 in boiler water should not have a marked effect on the rate of reaction should a leak occur. With the dissolved ions Fe^{3+} and Cr^{3+} in the water, however, there may

be prevention of product film formation, leading to the increased mixing of the reactants, and enhanced reaction rates.

10. 5 FURTHER WORK

10.5.1. Reverse (Water → Metal) injections

Since the main process occurring in a heat exchanger leak is the injection of water into metal, it is pertinent to consider how this may be set up and studied on a laboratory scale. Naturally, much data is already available for full scale reactions of this type, in which L.M.F.B.R. steam generator leaks are simulated under operating conditions i.e. high temperatures and pressures. [9,19] Scale models of these generators have been built for this purpose.[100]

These investigations were concerned with temperature rises, pressure surges, the corrosive nature of solutions of products and the plugging in flowing systems by solid products. On a small scale, however, it would be interesting to see if there was any separation of the reactants by hydrogen as occurs in the injection of metal into water. Hydrogen would now encapsulate a water globule instead of a metal sphere (see Figures 2.3 and 2.4). The opaque problem in observing the bulk metal may tackled in different ways:

(1) Injection of water into a very narrow glass walled cell, containing NaK or Na. Bubbles that form would then be visible, and could be recorded photographically if their diameter

was greater than the width of the cell. It seems possible to count the number of bubbles produced in a certain time, measure their average size, and knowing the flow rate of water into the reaction vessel, come to a measurement of the rate of reaction. There are, however, many complicating issues. For example, the hydrogen bubbles might also contain appreciable quantities of water vapour, thereby increasing the apparent production of hydrogen, and giving a contribution from the metal-water vapour reaction. The method also would not give any indication of the nature of bubble formation at the jet, but would only show up the completed bubbles when they reach the appropriate size.

(2) Observation by radiation other than visible. There is a 'window' in the far ultraviolet region of the electromagnetic spectrum, in which the alkali-metals are transparent to radiation.[101] Hence ultraviolet transmission pictures seem possible. X-rays also pass through thin films of the metals. The mass absorption coefficients of the metals are shown in Table 10.1. Clearly silver gives the most penetrating X-rays for the alkali-metals but molybdenum targets are more readily available

Using MoK_{α}, intensity 30kv/20 mA, samples of the alkali-metals sodium, potassium, caesium and NaK proved virtually transparent to X-rays when the source was placed adjacent to glass vessels containing the metals. Exposure times of 1 - 2 seconds completely blackened sections of the film which were sealed in black paper folders and taped to the reverse surface of the glass. The path length of metal was approximately

TABLE 10.1 THE MASS ABSORPTION COEFFICIENTS OF THE ALKALI-METALS (INCLUDING SCATTERING).[102]

Metal	Li	Na	K	Rb	Cs
At. No.	3	11	19	37	55
Ag kα 0.05609 nm	0.18	1.75	8.05	48.2	23.6
Mo kα 0.07101 nm	0.22	3.36	16.7	94.4	43.3
Cu kα 0.15418 nm		30.9	143	109.1	347
Ni kα 0.16591 nm		37.9	179	132.9	410
Fe kα 0.19373 nm		56.9	269	197	579
Cr kα 0.22909 nm		92.5	425	309	844

30mm. With radiation from the same source, Mo k_α, at intensity 40kv/20mA, NaK proved semi-transparent i.e. the film darkened but did not turn completely black, when the source was removed to a distance of 300 mm from the sample. The exposure time in this case was one second. When argon filled tubes were immersed in the liquid metal, under the same conditions as above, the shadowed shape of the tubes could clearly be made out from the developed film. These shapes appeared as areas of black in a field of light grey. The difference in absorption coefficients then, between NaK and argon, is sufficiently great to distinguish between metal and gas bubbles.

Method (2) is potentially more useful, therefore, for a detailed observation of the situation of a water jet in liquid NaK. Prior to studying the reaction via X-ray shadows, the feasibility of squirting water into NaK was investigated.

A reaction vessel (Figure 10.1) was designed and built along the lines of the vessel for metal ⟶ water injections (Figure 3.3). Some important modifications, however, were necessary. The ground glass taps were replaced with greaseless taps, and the injector was joined directly to the vessel, dispensing with the ground glass joint. The top of the vessel now consisted of a tap (A) with adaptor to fit the NaK filtration apparatus (Figure 3.2). Draining the vessel after use was naturally not so straightforward as before, so a ground glass joint (B) was fitted so as to allow drainage into a closed argon-filled vessel. The injector (C) was of the same pattern as used previously, with the omission of the sintered glass filter. It fitted into that part of the reaction vessel which comprised the 'observation cell', whose dimensions were approximately 50mm x 50 mm x 10 mm (depth). Both the argon cover gas and that used to supply the pressure for water injection were scrubbed by bubbling through liquid NaK (D and E respectively).

FIG. 10.1 Reaction vessel for $H_2O \longrightarrow$ NaK injections

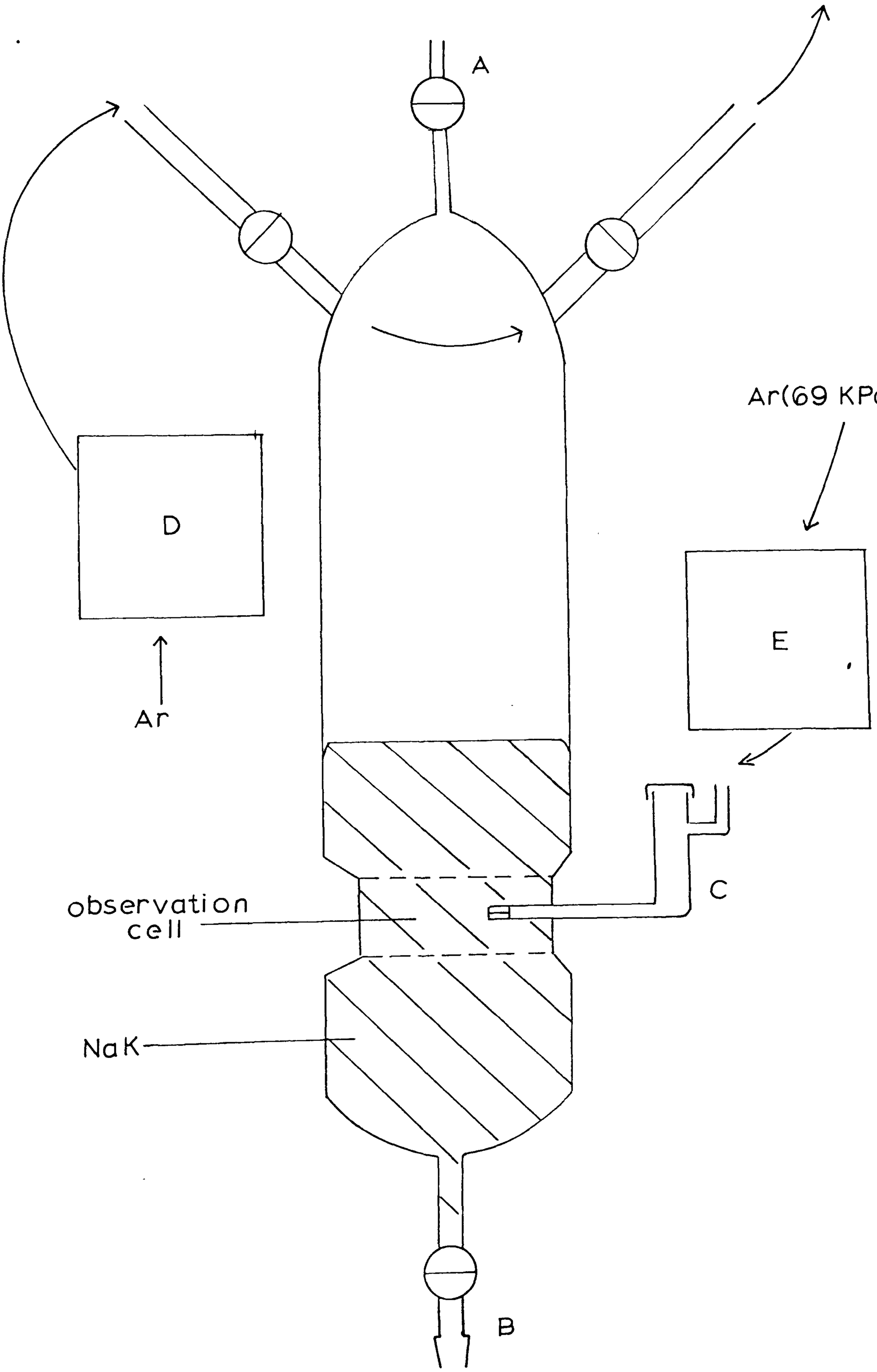

Water was introduced to the injector via the rubber septum cap (F) using a 2 cm^3 syringe and hypodermic needle. Two injections of water were carried out, one immediately after the other, into the same bulk metal. The gas pressure was 69 KPa for the first injection, of approximately 0.5 cm^3, and 30 KPa for the second, of 2 cm^3 of water. This lower pressure for the second injection gave a longer injection time, and hence more opportunity to observe the reaction. The observations are summarised as follows:

(a) The reaction was smooth and controllable.

(b) Gas bubbles were produced, and observed in contact with the walls of the 'observation cell'. Whether these were bubbles of water vapour or product (hydrogen) could not be determined, since visual observation of the end of the capillary was of course not possible. This preliminary experiment did not reveal whether all of the reaction took place in the vicinity of injection or whether, as with metal → water injections, part of the reaction took place some distance from the site of the injection.

(c) The solid reaction products, presumed at this temperature to be entirely sodium and potassium hydroxide, rose to the surface of the metal as a 'slag'.

(d) The reaction vessel and contents heated up rapidly. Unlike the system described in previous chapters, heat was transferred quickly from the reaction site into the bulk metal due to the greater thermal conductivity of NaK over water.

(e) With the first injection (but not the second) a blue colouration appeared around the site of injection in the metal/water/hydroxide reacting mixture. This spread slowly away from the capillary opening, and

appeared mainly at the space between the metal and the glass of the reaction vessel walls. This corroborates the formation of the reaction intermediate $e^-_{(aq)}$.

These experimental results, when combined with X-ray transmission photography should allow a thorough examination of the reaction between excess liquid NaK and liquid water at room temperatures.

7.5.2 The detection of $e^-_{(aq)}$

A spectroscopic observation of the probable intermediate $e^-_{(aq)}$ during an alkali-metal/water reaction would provide positive proof that this species is involved. This might be achieved by vastly increasing the hydroxide content. It has already been noted that the alkali-metals are soluble in fused sodium hydroxide to give a blue solution,[68] the absorption spectrum of which would be similar to, but not exactly the same as that for the hydrated electron, since the metals dissociate to M^+ and $e^-_{(solvated)}$ in both of the above solvents. The spectroscopic analysis of solutions in molten salts requires special techniques, but is well advanced.[103]. The addition of small quantities of water to such a solution may give rise to the species $e^-_{(aq)}$, which could exist in such a solution for long enough to be detected spectroscopically at 715 nm. The life of the species would certainly be longer in such a solution than in water, especially if dilute solutions were prepared. The only major reaction of $e^-_{(aq)}$ in $NaOH_{(l)}$ would be that with another electron (Equation 9.10)) since reaction with the species H_3O^+ would be eliminated. Alternatively, continuous generation of the species by regular addition of water may give rise to a satisfactory spectrum.

APPENDIX I METAL SURFACE AREAS

For a body centred cubic cell, the area of the 100 plane is a^2, where a is the unit cell dimension. The area of the 110 plane is $\sqrt{2} \times a^2$. The 100 plane contains one

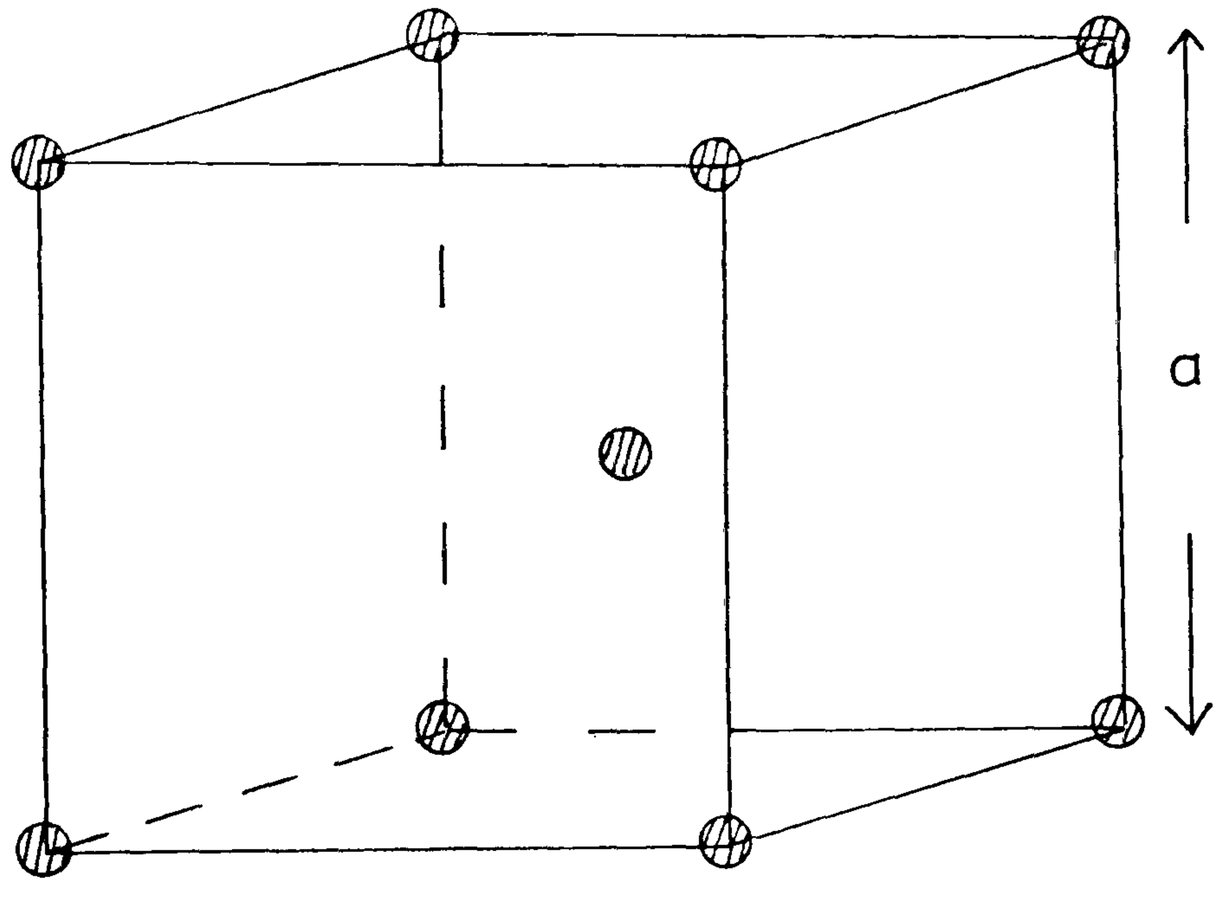

FIGURE X.1 B.C.C. UNIT CELL

atom ($4 \times \frac{1}{4}$). The number of atoms per square millimetre is therefore $1/a^2$ if a is in millimetres. The 110 plane contains two atoms ($1 + 4 \times \frac{1}{4}$). The area occupied by one atom is therefore $\frac{1}{2}\sqrt{2}.a^2 = a^2/\sqrt{2}$. The number of atoms per square millimetre is therefore $\sqrt{2}/a^2$ if a is in millimetres.

APPENDIX II ANALYSIS OF NaK FOR HYDRIDE CONTENT (Chapter 8)

Experiment 1

Moles Na, 3.025×10^{-3}. Moles K, 2.052×10^{-3}

Total metal 5.08×10^{-3}

Frame volume 183.0 cm^3

Pressure of H_2 255.3 mm Hg

Temperature 22.0°C

Moles H_2 2.54×10^{-3} †

2.54×10^{-3} *

Experiment 2

Moles Na, 4.759×10^{-3}. Moles K, 3.313×10^{-3}

Total metal, 8.08×10^{-3}

Frame volume 191.4 cm^3

Pressure of H_2 452.3 mm Hg

Temperature 20.5°C

Moles H_2 4.73×10^{-3}

4.04×10^{-3}

Experiment 3

Moles Na, 5.18×10^{-3} Moles K, 3.37×10^{-3}

Total metal, 8.56×10^{-3}

Frame volume 156.0 cm^3

Pressure of H_2 530.2 mm Hg

Temperature 18.5°C

Moles H_2 4.55×10^{-3}

4.28×10^{-3}

* Expected yield from the reaction $M + H_2O \rightarrow MOH + \frac{1}{2}H_2$

† Actual yield from the reaction $M + MH + H_2O \rightarrow MOH + H_2$

Experiment 4

Moles Na, 3.66×10^{-3}. Moles K, 2.46×10^{-3}

Total metal 6.12×10^{-3}

Frame volume $216.5 . cm^3$

Pressure of H_2 280.3 mm Hg

Temperature 21.0°C

Moles H_2 3.31×10^{-3} — 3.06×10^{-3}

Experiment 5

Moles Na, 5.01×10^{-3} Moles K, 3.89×10^{-3}

Total metal 8.90×10^{-3}

Frame volume 191.3 dm^3

Pressure of H_2 475.7 mm Hg

Temperature 22.0°C

Moles H_2 4.95×10^{-3} — 4.45×10^{-3}

Experiment 6

Moles Na, 1.71×10^{-3} Moles K, 3.40×10^{-3}

Total metal 5.11×10^{-3}

Frame volume 217.4 cm^3

Pressure of H_2 226.9 mm Hg

Temperature 20°C

Moles H_2 2.70×10^{-3} — 2.56×10^{-3}

Experiment 7

Moles Na 0.60×10^{-3} Moles K 0.83×10^{-3}

Total metal 1.43×10^{-3}

Frame volume $181.4\ cm^3$

Pressure of H_2 73.5 mm Hg

Temperature 20.0°C

Moles H_2 0.73×10^{-3}

6.72×10^{-3}

Experiment 8

Moles Na, 2.83×10^{-3} Moles K 5.78×10^{-3}

Total metal 8.61×10^{-3}

Frame volume $192.6\ cm^3$

Pressure of H_2 420.7 mm Hg

Temperature 21.0°C

Moles H_2 4.42×10^{-3}

4.31×10^{-3}

Experiment 9

Moles Na, 2.64×10^{-3} Moles K, 4.68×10^{-3}

Total metal 7.32×10^{-3}

Frame volume $214.3\ cm^3$

Pressure of H_2 322.8 mm Hg

Temperature 20.5°C

Moles H_2 3.78×10^{-3}

3.66×10^{-3}

Experiment 10

Moles Na 3.27×10^{-3} Moles K 3.21×10^{-3}

Total metal 6.48×10^{-3}

Frame volume $206.7\ cm^3$

Pressure of H_2 281.4 mm Hg.

Temperature 18.5°C

Moles H_2 3.20×10^{-3} 3.74×10^{-3}

Experiment 11

Moles Na 5.62×10^{-3} Moles K 3.10×10^{-3}

Total metal 8.72×10^{-3}

Frame volume $168.0\ cm^3$

Pressure of H_2 457.7 mm Hg

Temperature 22.0°C

Moles H_2 4.18×10^{-3} 4.36×10^{-3}

Experiment 12

Moles Na 3.89×10^{-3} Moles K 2.33×10^{-3}

Total metal 6.22×10^{-3}

Frame volume $193.2\ cm^3$

Pressure of H_2 281.8 mm Hg

Temperature 20.0°C

Moles H_2 2.98×10^{-3} 3.11×10^{-3}

Experiment 13

Moles Na 4.76×10^{-3} Moles K 4.23×10^{-3}

Total metal 8.99×10^{-3}

Frame volume 169.9 cm^3

Pressure of H_2 451.6 mm Hg

Temperature 20.0°C

Moles H_2 4.20×10^{-3} 4.50×10^{-3}

APPENDIX III DERIVATION OF EQUATION 8.7

In the sample, there are x moles of M and y moles of MH. On hydrolysis:-

$$xM + H_2O \longrightarrow x/2\ H_2$$

$$yMH + H_2O \longrightarrow yH_2$$

(i) a (total moles of metal) = x + y

(ii) b (total hydrogen) = x/2 + y

From (i) $x = a - y$

Sub. in (ii) $a/2 - y/2 + y = b$

$$y = 2(b - a/2)$$

$$\text{Mole \% y in y + x} = \frac{2(b - a/2) \times 100}{a}$$

APPENDIX IV MATERIALS

(a) Sodium

Supplied by British Drug Houses (B.D.H.) in 500g ingots (dry). The major quoted impurity was calcium (0.069%) with traces of the transition metals iron, copper, manganese and nickel (all less than 0.001%). In addition, the surface was contaminated with oxide, hydroxide and carbonate, which had to be cut away under an inert atmosphere, or alternatively, the melted metal was filtered through a grade - 0 sintered glass filter.

(b) Potassium

Supplied by Koch Light Laboratories Ltd. The assay gave K (99.4%), Na(o.4%), Si (0.05%). The metal was in the form of cylindrical rods (approximately 20g) under paraffin oil, sealed in plastic bags. Impurities were present in the surface, as with sodium.

(c) Argon

Supplied by Air Products Ltd., with a quoted purity of 99.999%. The impurities of concentration 1 p.p.m. and above were nitrogen (5 p.p.m.), carbon monoxide (1 p.p.m.) water (5 p.p.m.), oxygen (1 p.p.m.), and hydrogen (1 p.p.m.)

For most purposes, e.g. as reaction vessel cover gas, the argon was fed directly from the cylinder. In certain situations, it was necessary to clean the gas by passage through sodium-potassium alloy. This removed all the impurities with the exception of nitrogen.

(d) Water

After passage through an ion-exchange column, the water used was distilled three times:

(i) from acidic potassium permanganate.

(ii) from alkaline sodium dichromate.

(iii) from distilled water.

(e) Acids

The details of the acids used in the present work are contained in Table X.

(f) Glassware

The glass capillary was supplied by Jencons (Scientific) Ltd. as 'UNIFORM' Precision Bore Heat Resistant Glass Tubing, Cat. No. 3 (0.1 mm).

TABLE X ACIDS USED IN THE PRESENT WORK

Acid	HAc	HCl	H_2SO_4	HNO_3	HBr	HI
Source	M & B†	M & B	Laporte	M & B	EAC‡	M & B
Assay	99.6%	36%	98%	70%	65%	55%
Chloride	< 0.0005%			< 0.005%		<0.05% *
Sulphate	< 0.0005%	< 0.002%		< 0.01%		<0.005%
Iron	< 0.0002%	< 0.0002%		<0.002%		<0.001%
Arsenic	< 0.0002%			<0.0001%		<0.0002%
Lead	< 0.0002%	< 0.0002%		<0.0002%		<0.0005%
Sulphated Ash		< 0.01%				
Phosphorus compounds						<0.0005%
Non volatile residue	<0.01%			<0.01%		<0.02%

† May and Baker Ltd.

‡ East Anglia Chemicals

* Chloride + Bromide

REFERENCES

1. P.C. Putnam, 'Energy in the future', Macmillan (London), 1954.
2. A. Salmon, 'The nuclear reactor', Methuen and Co. Ltd. (London) 1964
3. D.M. Donald, 'Symposium on Liquid Metals', Aix-en-Provence; Cadrache (France), October 1963
4. S. Catchpole, Chem & Ind., 1972, 15 , 592
5. C.C. Addison , Endeavour, 1967, 26, 91
6. S. Glasstone, 'Principles of Nuclear Reactor Engineering', Macmillan (London), 1956, p. 525
7. 'Handbook of Chemistry and Physics' (53rd ed.) Chemical Rubber Publishing Co. 1973
8. K. Tregonning, 'Liquid Alkali Metals', Proc. Internat. Conf. B.N.E.S. (Nottingham), April 1973, p.115
9. J.L. Henry, USBM - RC - 1469, March 1970
10. S.C. Furman, 'Metal-water reactions', GEAP - 3208, V, July 1959
11. P.B. Longton, 'Reactions of the Alkali-metals with Gases', Part VI, IGR - TN/C, 435, January 1957
12. D.D. Adams, G.J. Barenborg and W.W. Kendall, KAPL - P - 1512
13. N.A. Bischel, BAW - 1105, September 1958
14. D.D. Williams, NRL Memo Report 33, June 1952
15. J.W. Weber, HW - 56588, September 1958
16. M.A. Salmon, NAA - SR - 840
17. H.H.Higgens and R.D. Schultz, IDO - 28000, April 1957
18. H.F. Coward and G.W. Jones, Bulletin 503, Bureau of Mines,(1952).
19. J.A. Ford, APDA - 167, March 1965
20. G. Long, ref 8, p. 31
21. V.V. Rachev, B.K. Maslennikov and A.A. Lbov, Zh. Prik. Khim., 1962, 35, 189.

22. A.I. Belyaev, L.A. Firsanova and I.I. Pomerantsev, Sbornik Nauch. Trudov. Moskov. Inst. Tsvetnykh Metal. i Zolota, 1955, No. 25, 172

23. J. Besson and W. Muller, Compt. Rend. 1958,247,2370

24. B.E. Deal and H.J. Svec, J.Am. Chem. Soc. 1953, 75, 6173

25. W.R Irvin and J.A. Lund, J. Electrochem. Soc., 1963, 110, 141.

26. J. Besson and A.Pelloux, C.R. Acad. Sci. Paris(c), 1967,265,816

27. A Hatterer and M. Thevenin, Chem. Soc(London), Spec. Publ., 1967, 22, 167

28. G. Cornec and J. Sannier, C.R. Acad. Sci. Paris. Ser., 1967, C265 (3), 137

29. A. Pelloux and J. Besson, Rev. Chim. Miner. 1970, 7(5), 955

30. R.J. Pulham and P.A. Simm, 'Chemical Aspects of Corrosion and Mass Transfer in Liquid Sodium', T.M.S. Symposium, Detroit, October, 1971.

31. L.G. McKnight and L.O. Brockway, Inorganic Chemistry 1966, 5, 1556

32. W.B. Wollen, D. Scott and F.R. Dell, Report A.E.R.E. CE/R2518, 1956

33. C.C. Addison and J.A.Manning, J.C.S. 1964, 4887.

34. H.M. Saltzburg, Report KAPL - 1945, April 1956.

35. H.M. Saltzburg, Report KAPL - 1763, April 1957.

36. M.M. Markowitz, J. Chem. Education, 1963, 40, 633

37. W.J. Moore, 'Physical Chemistry' (5th Ed), Longman, 1972. p. 402.

38. K, Dumm, H. Hausbeck and W. Schnitker, Atomkernenergie, 1969, 14(5), 309

39. I.Iiatika, J. Chem. Soc. Japan, 1930, 51, 301

40. W.D. Halstead, Report CEGB - RD/L/N 166/72, July 1972

41. A.G. Newlands and W.D. Halstead, Report CEGB - RD/L/N 130/75, September 1975

42. A.D. Bogard and D.D. Williams, Report NRL -3865, September 1951.

43. L. Corrsin, H. Steinmetz and B. Marano, NDA -89-19, May 1959

44. T.K. Rice, F.J. Woods and R.R.Miller, Report NRL - 2508, June 1949.

45. Data Sheets, APDC, NaK-water reaction tests, 1955/57

46. R.H. Jones, H.J. Williams and J.A. Murphy, APDA NaK-water reaction tests, Report AECU - 3193, Dec. 1956

47. M.D. Bonus, J.J. McSharry and E.A. Sullivan, J. Am. Chem. Soc., 1955, 77, 2007

48. W.M. Mueller, J.P. Blackledge and G.G. Libowitz, 'Metal Hydrides', Academic Press, 1968.

49. M. Dowling, Ph.D. Thesis, Nottingham, 1976

50. O.J. Faust, 'Sodium-NaK Engineering Handbook' (vol. I) Gordon and Breach (London) 1972

51. W.J. Price, 'Analytical Absorption Spectrometry', Heyden and Son Ltd.,1972

52. W.B. Pearson, ' A Handbook of Lattice Spacings and Structures of Metals and Alloys (vol II), Pergamon Press Ltd., 1967.

53. Ref. 50, p. 19

54. O. Miyagi, Phil Mag., 1925, 50

55. H.S. Allen, Phil. Mag., 1900, 50, 323

56. K.J. Laidler, 'Chemical Kinetics', McGraw-Hill,1950

57., A. Hérold, Ann. de Chim. 1951, 12, 536

58. A. Seidell and W.F. Link, 'Solubilities - Inorganic and Metal Organic Compounds' (4th Ed), D. van Nostrund Co. Ltd., 1958

59. W.D. Halstead, J. App. Chem.,1970, 20, 45

60. N.A. Lange, 'Handbook of Chemistry' (10th ed). McGraw-Hill,1966

61. T. Moeller and R.O'Connor, 'Ions in Aqueous Systems', McGraw-Hill, 1972.

62. R.J. Pulham, J.C.S. , A, 1971, 1389

63. G. Parry and R.J. Pulham, J.C.S. Dalton,1975, 446

64. C.C. Addison , R.J. Pulham and R.J. Roy, J.C.S., 1965, 116

65. K.M. Mackay, 'Hydrogen compounds of the metallic elements', E & F.N. Spon Ltd.(London),1966

66. C.A. Kraus, J. Am. Chem. Soc.,1908, 30, 1323

67. W.C. Johnson and H.J. Wolthorn, J.Chem. Ed.,1929, 6, 20

68. W.C. Fernelius and F.W. Bergstrom, J. Phys. Chem. 1931, 35, 746.

69. H.J. Wolthorn and W.C. Fernelius, J. Am. Chem. Soc., 1934, 56, 1551

70. J.N. Bronsted and N,L. Ross Kane, J. Am. Chem., Soc.,1931, 53, 3624

71. G. Stein, Disc. Faraday Soc.,1952, 12, 227.

72. M. Anbar, Chem. Soc. Quart. Rev.,1968. 22(4), 578

73. D.C. Walker, Chem. Soc. Quart. Rev.,1967,21(1) 79

74. E.J. Hart and M. Anbar, 'The hydrated electron', Wiley Interscience, 1970

75. E.A. Shaede and D.C. Walker, Chem. Soc. Spec. Publ., 1967, 22, 277

76. D.C. Walker, Can. J. Chem., 1966, 44, 2226

77. G. Hughes and R.J.Roach, Chem. Comm., 1965, 600

78. ref. 74, p 230

79. M. Gold and W.L. Jolly, Inorg. Chem.,1962, 1, 818

80. G.Nilson, H.C. Christensen, J. Fenger, P. Pagsberg and S.O. Nielson, A.C.S. Adv. in Chem., 1968,81,71

81. E.M. Fielden, and E.J. Hart, Trans. Faraday Soc., 1967, 63, 2975

82. E.J. Hart, 'Radiation Chemistry of Aqueous Systems', G. Stein,ed.., Weizmann Science Press of Israel, Jerusalem, 1968 p.73.

83. J. Bennett, B. Mile and A. Thomas, Nature,1964,201,919

84. J. Besson and A. Pelloux, C.R. Acad. Sci. Paris (c), 1966, 262, 1579

85. A. Pelloux, Ph.D. Thesis, Grenoble, 1969

86. P.B. Longton, Report IGR -TN/C, 418, December 1956
87. T.A. Miskinova and L.G. Giddin, Doklady Akad. Nauk. S.S.S.R., 1957, 117, 1027
88. ref. 74, p. 42
89. W.C. Gottschall and E.J. Hart, J. Phys. Chem, 1967, 71, 2102
90. M.S. Matheson, ACS Adv. in Chem., 1965, 50, 45
91. M. Sittig 'Sodium - its Manufacture, Properties and Uses' Reinhold (New York), 1956, p. 241
92. M. Anbar and D. Meyerstein, Trans. Faraday Soc., 1966, 62, 2121.
93. M. Anbar and D. Meyerstein, Chem. Comm., 1966, 57.
94. W.S. Cathro and J.C. Mackie, J.C.S. Faraday, I, 1972
95. R.M. Bowie and J.M. Woodrow, Phys. Rev., 1930, 35, 1423.
96. D.O. Hayward, B.M. W Trapnell, 'Chemisorption', Butterworths (London), 1964, p. 247
97. G.C. Bond, 'Catalysis by Metals', Academic Press (London), 1962, p. 375
98. V. Panec, Z. Knor, S. Cerny, 'Adsorption on Solids', Butterworths (London), 1974 (English translation) p.478
99. D.T. Hurd, 'An Introduction to the Chemistry of the Hydrides', Wiley (New York), 1952
100. J. Bray, J. Brit. Nucl. Energy Soc., 1971, 10. 107
101. G.A. Garzadyarn and V.M. Novikov, Dokl. Acad. Nauk., Armyanski, S.S.S.R., 1966, 42, part I, p. 15
102. H.P. Klugg and L.E. Alexander, 'X-ray Diffraction Procedures,' John Wiley and Son Inc., 1970, p.677
103. G.P. Smith, 'Electronic Absorption Spectra of Molten Salts' in 'Molten Salt Chemistry (ed.M. Blander), Wiley Interscience, 1964.